2011

Surface Characteristics of Silica Polyamine Composites

Jesse James Allen
The University of Montana

SURFACE CHARACTERISTICS OF SILICA POLYAMINE COMPOSITES

By

Jesse James Allen

B.S. in Chemistry, Oregon State University, Corvallis, OR, USA, 2005

Dissertation

Presented in partial fulfillment of the requirements
for the degree of

Doctor of Philosophy
in Chemistry, Inorganic

The University of Montana
Missoula, MT

Spring 2011

Approved by:

J.B. Alexander Ross, Assoc. Dean of the Graduate School

Dr. Edward Rosenberg, Committee Chairperson
Department of Chemistry

Dr. Nigel Priestley, Committee Member
Department of Chemistry

Dr. Bruce Bowler, Committee Member
Department of Chemistry

Dr. Earle Adams, Committee Member
Department of Chemistry

Dr. Nancy Hinman, Committee Member
Department of Geosciences

Allen, Jesse J., Ph.D., Spring 2011 Chemistry

Surface Characteristics of Polyamine Composites

Chairperson: Dr. Edward Rosenberg, Department of Chemistry

Abstract

The goals of this thesis were to explore the surface characteristics of silica polyamine composites (**SPC**) by elucidating coordination environments, measuring surface stability, and comparisons with analogous materials. Application of **SPC** materials as supports for heterogeneous catalysts was also investigated. Analytical techniques including NMR (both solution state and solid state), mercury porosimetry, and scanning electron microscopy (SEM) were used to characterize the materials.

Cobalt was found to irreversibly bind to the chelating polymer polyethyleneimine (**PEI**). This was due to oxidation of Co^{2+} to Co^{3+}, which was enabled by the chelate's ligand field stabilization. Detailed analysis of **SPC** surface coordination environments elucidated the types of coordination environments present. The use of model complexes further clarified the complexes forming on the composite surfaces.

Silica surfaces, including those of composite materials, are sensitive to alkaline conditions. Composite surface modifications such as the silanization step of **SPC** synthesis are shown to affect alkaline stability. Increasing surface group bulkiness and hydrophobicity circumstantially increased material stability. Anisotropy calculations utilizing solid-state CPMAS NMR spinning side bands were used to characterize some of the bulky, aromatic surface modifications.

A sol-gel method initially based upon the work of Dong and Brennan was developed to synthesize a composite material analogous to **SPC** materials. Initial materials were formed using methyltrimethoxysilane (**MTMOS**) and 3-chloropropyltrimethoxysilane (**CPTMOS**). Some control over surface morphology was achieved by adjusting synthetic conditions. Due to relatively low metal capacities, tetramethoxysilane (**TMOS**) was introduced as a structural support. Materials incorporating **TMOS** had metal capacities comparable with **SPC** materials, as well as narrower average pore size distributions.

Second row transition metal catalysts immobilized on **SPC** materials were investigated for olefin hydrogenation activity. Hydrogenation of monoenes and dienes was investigated and found comparable to currently used catalysts in some cases. The most potentially useful result of this catalysis work was the selective hydrogenation of a conjugated diene to a monoene. Selective heterogeneous hydrogenation of dienes to monoenes has potential industrial applications.

ACKNOWLEDGEMENTS

The time I have spent at the University of Montana has been a wonderful time in my life, filled with joy and new friendships, as well as a few old ones. I would like to thank first and foremost my professor Edward Rosenberg, who has provided unending guidance in my time here. The assistance and opportunities provided by Professor Rosenberg have been immense, and I will forever be grateful for the effort he has put forth in helping me. I will do my best throughout the future of my professional career to represent the Rosenberg group strongly and with the respect that it deserves. I would also like to thank those who helped share their experience as I was learning my way in the group, particularly Varadharajan Kailasam, Mark Hughes, and Bill Gleason. I would like to thank all of the rest of the Rosenberg group who has been involved in my education and research, particularly Erik Johnston, whose help on the sol-gel research has proved invaluable. The entire faculty of the Department of chemistry has been very supportive, however; a special thanks must go out to Earle Adams, without whose experience and support, the absolutely crucial solid-state NMR studies of these materials could not have been performed. My time at the UM would not have been so pleasant had it not been for the unconditional support of my family, who have always encouraged me to pursue my goals in whatever ways I find appropriate, and who I know will always continue to do so. Finally, I wish to express love and thanks to the beautiful and charming Sheryl, whose motivation and input was a tremendous help in the writing of this thesis.

TABLE OF CONTENTS

LIST OF FIGURES

LIST OF TABLES

LIST OF ABBREVIATIONS

1	$[Ru(CO)_3(TFA)_3]^-K^+$
AA	Atomic Absorption
AES	Atomic Emission Spectroscopy
AFM	Atomic Force Microscopy
BP-1	PAA based silica polyamine composite
BP-2	BP-1 modified with acetate groups
BP-NTA	BP-1 modified with NTA groups
BPAP	BP-1 modified with phosphorus acid
BPED	BP-1 modified with EDTA
CMPh	4-chloromethylphenyl
CPMAS	Cross Polarization Magic Angle Spinning
CPTCS	3-chloropropyltrichlorosilane
CPTMOS	3-chloropropyltrimethoxysilane
CuSelect	BP-1 modified with pyridine 2-carboxaldehyde
CuWRAM	See CuSelect
Dien	Bis(2-aminoethyl)amine
EDTA	Ethylenediaminetetraacetic acid
EXAFS	Extended X-Ray Absorption Fine Structure
FRET	Free Resonance Energy Transfer
ICP	Inductively Coupled Plasma
IR	Infrared
M	Methyl

MLCT	Metal to Ligand Charge Transfer
MTCS	Methyltrichlorosilane
MTMOS	Methyltrimethoxysilane
NMR	Nuclear Magnetic Resonance
NTA	Nitrilotriacetic acid
PAA	Polyallylamine
PEI	Polyethyleneimine
Ph	Phenyl
Q_4	Bulk Siloxane site with no unreacted Si-O bonds
Q_3	Bulk Siloxane site with one unreacted Si-O bond
Q_2	Bulk Siloxane site with two unreacted Si-O bonds
SEM	Scanning Electron Microscopy
SPC	Silica Polyamine Composite
T1ρ	The time constant for the decay of magnetization along the radio frequency field, B_1
T_3	Alkyl silane with no unreacted Si-O bonds
T_2	Alkyl silane with one unreacted Si-O bonds
T_1	Alkyl silane with two unreacted Si-O bonds
T_0	Alkyl silane with all unreacted Si-O bonds
TEM	Tunneling Electron Microscope
TEOS	Tetraethoxysilane
TFA	Trifluoroacetic acid
TMCS	Trimethylchlorosilane

TMOS	Tetramethoxysilane
TOF	Turn-Over Frequency
TON	Turn-Over Number
Tren	Tris(2-aminoethyl)amine
WP-1	PEI based silica polyamine composite
WP-2	WP-1 modified with acetate groups
WP-4	BP-1 modified with 8-hydroxyquinoline
WP-NTA	WP-1 modified with NTA groups
WPED	WP-1 modified with EDTA groups
XPS	X-ray Photoelectron Spectroscopy

CHAPTER 1: BACKGROUND

1.1. Introduction

Separation of materials is a necessity in modern society. The smelting of ores allows us to make metal. The refining of oil allows the production of plastics and gasoline. These examples and countless others are ways in which separations processes are absolutely necessary for the sustainability of society.

One unifying principle behind separations processes is that they require a driving force. Entropy must favor the mixing of like materials. Thus, a driving force must be provided for the separation of like materials. Whether this is the heating and cooling of a distillation or the application of a material that binds some part of the mixture more effectively than another portion, this driving force is always a necessity.[1,2]

Surfaces form the basis for almost all separations. The characteristics of these surfaces may strongly impact the characteristics of these separations, whether it's the number of plates in a column or the accessibility of pores in a gel.[2,3] Greater understanding of the surfaces involved can result in improved separations as well as further applications for these materials. There are many separation materials currently being used industrially, and the focus of this research is on silica polyamine composites (**SPC**) and their use not only as a separation material, but also as a platform for heterogeneous catalysts and as a support for other types of chemical modifications.

Amorphous silica gels have been effective materials for chromatography and catalytic supports since the middle of the 20th century.[4-7] Their use as solid-phase adsorbents for metal recovery and aqueous remediation has been increasing due to gains in efficiency and decreases in environmental impact relative to previously predominant methods such as solvent extraction.[8]

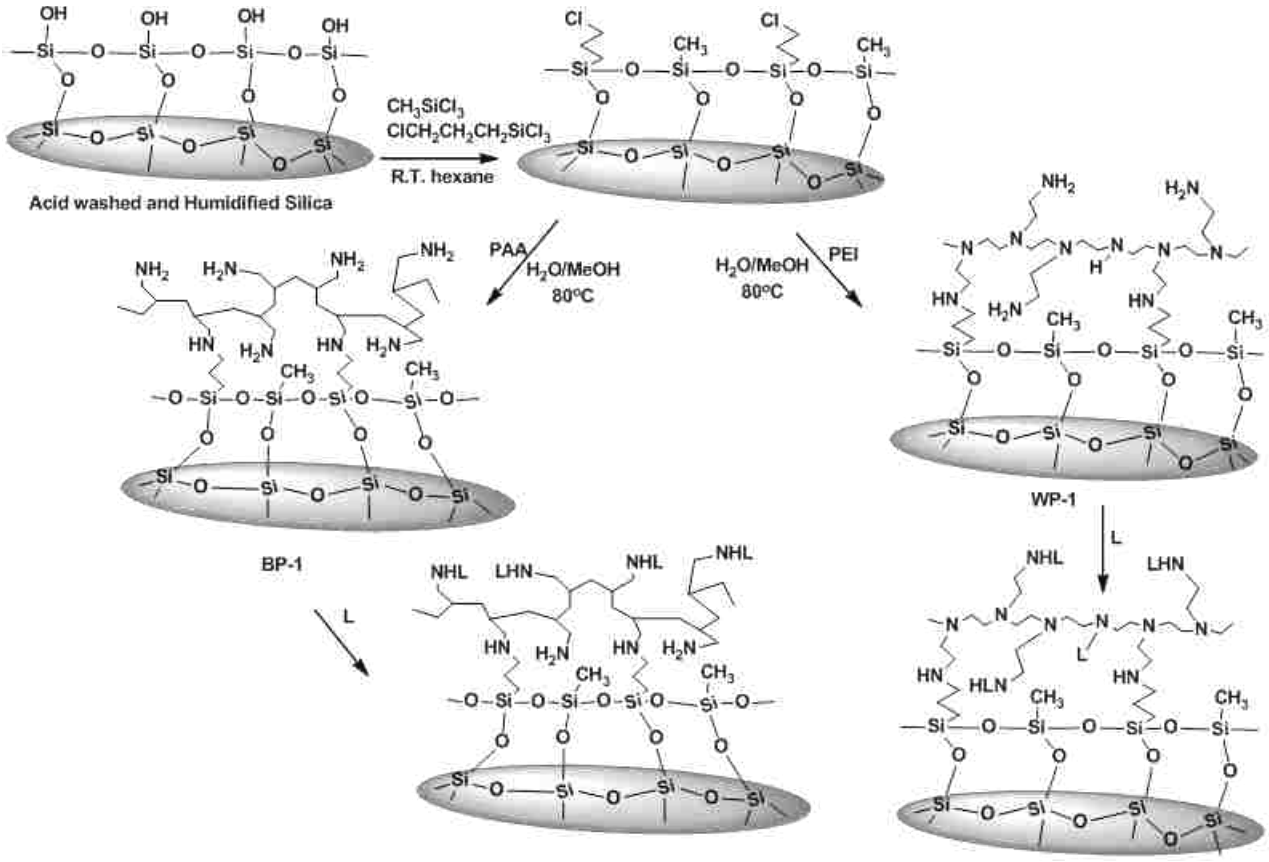

Figure 1.1: Schematic for the synthesis of **SPC** materials

Surface modification of silica gels and further covalent modification with polyamines has been one area of focus for the remediation of ionic pollutants in aqueous media.[9-24] Figure 1.1 shows the schematic for the synthesis of **SPC** materials. Silica is initially acid

washed to ensure removal of any surface cations. The silica is then fully dried, followed by a humidification step to leave a monolayer of water on the surface. The water monolayer then promotes lateral polymerization of the alkyltrichlorosilanes. A polyamine is then covalently bound to the surface by nucleophilic attack on the halocarbon of the 3-chloropropyl group. The surface-bound polymer can then be modified by ligand addition to give metal selectivity.[14,16-19,25-28] **SPC's** have found use industrially as well in research laboratories, and the technology developed has begun to branch out into applications other than metal sequestration, such as catalysis and luminescence.

1.2. Potential Applications

1.2.1 Surface Investigations

Improvements can be made in the uses of **SPC**'s. **SPC** characterization has led to new uses for these materials.[14,16-19,29-32] The ligand structure and geometry on the surface of a material gives vital information regarding potential interaction with ions on the surface. Studies into the surface environment including the method and level of coordination can, for example, improve performance and enable development of immobilized luminescent metal complexes as potential metal sensors.[31,33,34] These investigations can also lead towards more cost efficient metal separations[17,32,35] and even potentially towards catalytic reactions that could increase the efficiency of fuel production.[29,30]

1.2.2 Metal Separations

Heavy metal contamination of aqueous media is a worldwide concern, with examples ranging from Chernobyl, to contaminated ground water in Bangladesh, to the Berkeley Pit right here in Montana. More efficient methods of addressing this issue are being constantly sought out.[17,35,36-40]

The damage caused to the ecosystem by these anthropogenic sources of heavy metal contamination can be tremendous. Heavy metal contamination of ground water can cause major environmental concerns such as pollution of streams and subsequent destruction of wildlife, contamination of groundwater, and runoff into riverian systems, to name a few. This contamination not only affects the exposed wildlife, but will also continue to affect these areas for generations to come. Many heavy metals are persistent in ecological systems. For example, mercury and hexavalent chromium can slowly seep from soil and bioaccumulate in predatory animals, eventually reaching toxic levels.[41,42]

The damage to humans from environmental contaminants is a major concern leading to the immediate importance of developing remediation technologies. One topic of utmost importance is the incidence of arsenocosis. Arsenic present in aqueous form is mainly found in either the trivalent form as arsenite or the divalent form as arsenate.[43] Both forms are toxic, and exposure has raised concern worldwide. While there are natural sources of arsenic contamination, such as the thermal springs running from Yellowstone National Park, the majority of issues related to arsenic exposure have been due to anthropogenic effects such as

the drilling of wells, irrigation in Bangladesh, or mining tailings such as from the Berkeley Pit.[37-39]

Acid leaching of metals from ore is commonplace in mining processes. This process results in solutions with high metal ion concentrations, which often have very little of the metal removed for processing. These aqueous solutions rich in metal ions have the potential to be harvested for profit if metal separations can be effectively achieved while maintaining economic viability.[44-46]

Many technologies have shown efficacy in the binding of metal ion solutions in the previously mentioned circumstances. Solvent extraction, and ion exchange are among three of the many separation processes commonly used.[44-48] Each has its benefits and its own potential for remediation. Solvent extraction has found extensive use in the mining industry for high-throughput and high capacity purifications such as the isolation of cobalt and nickel from laterite ores[45], as well as the separation of gallium from solutions containing large concentrations of aluminum.[49] These technologies will be discussed in greater detail in Section 1.3.1.

1.2.3 Catalysts

Surface interactions are of monumental importance in the separation of materials. Around 90% of industrially produced materials are the product of heterogeneous catalysis.[3] Industrial catalytic systems using heterogeneous systems have shown many advantages over homogeneous systems. Increased stability of immobilized catalysts and ease of product

separation from catalysts are two such effects that have resulted in the wide range of processes employing the use of heterogeneous catalysts. Hydrogenation in particular has received a large amount of attention due to the many areas in which it has found a central role: hydrogenations of unsaturated oils into saturated oils in the food industry as well in the petroleum industry are just two examples of hydrogenations that have been widely implemented commercially.[50]

The performance of catalysts in heterogeneous systems is strongly affected by the support upon which the catalyst is immobilized. The surface where catalytic reactions take place as well as the access of the molecule to active sites greatly influences the activity of catalysts, and a further understanding of the surface environment of the active sites can lead to development of new catalytic systems as well as improvements upon existing ones.[30,31,51,52]

Though homogeneous catalysts are commonly used in selective organic transformations, heterogeneous catalysts have seen increasing use in the targeted hydrogenation of olefin bonds.[53] One particular case of interest is the selective hydrogenation of butadienes. Butadienes have the effect of poisoning some catalysts in petroleum processing, and their removal is necessary for efficient petrol processing. Additionally, butene is currently produced by the catalytic cracking of petrol products, and an efficient, targeted method for its formation during the purification process has the potential to produce this chemical by a more cost-efficient method.[54]

The complex mixtures found in petroleum processing methods make the use of heterogeneous catalysts very desirable, due to the ease of separation and recovery of these catalysts. Additionally, the use of a well-defined homogeneous catalyst which can be

immobilized on a heterogeneous support has the potential to exhibit the characteristics of a heterogeneous catalyst while maintaining some of the activity and selectivity of well-known homogeneous catalysts.[55,56]

There are several traits which are necessary for a catalyst to be considered viable for industrial use including high turnover number (**TON**), high turn-over frequency (**TOF**), and substrate selectivity. **TON** is defined as the number of moles of substrate that one mole of catalyst can convert on average before inactivation. A high **TON** is important for catalyst lifetime, and many of the potentially useful catalytic systems are relatively expensive. **TOF** is defined as the average number of turnovers per unit time. This term defines the level of activity of the catalyst, which is of the utmost importance not only for minimizing the amount being used, but also for minimizing the time required for reaction completion.

Classical homogeneous catalysts have exhibited much higher **TOF** than heterogeneous catalysts, as their behavior is a solution-state phenomenon rather than the surface phenomenon exhibited by heterogeneous catalysts.[57] Combining a tethered polymeric ligand system with a heterogeneous support has the potential to create a scaffold for the immobilization of well-known homogeneous catalysts. The high mobility of the tethered polymer as well as the kinetically accessible pores of **SPC** materials provides an opportunity to exploit the ease and economic benefits of heterogeneous catalysts while still maintaining some of the high activity of homogeneous catalysts.[30,57]

1.3. Competing Technologies

1.3.1. Ion Exchange

Many different methods have been used for the removal of aqueous metal ions from solution, including precipitation,[58] solid-phase adsorption,[48] solvent extraction,[45-47] membrane filtration,[59] bio-sorption,[42] among others.[8] Solid-phase adsorption, solvent extraction, and membrane filtration are all examples of ion exchange materials which have been used extensively for metal ion removal whether for remediation, sequestration, or for further purification. Some characteristics are desirable for all ion exchange materials in order to be viable for these uses, all of which together delineate the economic viability of the materials. Integrity and long usable lifetimes are necessities, as well as high capacities and sharp separations, even at low metal ion concentrations. In addition, the material must possess kinetically favorable characteristics as well as a broad range of operational environments.

1.3.2. Solvent Extraction.

Solvent extraction is a process in which the aqueous solution containing the ion or ions of interest is mixed with an organic solution of an extractant, often an organic-soluble chelating agent. This extractant is designed to be specific for the species of interest and, upon coordination of the ion, will bring it into the organic layer, often kerosene, as seen in Figure 1.2.

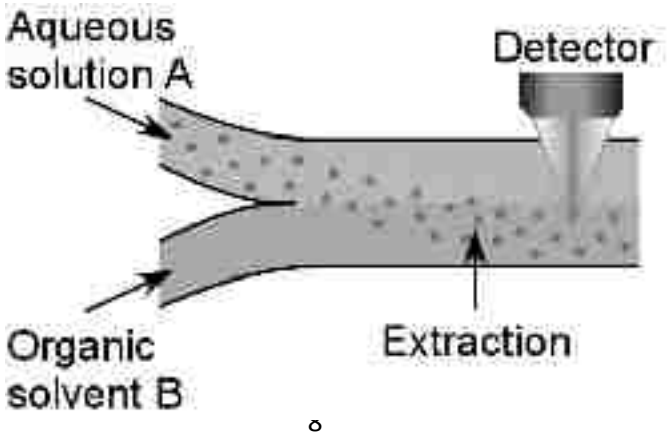

o

Figure 1.2. General schematic of the process of solvent extraction.

Solvent extraction has some unique advantages relative to other separatory processes. As the extractant is solubilized, these materials can be used under flow conditions, allowing the process time to be significantly reduced relative to other methods in systems which do not require extended equilibration times. These flow conditions also allow for the use of very high-throughput systems and versatility in the conditions used for individual systems. However, the lack of a solid-state matrix for immobilization of these extractants is a disadvantage. Some of the extractants are lost to the aqueous layer every time, and though for some processes they can be regenerated, there is always notable loss, resulting in the requirement of constant input of extractant. In addition, the build-up of emulsions and crud in the interfacial region of the immiscible solvents leads to both loss of species of interest, and loss of extractants. The two most industrially important disadvantages of solvent extraction, however, are the inability to have complete removal of species of interest from the aqueous solutions, and the large amounts of organic solvent that are required to be evaporated for recovery.[46]

1.3.3. Solid-Phase Ion Exchange Resins.

In addition to the aforementioned solvent extraction techniques, there are also many solid-phase ion exchange materials which are widely used in both metal ion remediation and recovery. Ion exchange materials typically have a solid matrix upon which functional groups are immobilized, typically by covalent binding, but also by precipitation or coordination of

metal cations for anion exchange. These materials possess many advantages related to the insoluble nature of the matrix which can be exploited for facilitation of separations and concentration of desired species.

Ion exchange materials using organic support matrices are the most commonly used ion exchange materials. Three common organic supports are cellulose, methacrylate, and polystyrene based resins. All three are relatively inexpensively synthesized and exhibit different characteristics. For the purposes of metal ion purification and decontamination, the most commonly used by far are polystyrene beads.

Polystyrene beads are generally crosslinked using divinylbenzene in order to provide more stable beads as well as to define some of the characteristics of the materials such as pore size and particle density.[60] Polystyrene resins can either be synthesized using modified monomeric units to include functional groups during the polymerization, or the modifications can be made post-polymerization. These functional groups then provide the metal binding sites which provide both capacity and selectivity for the species targeted for separation, just as the extractant does in solvent extraction systems. However, in opposition to solvent extraction systems, the matrix upon which the functional groups are immobilized has strong effects on the geometry in which these materials can interact with the species of interest, resulting in differences in the coordination environments present. This effect results in significant changes in the geometry at the binding site, and can result in changes in the specificity of functional groups for different species. This specificity can then be utilized for separations that would be otherwise unobtainable with solvent extraction techniques.[16]

Ion exchange resins such as polystyrene which use organic matrices do however have some undesirable characteristics. These materials are known to shrink and swell in acidic

and basic solutions, respectively, and, in addition to increased head pressures under column conditions, this characteristic is known to cause increased attrition of the material, resulting in a decreased lifetime of operation relative to those made on inorganic support matrices. Thermal stability of polystyrene supports has also been shown to be less than that of similar materials on inorganic supports.[61]

1.3.4. Hydrogenation Catalysts.

Many metals have been shown to be effective hydrogenation catalysts, the most active have been based upon the metals Pt, Pd, Rh, and Ru, and many catalysts have been shown to be active in activating carbon-carbon double bonds for hydrogenation by diatomic hydrogen gas.[51,57,62] For the particular goals of this research, however, Pt based catalysts were not investigated due to previous studies elucidating decreased substrate selectivity relative to Pd based catalysts.[63,64] Hydrogenation of alkenes, particularly aromatic systems, is generally too slow of a process to occur without the assistance of a catalyst.

Homogeneously catalyzed hydrogenations generally have higher TON and TOF. Homogeneous hydrogenation catalysts, however; have seen a relatively small role in industrial applications due to the difficulties in separation of the catalyst from substrate and loss of catalyst, many of which are quite expensive. Therefore, it is desirable to form catalysts which mimic some of the activities of the highly active homogeneous catalysts while maintaining a solid support which will facilitate industrial application of the catalyst. From this regard, a brief overview of some of the more extensively used and investigated catalytic systems for both homogeneous and heterogeneous hydrogenation is necessary.

Studies similar to those presented in this research have been performed where Rh heterogeneous hydrogenation catalysts were synthesized by the immobilization of the $Rh(III)Cl_3$ salt on iminodiacetic acid functionalized polystyrene-based resins which showed less activity than homogeneous catalysts, but were nonetheless shown to be catalytically active materials similar in structure to the polyamine composites researched in this work.[65]

Ruthenium based catalysts are well known in most circumstances to have less effective catalytic activities relative to rhodium and palladium based catalysts. These mild reactivities as well as the varied coordination environments available for different ruthenium species present the potential for chemoselective hydrogenation of olefins, and several examples of these types of transformations are present in literature.[66]

Palladium complexes as well as nanoparticles have found extensive use as hydrogenation catalysts due to the very high TOF expressed as well as the level of selectivity that can be observed in some circumstances. Pd on carbon is currently one of the most commonly used hydrogenation catalysts. It consists of zero valent palladium particles immobilized on activated carbon to provide greater surface area. Other derivatives of this such as Pd on alumina and Pd on silica are also commonly used. The high levels of activity expressed by this system are ideal for a commercially viable process, and new materials with increased kinetic accessibility to catalytic sites are often being investigated, particularly due to the expensive nature of the compounds.[64]

1.4. Silica-based Polyamine Composites

1.4.1. Silica Polyamine Composites.

Amorphous silica gel is produced via the precipitation of sodium silicate with mineral acids. Depending upon the method of production, silica gel may be manufactured in spherical or irregular shapes with some control over particle and pore sizes. Silica gel used in the context of this research was silica gel which was formed in irregular shapes and was ground to either 150-250μm particle size or 250-600μm particle size. 97-99% of the surface area of these silica gels is from the porous interior, and as such, the crushing and sieving process for production of the gels has little effect on the actual surface area of the materials.

Pore characteristics greatly affect the diffusion of dissolved species into the porous interior of the gels. Large pores will result in highly kinetically accessible materials, while smaller pores will increase the effective surface area of the material, increasing the number of active sites or binding sites available. In addition to these effects, smaller pores have the ability to be blocked upon surface modification by both polymers and ligands, especially when hydrophobic functional groups are present.

In order to take advantage of the porous nature of amorphous silica gels, surface modification with tether groups active towards further modification is necessary. 3-chloropropyl tethers have been effectively used to provide an anchor upon which further modifications can be made. The current synthesis of this surface proceeds by the hydration of the silica surface with a monolayer of water, followed by surface polymerization with alkyltrichlorosilanes which undergo lateral polymerization due to the presence of the monolayer of water. Currently, a mixture of both methyltrichlorosilane (**MTCS**) and 3-

chloropropyltrichlorosilane (**CPTCS**) is being used in varying ratios dependent upon the further modifications that will be made. The dilution of the chloropropyl anchoring groups with methyl groups has been shown to increase the number of available nitrogen groups upon polymer addition. The entire synthetic schematic can be seen in Figure 1.1.[14]

The further modification of this surface with a water soluble large molecular weight polymer provides a surface to which metal ions can bind, and further modification of the polyamine can make the **SPC** metal selective. Polyamines in particular make a good choice due to the facile modification of the amine groups with other ligands as well as the ability of the polyamine itself to coordinate metal ions. These polyamines are easily grafted onto the surface of the silanized silica gels via the halocarbon undergoing nucleophilic attack by the amine. Two particular polymers have been investigated in this regard, polyallylamine (**PAA**), and polyethyleneimine (**PEI**).

PAA is a non-chelating linear polyamine consisting of exclusively primary amines. The composite material obtained from the covalent binding of this polymer to silica is labeled as **BP-1**. **BP-1** is currently synthesized using a silanized surface ratio of 7.5:1 of **MTCS:CPTCS**. The regular structure of this polymer provides effectively regular surface environments upon which metal coordination can occur. Primary amines can also be later either mono- or di-functionalized to provide a resultant material selective for species of interest.

PEI is a chelating branched polyamine consisting of approximately 35% primary amines, 35% secondary amines, and 30% tertiary amines. The composite material obtained from the covalent binding of this polymer to silica is labeled as **WP-1**. **WP-1** is currently synthesized using a silanized surface ratio of 12.5:1 of **MTCS:CPTCS**. The chelating

nature of this polymer provides an average coordination number of 4 when **PEI** is bound to the surface of the silica composite.[31] Additionally, the presence of secondary and tertiary amines allows for stronger ligand field stabilization relative to the exclusively primary amines found in **BP-1**.[31]

Figure 1.3 shows six different ligands which have been attached to the amine groups to establish specificity for metal ions. Ligand immobilization is also utilized to enhance composite performance at low pH by using ligands which exhibit low pKa values, enhancing the concentration of the deprotonated state under acidic conditions.

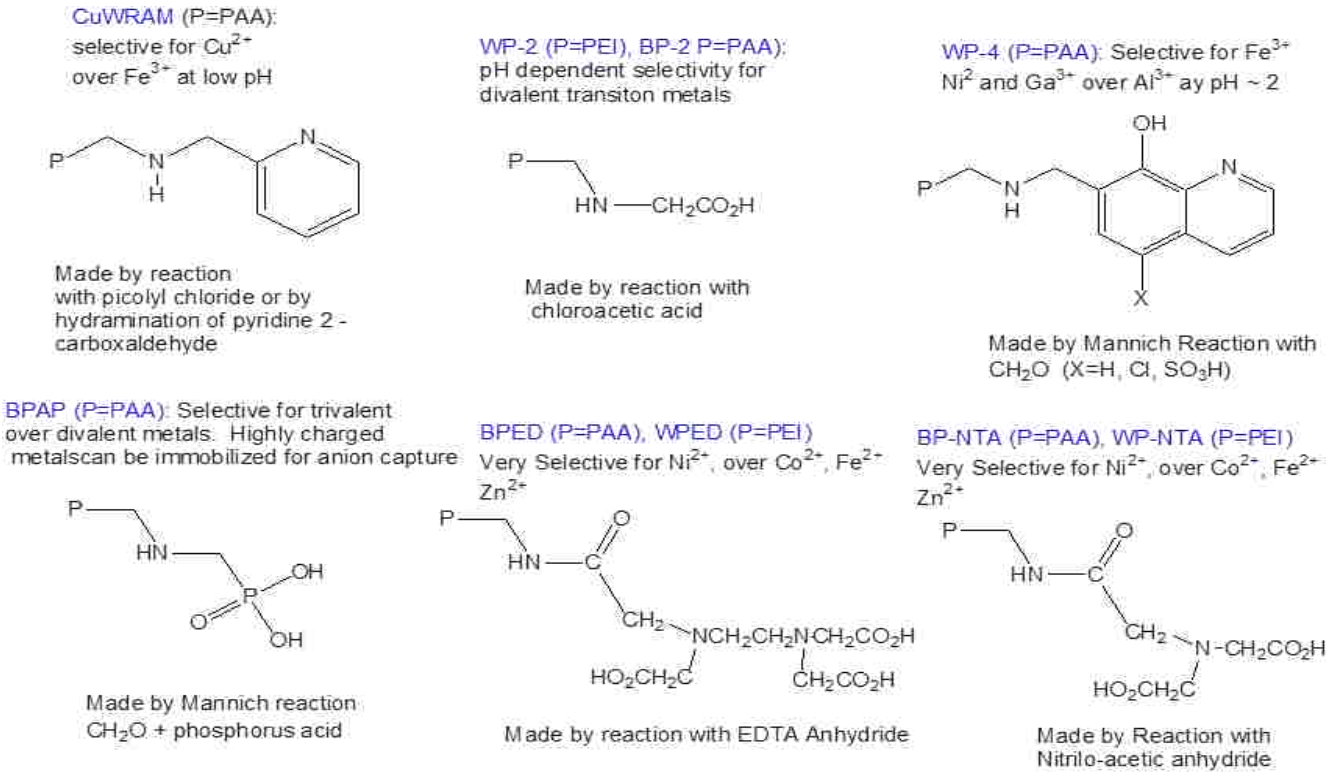

Figure 1.3. Ligand modifications of polyamine composites for metal selectivity

Picolylamine has been covalently bound to the composite **BP-1** to form a composite known as **CuWRAM** or **CuSelect**, as seen in the top left of Figure 1.3. This composite

material was designed to be selective for Cu(II) over iron(III) and Zn(II). **CuSelect** is currently in production commercially.

Acetate ligands have been covalently bound to the amine surfaces nucleophilic attack of the sodium chloroacetate salt by the polymeric amines. The products of this synthesis method for reaction with **BP-1** and **WP-1** are labeled **BP-2** and **WP-2** respectively, and are shown in the top middle of Figure 1.3. The acetate functional group imparts greater affinity at lower pH for Cu(II), Ni(II), Zn(II), and Co(II) at lower pH values than the parent composites **BP-1** and **WP-1**.[19]

8-hydroxyquinoline has been covalently bound to **BP-1** to form a composite known as **WP-4**, which is shown in the top right of Figure 1.3. This composite has been found to be selective for Ga(III) in the presence of hich concentrations of Al(III), and has potential to be used in the isolation of gallium from zinc mine tailings.[19]

A phosphonic acid derivative of **BP-1** has been synthesized by covalent binding of the functional group via a Mannich-type reaction. This is shown in the bottom left of Figure 1.3. Approximately one third of polymer amines are difunctionalized in this reaction. This composite was given the name **BPAP** and has been found to be selective for trivalent metals over divalent metals.[19]

Modification of **BP-1** surface amines by reaction with ethylenediaminetetraacetic acid (EDTA) anyhydride results in the composite **BPED**, which can be seen in the bottom middle of Figure 1.3. **BPED** has been shown to be very selective for Ni^{2+} over Co^{2+}, Fe^{2+}, and Zn^{2+}.[16]

Modification of **BP-1** surface amines with nitrilotriacetic acid anhydride (NTA anhydride) results in the composite **BP-NTA**, which can be seen in the bottom right of Figure 1.3. **BP-NTA** has been shown to have similar selectivities to **BPED**, which is expected considering the similarities between the ligands.[16]

In addition to their use as ion exchange materials, silica polyamine composites have recently been investigated as to their use for other applications such as the reactive sorption of hydrogen sulfide[29] and as supports for hydrogenation catalysts.[30]

1.4.2. Sol-gel Polyamine Composites.

Sol-gel methods for the formation of mesoporous gels have received considerable interest, however; the functionalization of these materials and their use as ion exchange materials is still a developing field.[67,68]

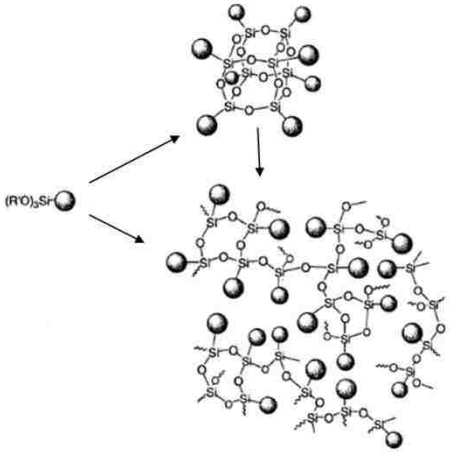

Figure 1.4. Chain elongation and oligomer formation during the acid-catalyzed step

A sol-gel process is one in which a specific series of events occur, leading to the precipitation of a solid out of its initial solvated form. The 'sol' in sol-gel refers to the fact that the initial mixture of monomeric units is fully solvated. Hydrolytic polymerization causes a colloidal suspension of oligomeric and polymeric clusters to form. This is shown in Figure 1.4. Figure 1.4 also shows the reopening of cyclized oligomers leading to linearly polymerized polymeric clusters. Pores begin to form due to solvent hydrogen bonding interactions as well as cluster-cluster binding, and then gelation and precipitation are observed (not necessarily in that order). Figure 1.5 shows a representation of a polysilsesquioxane formed using a mixture of methyltrimethoxysilane (**MTMOS**) and 3-chloropropyltrimethoxysilane (**CPTMOS**). Precipitation of these sol-gel materials is due to increased hydrophobicity resulting from the hydrolysis reaction. It can be seen in Figure 1.5 that the hydrophobic alkyl groups are centered towards the outside of the structure, resulting in increased hydrophobicity. The way in which the precipitation and gelation occur can be seen to have significant impacts upon both the macroporous and mesoporous characteristics of the gel. Gels formed in this way have shown many uses in industrial and research applications, including the formation of thin films, mold casts of highly dense material, drawn fibers, and precipitates which can either be powders or monoliths.[68-71]

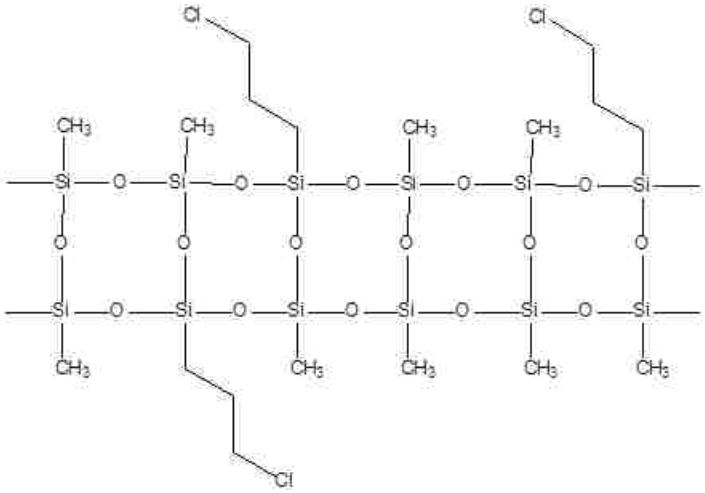

Figure 1.5. Idealized representation of a very hydrophobic polysilsesquioxane surface

For the method of formation of these materials, the two types of materials that are most desirable for the aforementioned purposes are the formation of highly uniform powders and the formation of monoliths. The formation of these highly uniform powders has only been shown to occur in rare circumstances with specific alkyl groups and under a limited set of circumstances, and while more desirable due to their very high level of uniformity, it is not reasonable to expect that materials formed will have this character. The formation of a monolith, however, can still yield very uniform pore size distributions, and the resultant materials can be crushed and sieved to desired particle sizes.[71]

The potential to create a hybrid sol-gel material which can easily be modified with the use of a polyamine has the potential to create a composite comparable to the previously mentioned silica polyamine composites, but with the potential advantages of increased uniformity as well as chemical stability. The methods used to produce these mesoporous sol-gel materials is also significantly more environmentally friendly, and could potentially be an economically viable alternative.

Pore definition and morphological control has been a matter of difficulty for sol-gel materials when a specific set of characteristics is desired, as in the case with ion exchange materials. This is due to the very high level of dependence of the gel's properties upon the substituents present on the starting monomeric units. Recently, however, the use of a two-step method utilizing first acid- and then base-catalyzed polymerization has been developed which allows for increased control of pore definition without necessitating changes in the substituent groups used.[71,72] This increased level of control allows for the formation of a sol-gel based material which can be designed to mimic the characteristics of the currently synthesized silica polyamine composites.

1.5. Research Goals

1. To investigate surface metal-binding characteristics of silica polyamine composites, including coordination environment, by following the reduction of divalent cobalt to trivalent cobalt on the surface of **WP-1**, as well as the use of model complexes to investigate these characteristics on the surfaces of both **WP-1** and **BP-1**.

2. To investigate surface stability of silica polyamine composites using bulky and sterically hindering anchor group modifications. NMR investigations of the surfaces will be performed, and silica leaching under alkaline conditions will be measured.

3. To investigate the production of a new matrix for polyamine immobilization via a sol-gel process. The materials will be synthesized with the goals of obtaining control of pore formation while meeting established standards for stability and metal capture properties.

4. To investigate the use of transition metal salts immobilized on silica polyamine composites for catalytic hydrogenations of monoenes and the selective hydrogenation of conjugated dienes.

CHAPTER 2: SPC SURFACE COORDINATION ENVIRONMENTS[‡]

2.1. Introduction

The use of solid phase adsorbents for the removal and recovery of metal cations and oxoanions from industrial and mining waste streams has been gaining in popularity due to the greater efficiency and environmental friendliness of this method relative to bulk hydrometallurgy or solvent extraction.[8] In general, the solid phases of choice have been lightly cross linked polystyrene or methyl methacrylate polymers.[73] In cases where dilution of a waste stream is not practical, or in the case of waste streams containing valuable metals, ion exchange offers a viable method for offsetting the price of environmental remediation using relatively simple and safe process designs. Moreover, the increased use of oxidative pressure leaching and bioleaching for metal extraction of sulfide ores in the mining industry is even more compatible with ion exchange than with solvent extraction because it avoids the use of flammable solvents and takes metal concentrations to lower effluent values.[74,75]

Polymer based matrices, however, are not particularly well suited to these large scale applications because they often involve the use of hot solutions and wide swings in pH where the shrink–swell properties of the polymers lead to shorter life times or require the use of dead volumes in plant design. In order to overcome these disadvantages we have turned to amorphous silica gel polyamine composites. These materials do not shrink or swell, and the

[‡]This chapter was published as reference #31

polar nature of the silica polyamine surface makes for better mass transfer kinetics in the case of aqueous solutions.[22-24,26,27,76-79] The surface bound polyamine can be easily modified with metal selective functional groups in similar ways to those used for polystyrene resins[80], without the use of swelling solvents, to form robust carbon-nitrogen single bonds.[22] The advantages of these composites have been demonstrated through studies that directly compare the properties of the polyamine composites with commercially available polystyrene resins.[76,78]

These composite materials are synthesized by coating an amorphous silica gel surface with a mixture of methyltrichlorosilane (**MTCS**) and 3-chloropropyltrichlorosilane (**CPTCS**) and then reacting with the branched polymer polyethylenimine (**PEI**, MW = 23 000) to yield the composite **WP-1** or with the linear polymer polyallylamine (**PAA**, MW = 15 000) to yield the composite **BP-1** (Fig. 2.1). The **WP-1** used in these studies was made from a mixture of 12.5:1 molar ratio of **MTCS:CPTCS**. The **BP-1** used in these studies was made from a mixture of 7.5:1 molar ratio of **MTCS:CPTCS**. The polyamine is covalently bound at multiple points to the silane layer. In this way, the chelating moiety becomes an integral part of the coating matrix. These are key factors in creating a material with remarkable durability.[76,78] These composites have been tested through 7000 cycles with no visible loss of physical stability and less than 10% loss in capacity.[22] **PEI** is a highly branched, water soluble amine polymer containing 1°, 2°, and 3° amino groups in a ratio of 7:7:6, respectively. **PAA** is a linear water soluble polyamine containing primary amino groups only.

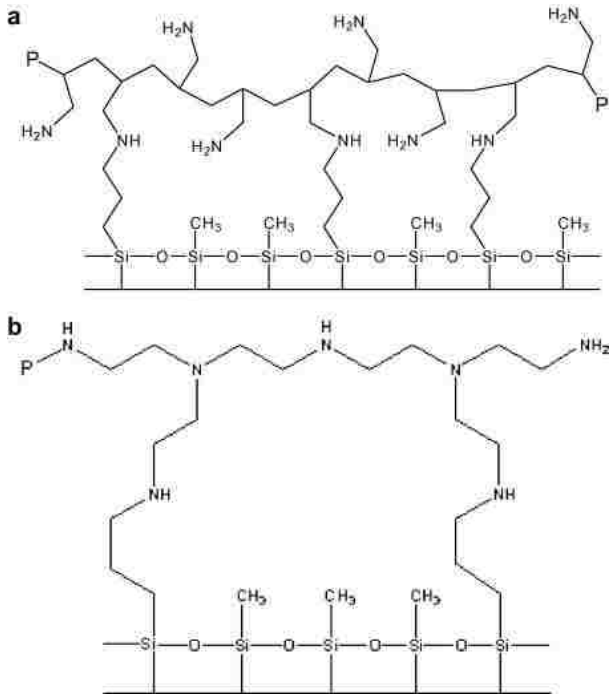

Figure 2.1. Structures of mixed silane **BP-1** and **WP-1**, showing the diluted anchor points present in both composites, as well as the branched nature of **BP-1** (a) and the linear nature of **WP-1** (b).

In the course of our studies on the binding of Co^{2+} to **WP-1** and **BP-1,** we noted that a considerable fraction of the Co^{2+} was irreversibly bound to **WP-1** but not to **BP-1**. This suggested that the Co^{2+} was being oxidized to Co^{3+} and the greater ligand field stabilization associated with a multi-amine coordinated Co^{3+} prevented desorption from the composite. For example, the reduction potential of the $[Co(H_2O)_6]^{3+}$ is 1.92 V while that of the pentamine complexes $[Co(NH_3)_5L]^{2+}$ or $[Co(NH_3)_5L]^{3+}$ range from 0.22 to −0.47 V, depending on L. Tetramine complexes of Co^{3+} have reduction potentials in the range of 0.47–0.98 V.[81,82] In the case of the linear polyamine composite, **BP-1**, one would expect amine coordination numbers lower than four, which would not provide enough ligand field stabilization energy to promote Co^{2+} oxidation. We report here a study of the coordination of

Co^{2+} to **WP-1** as well as a comparison of the UV–Vis spectra of **PEI**–Co^{3+} in solution with a series of model Co^{3+} amine complexes. Furthermore, we have studied the adsorption of $[Ru(CO)_3(TFA)_3]^-K^+$ (**1**, TFA = trifluoroacetate) onto **WP-1** and **BP-1** where the carbonyl stretching frequencies in the IR spectra and the solid-state ^{13}C CPMAS spectra are used to define amine coordination on the two composites.

2.2. Results and discussion

2.2.1. Characterization of the oxidation of Co^{2+} on the polyamine composite WP-1

Illustrated in Figure 2.2 is the total cobalt loaded onto the polyamine composite **WP-1** as a function of time. It can be seen that cobalt loading initially increases until 215 min, after which the cumulative uptake of cobalt actually decreases. We interpret this as initial binding of Co^{2+} to the polyamine at a relatively low coordination number, followed by reorganization to higher amine coordination numbers and oxidation to Co^{3+} with associated desorption of Co^{2+} from the surface. Related experiments with **BP-1** showed only initial increase in Co^{2+} adsorption to composite saturation.

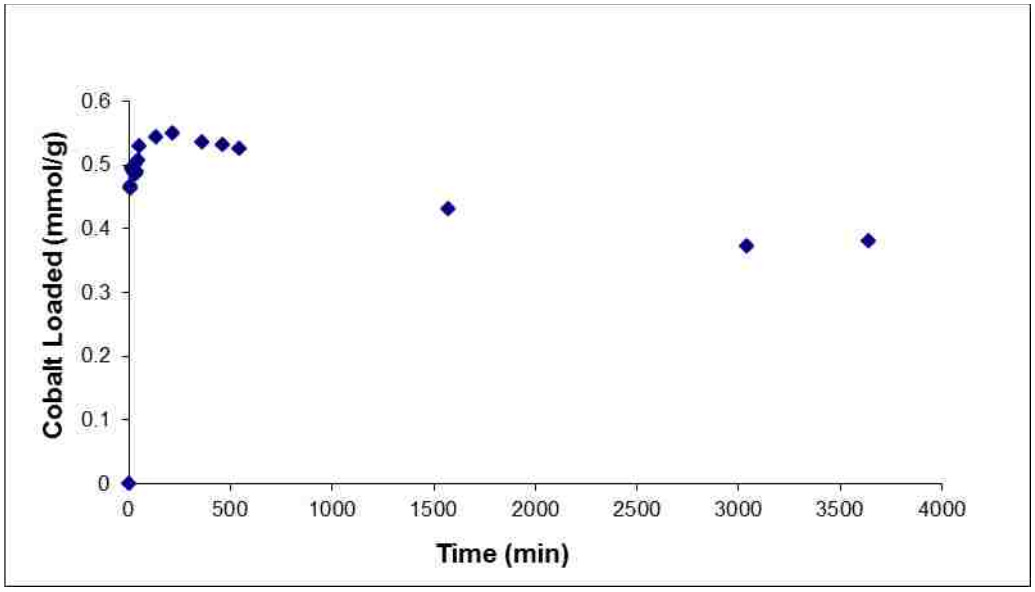

Figure 2.2. Kinetics of cobalt loading on **WP-1**, showing the total cobalt species loaded onto the surface of the silica polyamine as a function of time.

In a separate experiment, Co^{2+} was allowed to equilibrate for 24 h with **WP-1** and the adsorbed cobalt (28 mg cobalt/g composite) was exposed to increasing concentrations of sulfuric acid. Even with concentrated sulfuric acid, less than 1% of the cobalt was leached from the polyamine surface as measured by atomic adsorption spectroscopy. In the case of **BP-1**, adsorbed Co^{2+}(32 mg/g) stripping was complete with 1 M sulfuric acid.

It seems reasonable to propose that surface adsorbed and dissolved O_2 is responsible for the oxidation of Co^{2+}–Co^{3+} according to Eq. (1).

$$(1)\quad 4nL + O_2 + 4H^+ + 4Co^{2+} \rightarrow 2H_2O + 4Co(L)_n^{3+}.$$

According to previous work on the Co^{2+} to Co^{3+} oxidation, *n* must be greater than or equal to three.[83,84] In order to verify that oxygen was responsible for the Co^{2+} to Co^{3+} oxidation, we conducted an experiment where the composite solution mixture was degassed under a slight vacuum and the solution purged under a stream of nitrogen. After stirring for 24 h, workup and AA analysis revealed that the oxidation had proceeded to only 14% of the amount determined in the previous experiments, (3.9 mg/g). Clearly it was not possible to eliminate all of the oxygen, but this experiment indicates that O_2 was responsible for the oxidation.

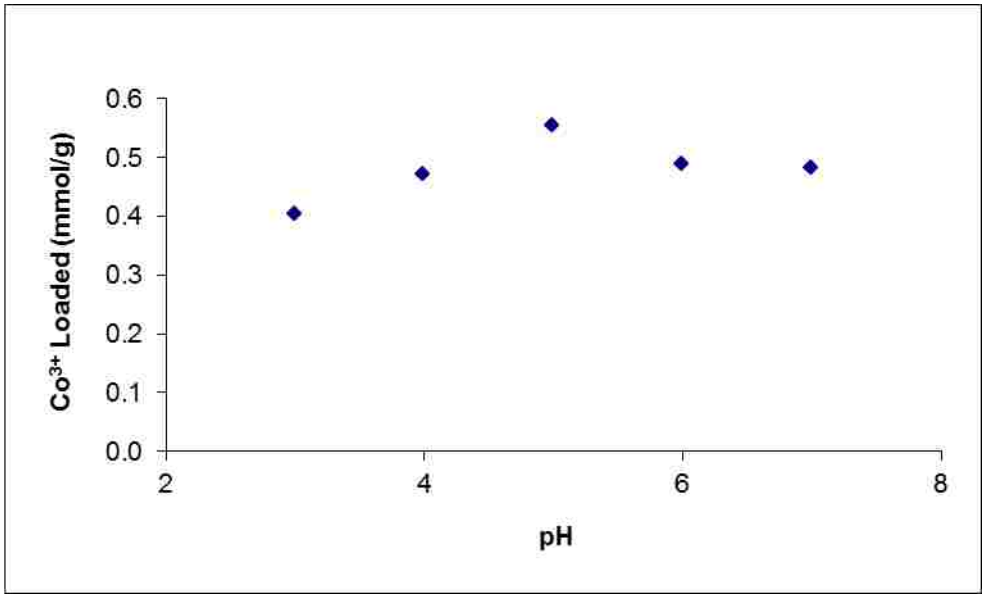

Figure 2.3. pH dependence of the oxidation of Co^{2+} to Co^{3+}. High pH favors coordination, leading to ligand field stabilization. Low pH favors oxidation by the increased presence of protons to push equilibrium. Balance is seen with maximum cobalt oxidation at pH = 5.

Illustrated in Figure 2.3 is the pH dependence of irreversible cobalt binding to **WP-1**. Clearly, this oxidation requires protons, but at pH's below three, **WP-1** is fully protonated and does not adsorb metal cations. Thus, the observed maximum at a pH of five represents an optimal value which is a balance of these two effects.

To gain a better understanding of the coordination environment for the Co^{3+} adsorbed on **WP-1**, we did an elemental analysis after irreversible binding and washing with 0.1 M HCl and then water to remove any adsorbed Co^{2+}. Elemental analysis along with AA analysis to evaluate adsorbed Co^{3+} gave a chloride to cobalt ratio of 4.66:1. The higher chloride to cobalt ratio than the expected 3:1 is undoubtedly due to the presence of uncoordinated amines on the surface which may be protonated, having a chloride counterion. To determine whether these chlorides were in the inner coordination sphere or acting as counter ions to amine-aquo cobalt centers, we then washed the sample with 1 M sulfuric acid and subsequent analysis revealed that there was one chloride for every four Co^{3+} ions. (Table 2.1) This suggests that the adsorbed cobalt species were either $[N_3Co(H_2O)_3]^{3+}$ or $[N_4Co(H_2O)_2]^{3+}$, along with a small number of cobalt centers with a chloride within the inner coordination sphere, and with sulfate or bisulfate as the necessary counterions. These data are also consistent with the Co^{3+} low spin d^6 configuration, which exhibits very slow ligand exchange.[85] The overall nitrogen to cobalt ratio of **WP-1** with irreversibly bound Co^{3+} was between 6:1 and 7:1 by elemental analysis and 5.7:1 to 7.9:1 by XPS measurements, thereby

indicating that not all of the nitrogen atoms are used for coordination of cobalt, making it impossible to determine the number of amines coordinated to each cobalt by these techniques. Sputtering the surface by XPS showed a decreasing N:Co ratio (4.6:1) indicating that N atoms are preferentially removed from the surface and suggesting that there is no cobalt gradient as one approaches the silica surface.

Elemental analyses	molar ratio Nitrogen	molar ratio Chlorine	molar ratio Cobalt
WP-1 12.5:1 **MTCS:CPTCS**	34.6	1.72	0.00
WP-1 12.5:1 **MTCS:CPTCS** Co loaded, H_2SO_4 stripped	22.0	2.57	3.12
WP-1 12.5:1 **MTCS:CPTCS** Co loaded, HCl stripped	18.9	16.2	3.12
(%Co as determined by AA)			
(molar ratios are relative)			
(mol Cl / mol Co is calculated subtracting chloride content of **WP-1** before loading of cobalt.)			

Table 2.1. Results of elemental analysis and AAS to determine Co:N:Cl ratios on the surface of **WP-1** with no cobalt loaded, with cobalt loaded then stripped using H_2SO_4, and with cobalt loaded then stripped with HCl, respectively.

Additional evidence for complete conversion from Co^{2+} to Co^{3+} on **WP-1** comes from the fact that the solid-state ^{13}C CPMAS NMR spectra before and after binding of cobalt are virtually identical (Figure 2.4). Our previous molecular modeling and NMR studies indicate that **PEI** is rigidly bound to the silica gel surface and suggests that coordination sites for Co^{3+} are pre-templated on the surface.[22]

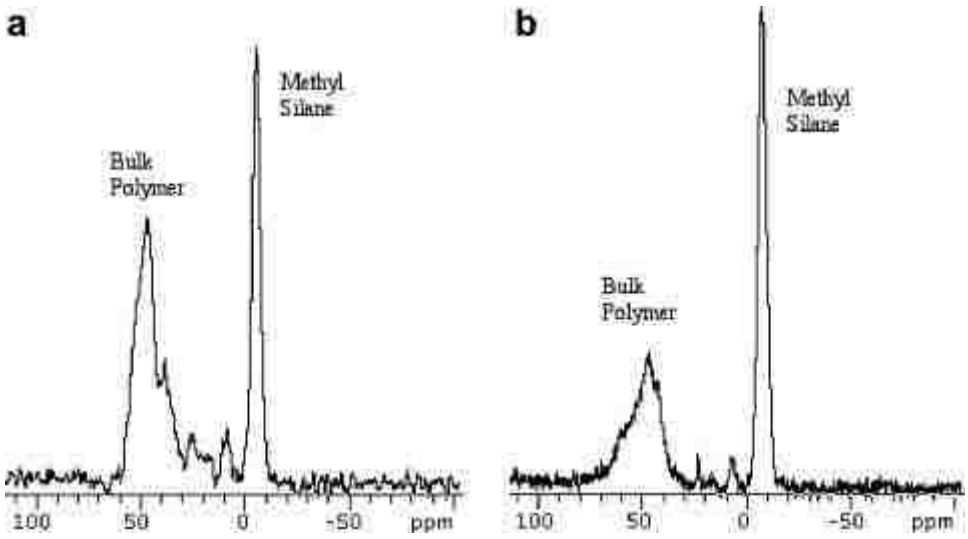

Figure 2.4. Solid-state ^{13}C CPMAS NMR spectra of **WP-1** (a) and Co-**WP-1** (b) using mixed silane, the similarity of the spectra indicates the complete lack of paramagnetic Co^{2+}.

2.2.2. Investigation of coordination number using model systems

The evaluation of coordination number and geometry of metal ions adsorbed onto amorphous surfaces is a daunting task. In an attempt to understand whether three or four amines were bound to each Co^{3+} on **WP-1**, we synthesized the complexes $[(tren)Co(H_2O)_2]^{3+}3Cl^-$ (tren = tris(2,2′,2″aminoethyl)amine) and $[(dien)Co(H_2O)_3]^{3+}3Cl^-$ (dien = diethylenetriamine) and compared their UV–Vis spectra with a solution of **PEI** loaded with cobalt (Figure 2.5). The tren and dien complexes were prepared according to literature procedures from the $[Co(NO_2)_6]^{4-}4Na^+$ complex.[83,84] Aspiration of air through the solutions of the hexanitrito species in the presence of dien and tren gives the desired complexes. To a solution of **PEI** was added $[Co(NO_2)_6]^{4-}4Na^+$. Air was aspirated

through that, and it was assumed that all of the Co^{2+} was oxidized to Co^{3+} as was the case for the dien and tren complexes. UV–Vis spectra of the two isolated complexes and the cobalt–**PEI** solution were then measured as shown in Figure 2.6. In a separate experiment, $CoCl_2$was added to a solution of **PEI**, let stand overnight, and then dialyzed with a cellulose membrane for 3 weeks, changing the solution outside the dialysis membrane daily. A UV–Vis spectra of this sample following dialysis was identical to that shown in Figure 2.6 for the **PEI**–Co complex. It can be seen that although the λ_{max} values in the 520 nm region, assignable to the MLCT band, are quite similar, the value for the **PEI**–Co^{3+} (528 nm) is closer to that for the tren complex (529 nm) relative to the dien complex (522 nm). Although this small difference is chemically significant, we sought additional evidence for the $[N_4Co(H_2O)_2]^{3+}3Cl^-$ complex.

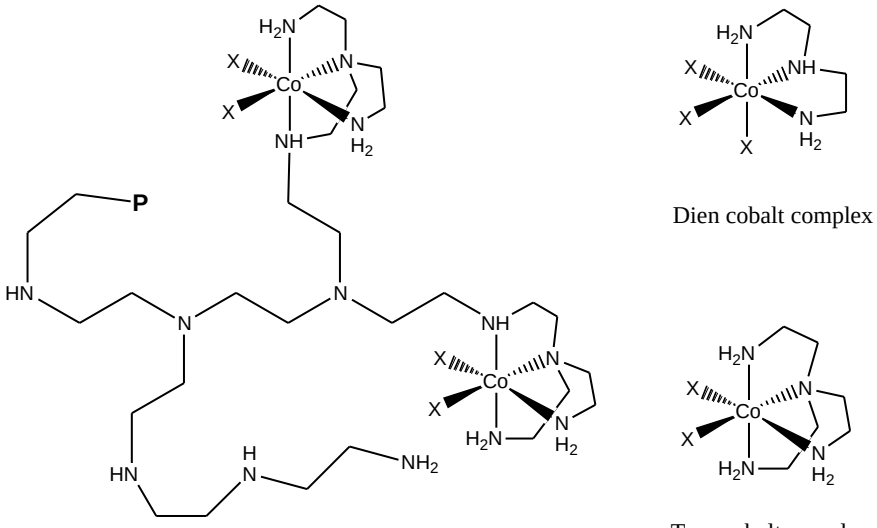

Figure 2.5. Structures of dien, tren, and **PEI** coordinated to cobalt, X indicates a ligand, likely the aquo complexes.

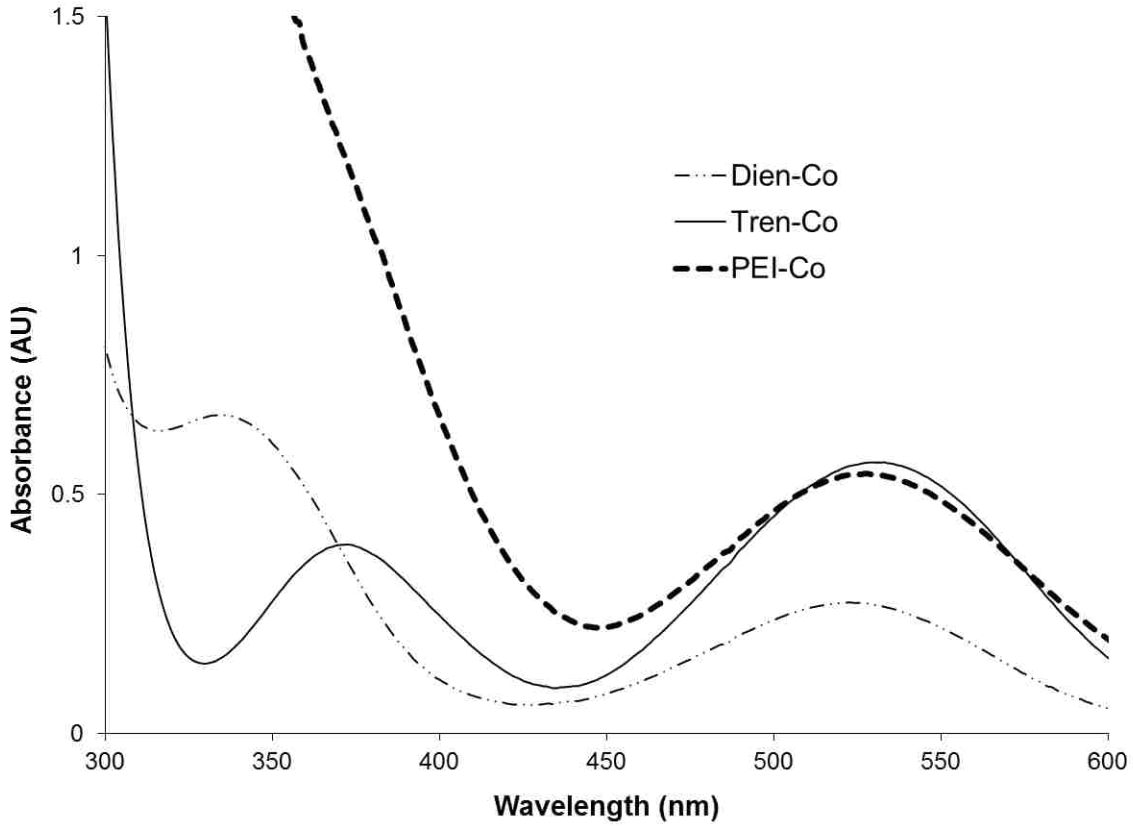

Figure 2.6. UV–Vis spectra of $[(tren)Co(H_2O)_2]^{3+}3Cl^-$, $[(dien)Co(H_2O)_3]^{3+}3Cl^-$, and **PEI** loaded with trivalent cobalt.

Also, a comparison of **PEI** in solution coordinated to Co^{3+} is not a particularly good analog to Co^{3+} coordinated to **WP-1** because in solution the **PEI** can undergo intermolecular crosslinking and is much less structurally rigid than the polymer grafted to the surface of the silica gel. We therefore sought a probe molecule that could give spectroscopic evidence for the coordination of metal ions to **WP-1** versus **BP-1**. Recently, we have been studying the coordination chemistry of the reactive ruthenium complex, $[Ru(CO)_3(TFA)_3]^-K^+$ (TFA = trifluoroacetate) (**1**).[33,86] This reactive ruthenium complex undergoes stepwise substitution of up to four ligands as seen in Figure 2.7. The overall pattern of substitution involves

replacement of one CO and one TFA followed by displacement of a second TFA and then a second CO (Figure 2.7).[33,86] The number of CO stretching frequencies observed in the IR can be used as a rough assessment of the number of ancillary ligands coordinated to the ruthenium center.[33,86] Using this complex as a probe of surface coordination geometry on **WP-1** and **BP-1** could provide a much clearer picture of amine coordination to octahedral metal centers. We therefore synthesized the tren complex of **1**, which gives $[(tren)Ru(CO)(TFA)]^{+}TFA^{-}$. We then compared its IR CO stretching frequencies with that of a sample of **1** equilibrated on the surface of **WP-1**. The IR spectra of KBr pellets of these two samples are shown in Figure 2.8. Both show single, strong CO stretches at 1952 cm^{-1} and 1958 cm^{-1} for $[(tren)Ru(CO)(TFA)]^{+}TFA^{-}$ and the Ru–**WP-1** complex, respectively. In addition to broad lower intensity bands at 2052 cm^{-1} and 2044 cm^{-1} for $[(tren)Ru(CO)(TFA)]^{+}TFA^{-}$ and the Ru–**WP-1** complex, respectively. These data give strong support for the coordination of four amine groups to Co^{3+} on **WP-1**.

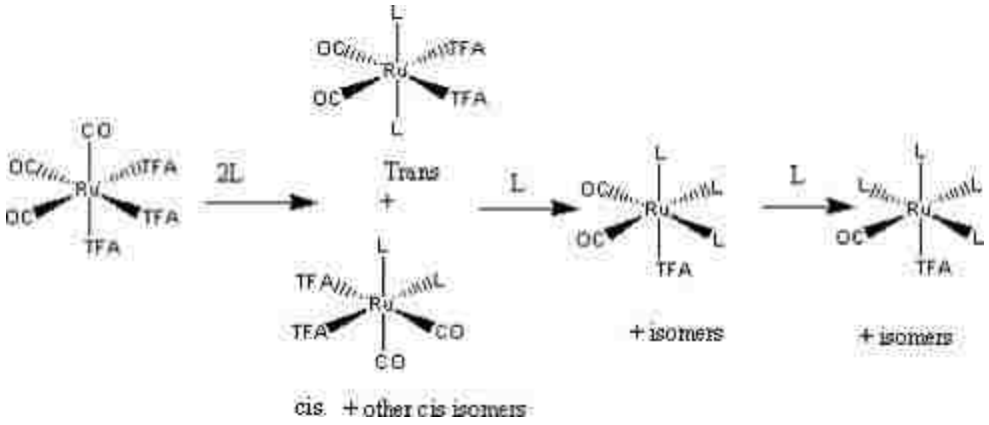

Figure 2.7. Ligand replacement motif for **1**, showing the pattern of ligand replacement sequentially as coordination number increases. First, one carbonyl and one TFA leave as two ligands are replaced. Then, sequentially, one TFA ligand leaves, followed by one carbonyl ligand.

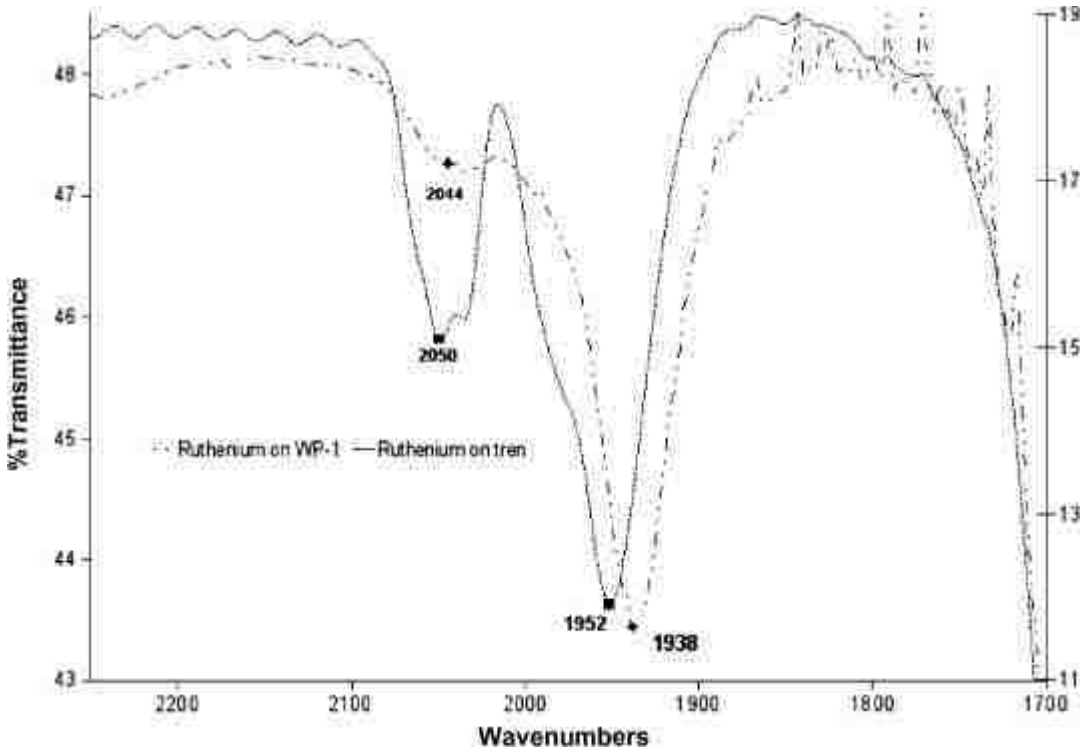

Figure 2.8. IR of **1** coordinated to **WP-1** and tren, showing the marked similarity of the carbonyl region of both, indicating the presence of one major species and its isomer.

For comparison, we then measured the IR spectra for a sample of **1** bound with the linear polymer composite, **BP-1**. This sample shows two partially overlapping dicarbonyl stretching patterns, indicating that for this composite, two amines coordinate to two adjacent sites on the linear polymer, **PAA**. Thus, as expected, the branched polymer, **PEI**, provides greater intrinsic coordination numbers sufficient to drive the oxidation of Co^{2+} to Co^{3+} while the linear polymer does not.

For both **BP-1** and **WP-1** loaded with **1**, and for $[(tren)Ru(CO)(TFA)]^{+}TFA^{-}$, the presence of multiple isomers is indicated. For the **WP-1**–Ru, one major and one minor

isomer is indicated, while for the **BP-1**–Ru, two isomers of similar intensities are suggested. The complex $[(tren)Ru(CO)(TFA)]^{+}TFA^{-}$ suggests the presence of one major and two minor monocarbonyl isomers, but there is also a shoulder on the high frequency side of the major monocarbonyl species.

Of course IR is not a very good indicator of the relative abundance of these different isomers, and so we decided to measure the solid-state ^{13}C CPMAS spectra of **BP-1**–Ru and **WP-1**–Ru using ^{13}CO enriched samples of **1**. Shown in Figure 2.9a is the ^{13}C spectrum of **WP-1** loaded with **1** at a spin rate of 11.5 kHz. It can be seen that there are two partially overlapping CO signals at 203 ppm in an approximate ratio of 3 to 7, with the high-frequency peak being the smaller one. Although, relative intensities of these peaks must be interpreted with caution because they were run under CPMAS conditions, it is thought that for CO in similar environments, CPMAS effects on intensity would be very similar. Most interestingly, we observe a broad, low intensity resonance at 258 ppm, which we tentatively assign to the presence of di-ruthenium μ-carbonyl species. It thus appears that the branched polymer, **PEI**, can coordinate two ruthenium atoms in close enough proximity to form a μ-carbonyl species, but that this takes place to a very minor extent relative to the two major terminal carbonyl peaks observed. Spectra were run at different spinning speeds to verify that these peaks were real and not just spinning sidebands. We also observe a resonance at 165 ppm which we assign to the natural abundance carboxyl carbon of the TFA ligand and a multiplet at 119.5 ppm (observed at a spin rate of 15 kHz, spectrum not shown) which we assign to the CF_3 group on TFA. In Figure 2.9a, this peak is overlapping with one of the major spinning sidebands for the metal carbonyls. The chemical shifts of both of these resonances are very similar to the peaks observed in the solid-state NMR for the parent complex, **1**, at 163 ppm

and 117 ppm, respectively. This indicates that the TFA that we observe is in the coordination sphere of the metal, and that additional TFA present as a counterion is not observed due to the much lower cross polarization expected for counterions.

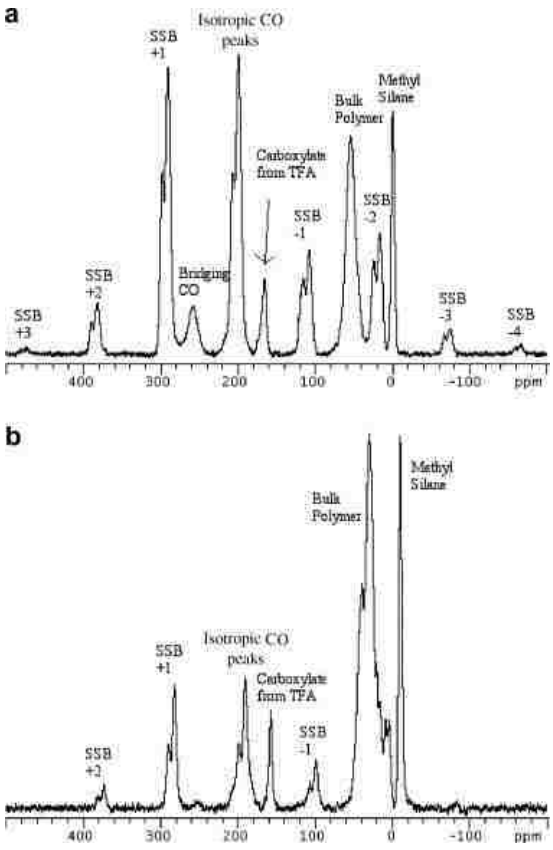

Figure 2.9. CPMAS NMR of **WP-1** (a) and **BP-1** (b) complexed with ^{13}CO enriched **1**, respectively. Peaks labeled "ssb" are spinning sidebands from the main pair of carbonyl peaks at 190 ppm. Spinning sidebands are labelled "+n" or "−n" where n is an integer relative to the peak's position downfield or upfield from the isotropic peak, respectively.

Figure 2.9b shows the ^{13}C CPMAS spectrum of ^{13}CO enriched **1** adsorbed on the surface of **BP-1** at a spin rate of 11.5 kHz. The IR evidence for the complexation of **1** on **BP-**

1 suggested the complexation of two dicarbonyl species. Assuming that **1** will bind to two adjacent primary amine groups on the linear polymer, **PAA**, there should be three isomers. (Figure 2.10). The ^{13}C spectrum shows the presence of two carbonyl peaks in ratio of 1:2.5 and one TFA carboxyl peak. Isomers **a** and **b** have equivalent carbonyls, and the two carbonyl peaks could be assigned to isomers **a** and **b**. However, we cannot exclude the possibility that the inequivalent carbonyl peaks of isomer **c** overlap with the peaks of other isomers. The assignment of the carbonyl peaks to isomers **a** and **b** must be considered with caution because we observe only one TFA carboxylate peak, where one would expect at least two with the presence of isomers **a** and **b**. Again, this could be due to the overlap of the broad solid-state peaks observed and/or the fact that the carboxyl carbon is one bond removed from direct interaction with the metal thus making their chemical shifts more similar. Significantly, we see no evidence of the formation of bridging carbonyls with this polymer. Thus, it can be concluded that the linear polymer does not have the ability to coordinate ruthenium complexes in close enough proximity to form dinuclear species on the surface.

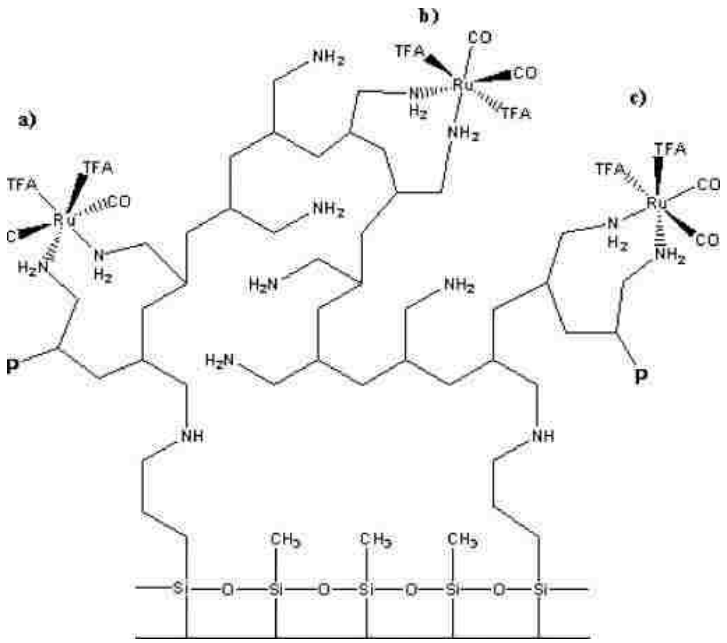

Figure 2.10 Structures of the three cis isomers of **1** with bidentate coordination to the surface of **BP-1**.

Previous work from our laboratories has shown that spinning sideband intensity patterns of ^{13}CO resonances from carbon monoxide metal complexes can be used to gain an understanding of transition metal complex mobility on a surface.[87] Anisotropy calculations were carried out using the Herzfeld Berger Analysis[88] using data obtained at a spin rate of 11.5 kHz. The calculated anisotropy, $\Delta\delta$, measured using the sum of the integration of both terminal carbonyl resonances for **1** complexed to **WP-1** was −366 ppm (δ_{11} = 316, δ_{22} = 316, δ_{33} = −50.0). The calculated anisotropy for the complex of **1** on **BP-1** gave a similar anisotropy of 378 ppm (δ_{11} = 361,δ_{22} = 287, δ_{33} = −53.8). The spectroscopic data for **1** on **BP-1** and **1** on **WP-1** suggest that the **WP-1** branched polymer provides a higher number of amines for coordination (2 for **BP-1** and 4 for **WP-1**). Despite the difference in coordination

number, the anisotropies are similar, indicating that both complexes are relatively rigid on the surface.

2.3. Conclusions

The studies reported here present convincing evidences that the coordination number of amines in the branched polymer **PEI** necessary to drive the oxidation of Co^{2+} to Co^{3+} is four. In the linear polymer, **PAA**, it appears that coordination of two amines is most likely and is insufficient to drive the oxidation of Co^{2+} to Co^{3+}. The studies with the complex **1** demonstrate that this molecule will be a useful probe for studying coordination geometries of surface bound ligands to transition metals. In addition, the branched polymer, **PEI**, appears to be predisposed for higher amine coordination numbers, and a certain small number of the branched sites are in close enough proximity to result in the formation of $M_2\mu CO$ species. The ^{13}C CPMAS NMR data also supports relatively rigid metal coordination sites for both polymers, and that the CO ligands are associated with isolated coordination sites. However, these studies say nothing about the distribution of coordination sites on the surface or on the number of microenvironments associated with metal complexation in amorphous composites of this type.

2.4. Experimental

2.4.1. Materials and methods

All chemicals were purchased from Sigma-Aldrich and used as received. $[(tren)Co(H_2O)_2]^{3+}3Cl^-$ and $[(dien)Co(H_2O)_3]^{3+}3Cl^-$ and **1** were prepared by published literature procedures.[32,83,84,86]

AA spectra were measured on an S series Thermo Electron corporation AA spectrometer. Cobalt concentrations were measured using a wavelength of 240.7 nm. Solutions were run in a 2% nitric acid solution using an air/acetylene method. Solutions were diluted to give approximately 0.1–0.2 absorbance units. AA analysis was used to determine the cobalt remaining bound on the surface of composites by measurement of the difference between the total cobalt in the initial solution and the total cobalt in the filtrate and rinses. Elemental analyses were done by Schwarzkopf Microanalytical Laboratory, Woodside, NY. X-ray photoelectron spectra were run by Zhiyong (Jahson) Suo, Ph.D. Research Scientist, ICAL – Physics Department Montana State University, Bozeman MT 59717.

Solid-state ^{13}C CPMAS NMR were taken on a 500 MHz Varian NMR spectrometer with a system description of MRCA 500/54/ASP. Parameter settings for both ^{13}C and ^{29}Si NMR are given in Figure 2.11. The parameter 'ct' was varied as needed to resolve peaks. Solution state NMR were taken on a 400 MHz Varian Unityplus NMR spectrometer. UV–Vis spectra were taken on an Agilent HP 8453 UV–Vis spectrophotometer in aqueous solutions at 1 cm path length. All samples were diluted to give approximately one absorbance unit. FT-IR spectra were recorded as KBr pellets on a Nicolet Nexus 670 FT-IR. KBr pellets of the composite materials were obtained by thorough grinding and drying of the composite prior to mixing with KBr. KBr pellets of the complex **1** bound with the tren ligand were prepared by evaporation of the complex solvated in CH_2Cl_2 on KBr powder.

Parameter	tn C13	tn Si29		Decouple	tn C13	tn Si29
pulse	tancpx	tancpx		dn	H1	H1
spin	5000 Hz	5000 Hz		dfrq	499.798	499.798
sfrq	125.686	99.29		dof	-3000	-2970.4
tof	0	-6207.8		dpwr	63	63
tpwr	61	61		aH90	4095	4095
sw	50000	25000		pwH90	3.7	2.8
at	0.05	0.05				
np	5000	2500		Decouple2		
d1	2	4				
ct	500-65536	808-65536		dn2	N15	Not Used
ss	0	0		dfrq2	50.649	Not Used
rd	4	4		dof2	0	Not Used
ad	12	4		dpwr2	54	Not Used
aX90	0	2711		aY90	2000	Not Used
pwX90	3.2	2.6		pwY90	4	Not Used

Table 2.11 Parameters used for solid-state NMR experiments.

2.4.2. Cobalt loading and oxidation

The kinetics of cobalt binding to the surface of **WP-1** were measured by adding 500 mL of a 1 g/L solution of $CoCl_2$ at pH 5 (adjusted to pH by addition of dilute HCl) to 5 g of the composite **WP-1**. The mixture was then degassed by applying a vacuum for 10 min to remove air from the pores. Measurements were then taken at regular time intervals by removal of 100 μL of the reaction solution, then dilution for measurement on the AA. The loading in mg of cobalt per g of composite is shown in Figure 2.4.

The dependence of the oxidation of Co^{2+} to Co^{3+} on the presence of oxygen was estimated by two procedures. To estimate the degree of oxidation in the presence of a limited amount of oxygen, a 20 mL solution of 1 g/L $CoCl_2$ at pH 5 was added to 200 mg **WP-1**. This solution was then sealed and allowed to sit overnight. The concentration of the filtrate combined with the washes the next day was measured by AA spectroscopy and showed a

loading of 12.3 mg/g. In order to estimate the degree of oxidation under nearly anaerobic conditions, the previous experiment was repeated, but using a solution that had previously been purged with nitrogen for 10 minutes and additionally purging the reaction flask containing the composite **WP-1** for 10 min with nitrogen. This procedure yielded a final loading of 3.9 mg/g after standing overnight.

The pH dependence of the oxidation of Co^{2+} to Co^{3+} was evaluated by adding 10 mL each of 1 g/L $CoCl_2$ solutions at pH 3–7 to different vials containing 100 mg of the composite **WP-1**. The solutions were allowed to equilibrate overnight, and then were stripped with 1 M H_2SO_4 and their strip concentrations measured by AA to calculate the cobalt remaining on the surface of the composite. The resultant mg/g loading of cobalt at each pH is shown in Figure 2.3.

The occupancy of the inner coordination sphere of the cobalt complex when immobilized on the surface of **WP-1** was determined by preparing six 100 mg samples of **WP-1** with 10 mL of 1 g/L pH 5 $CoCl_2$ solution. The samples were allowed to sit overnight, and were filtered individually, and then half were washed with 2 M H_2SO_4, and half were washed with 2 M HCl. The filtrate concentrations were measured by AA, giving a loading of cobalt on the surface of 18.4 mg/g. The solid samples were then sent out for elemental analyses, and their nitrogen:cobalt:chlorine ratio was investigated. The nitrogen:cobalt molar ratio was found to be 6–7 mol N/mol Co, however, the chlorine:cobalt molar ratio was found to be 0.26:1 and 4.66:1 for the samples washed with H_2SO_4 and HCl, respectively.

2.4.3. Modeling surface cobalt coordination in solution

Trivalent cobalt was generated in a solution of **PEI** by adding 0.2 g of $[Co(NO_2)_6]^{4-}4Na^+$ to a solution of **PEI**. Air was aspirated through the solution and it was assumed that all of the Co^{2+} was oxidized to Co^{3+}, as was the case for the dien and tren complexes. This solution was then converted to the chloride salt by boiling in concentrated HCl until dryness. This material was then redissolved in water and the UV–Vis spectrum was measured (Figure 2.6). In a related experiment, $CoCl_2$ was added to a solution of **PEI**, let stand overnight, and then dialyzed with a cellulose membrane for 3 weeks, changing the solution outside the dialysis membrane daily. A UV–Vis spectra of this sample following dialysis was identical to that shown in Figure 2.6 for the **PEI**–Co complex.

2.4.4. Reaction of tren with $K^+[Ru(CO)_3(TFA)_3]^-$

To a solution containing 6 μL of tren (0.04 mmol) in 0.75 mL of methanol-d_4 was added 23 mg (0.04 mmol) in a 5 mm NMR tube. The solution was allowed to equilibrate overnight and then ^{1}H NMR, ^{13}C NMR, and ^{19}F NMR of the solution were recorded. A portion of this solution was allowed to evaporate on dry KBr which was then converted into a pellet and the IR recorded.

- ^{1}H NMR, (methanol-d_4) 2.79, 2.57 ppm (CH_2); 3.08, 3.39 ppm (NH).
- ^{13}C NMR (methanol-d_4) 39.8, 55.9, 192.5, 193.8, 195.4, 196.1, 198.2, 204.1, and 207.5 ppm.
- ^{19}F NMR (relative to external trifluoracetic acid) −77.35 ppm.
- IR (KBr) (νCO) 1952, 2050 cm^{-1}, νCOOH 1689 cm^{-1}.

2.4.5. Complexation of 1 to the composites, WP-1 and BP-1

To a solution of 15–17 mg of **1** in 10 mL of MeOH was added 200 mg of the composite **WP-1** or **BP-1**. This mixture was allowed to equilibrate overnight, and washed three times with CH_2Cl_2. This was then dried at 60 °C to constant weight. Solid-state ^{13}C CPMAS NMR:

- **WP-1**, -6 (SiMe), 8–50 (aliphatic), 161.9 (carboxylate), 195.1 and 203 (CO) ppm;
- **BP-1,** -6 (SiMe), 33–60 (aliphatic), 160 (carboxylate), 194 and 201.3 (CO), 251.6 (bridging CO) ppm;
- IR (KBr) **WP-1** (ν*C*O)1938, 2044 cm^{-1}; ν*C*OOH 1678 cm^{-1};
- IR (KBr) **BP-1**(ν*C*O)1922, 1963, 2041 cm^{-1}; ν*C*OOH 1653, 1738 cm^{-1}.

2.4.6. Anisotropy calculations

Anisotropy calculations were done using the program HBA – Graphical Herzfeld-Berger Analysis, Copyright ©1995, 2005 K. Eichele, version 1.5.8. The measurements were made based upon the relative integration values of the spinning sidebands from the peak being measured in solid-state^{13}C CPMAS NMR, taking into account field strength and spinning speed. The measured anisotropies for **1** on **BP-1** and **WP-1** are 378 and 366, respectively, as measured at 11.5 kHz spinning and 2 ms contact time. The ^{13}C principal tensor components are reported according to the standard convention[88] where $\delta_{11} \geqslant \delta_{22} \geqslant \delta_{33}$ and the shielding anisotropy is defined as $\Delta\sigma = \sigma_{33} - (\sigma_{11} + \sigma_{22})/2$ with $\sigma_{11} \leqslant \sigma_{22} \leqslant \sigma_{33}$ and $\delta_{ii} = -\sigma_{ii}$.

CHAPTER 3: SPC SURFACE STABILITY[‡]

3.1. Introduction

Amorphous silica gels have been a favored solid state matrix for applications in chromatography, catalysis, colloid chemistry and as drying agents since the middle of the 20th century.[4-7] Recent developments in sol–gel chemistry have further expanded the scope and type of solid silica phases that can be made.[68,89] The surface modification of silica gels with organic ligands via silanization of surface hydroxyl groups has been an area of intense activity.[9-13] We have been making a systematic study of the characteristics and applications of the related silica polyamine composites (**SPC**s), which provide nanoporous hybrid organic–inorganic materials that have found applications in metal ion separations and in the remediation of toxic anionic and cationic pollutants.[15,16,18-24,29,31] These studies have focused on the impact of using a mixture of propyl and methyl silanes,[15,16] the thermal stability of the materials,[29] and the impact of polymer and ligand structure on metal ion selectivity.[16,18,20,31] Despite all of the useful information that was revealed regarding the surface features of these commercialized and industrially relevant composites, several important questions remain to be answered. For instance, it is well known that amorphous silica gels are attacked by base at elevated pH but it is not known how the silica leaching is impacted by the nature of silane anchors, the subsequent reaction of the silanized silica surface with the polyamine, and modification of the polymer with metal selective ligands (Figure 3.1). The impact of polymer

[‡]This chapter was published as reference #32.

binding on the distribution of the surface siloxane species is not well understood either. We report here an attempt to address these questions by a systematic study of surface silica leaching as a function of pH, silane anchor and polymer–surface interactions. Multinuclear, solid state NMR studies are used to elucidate the general surface features and the nature of the changes associated with surface functionalization. Finally, in order to further develop the **SPC** technology and to see how the synthetic method used to make the silanized gel impacts surface leaching, we have also examined leaching and surface structures of composites made via sol–gel chemistry. To our knowledge, this represents the first direct comparison of a composite material made by these two different routes.

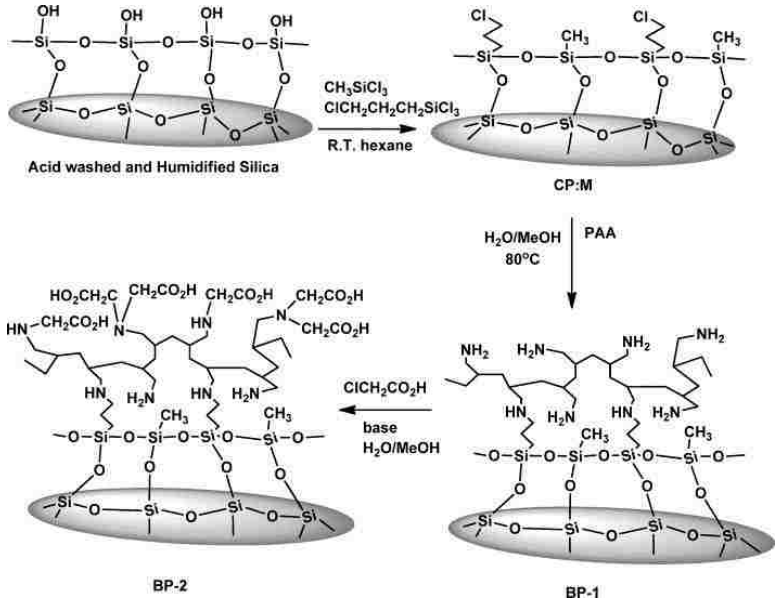

Figure 3.1. Schematic drawing of the stepwise synthesis of the poly(allylamine) composite **BP-1**.

3.2. Results and discussion

3.2.1. Relative silicate leaching rates for silanized silica surfaces versus silica gel

It is well known that amorphous silica gels are subjected to degradation by aqueous alkaline solutions.[4-7] This property represents a serious obstacle to the use of silica gels as ion exchange materials at elevated pH. In the case of the **SPC** materials under consideration here and related organic–inorganic hybrid materials, it is not understood how the relative rate of silicate leaching is influenced by silanization, polymer grafting and the subsequent ligand modifications that we have previously reported.[14-16,18-24,29,31] Hydrophobicity parameters based on measured surface tensions have been assigned to various silanes but these parameters have not been directly related to base induced leaching rates on amorphous silica gels.[4-7] We have previously reported that only 45–55% of the surface of **SPC**s are covered by the silane anchors used in their synthesis, suggesting that silicate leaching could still be a significant problem under alkaline conditions.[15,16] We therefore undertook a systematic study of silica leaching as a function of the nature of the silane anchors and the impact that the polyamine grafting and its subsequent modification has on the rate of this process. We previously reported that the use of a mixture of halogenated silane anchor with methyl trichlorosilane gave **SPC** materials with better capacities and mass transfer kinetics. Because of this, we have examined leaching rates for these mixed silane composites.[15]

All leaching experiments were conducted under identical batch conditions. We began these studies by first doing a leaching pH profile in order to bracket the rate of silicate dissolution from the composite and silica gels (see Section 3.4.4). The leaching data in the

pH range of 2–14 are shown in Figure 3.2 for the commercial silica gel, the chloropropyl silanized gel (CP gel) and the methyl:chloropropyl 7.5:1 mixed silane (M:CP 7.5:1). At pH = 14, 43%, 33% and 33% of the silica has been leached into the solution for the unmodified silica, CP gel and M:CP respectively. These results illustrate that the organic silanes offer minimal protection to the surface at this pH. At pH = 10 and below however, there is a significant difference in the leaching between the silanized materials and the starting silica gel with the M:CP material showing about the same degree of leaching as the CP (Figure 3.2). Thus, although silanization does not give complete surface coverage it does afford some protection from alkaline solutions.

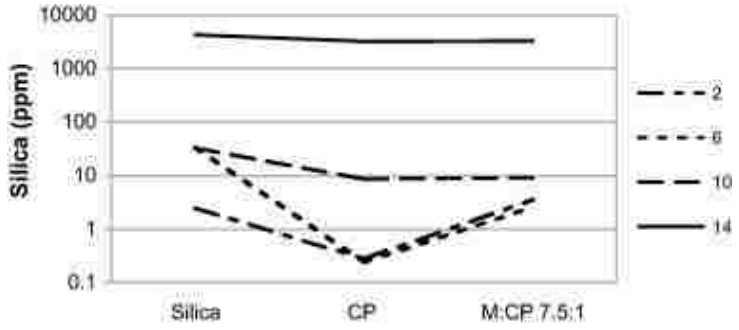

Figure 3.2. Silica leaching data for the commercial/conventional silica gel, the chloropropyl silanized gel (CP gel) and the methyl:chloropropyl 7.5:1 mixed silane (M:CP) in pH range of 2–14. Vertical axis is a logarithmic scale.

3.2.2. Synthesis of silanized silica surfaces made with different silanes and conversion to the corresponding composites

Based on these results we decided to examine the impact of varying the nature of the silane on the degree of silica leaching. We chose a pH = 10 for these studies because this was the lowest pH where significant leaching is observed and where significant protection of the

surface by the silane was realized. The silane anchors chosen for this study and the mixed silane combinations used are shown in Figure 3.11 in the experimental section. The silanized silica gels and the corresponding **PAA** composites were synthesized by the methods previously reported.[15,16] The ratio of the methyl or phenyl to the 4-(chloromethyl)phenylsilane of 7.5:1 was chosen because previous studies with methyltrichlorosilane and 3-chloropropyltrichlorosilane showed that this ratio was optimal for metal loading capacities. Characterization of the silanized gels and the corresponding composites was done by solid state CPMAS ^{13}C NMR (Table 3.1), elemental analysis and by measuring the copper capacities for the composites (Table 3.2). The copper capacities for all the 4-(chloromethyl)phenylsilane derivatives are slightly greater than the capacities of the chloropropyl analogs after conversion to the silica polyamine composite, **BP-1** (90–105 mg/g for **BP-1**, made with methyl/chloropropylsilane mixtures).[15,16] The chlorine analysis gives a measure of the silane loading and it can be seen that the 4-(chloromethyl)phenylsilane (**CMPh**) has a chlorine content similar to the corresponding composite made with only chloropropyl silane.[15,16] The somewhat higher copper capacities reflect the higher polymer loading and this can be attributed to the greater reactivity of the benzylic halide relative to the alkyl halide. The mixed silane silica gels phenyl:4-(chloromethyl)phenyl 7.5:1 (**Ph:CMPh**) and methyl/4-(chloromethyl)phenyl 7.5:1 (**M:CMPh**) both show much lower chlorine content because the phenyl and methyl silanes effectively compete with the 4-(chloromethyl)phenylsilane for binding to the surface (Table 3.2). However, polymer loading is relatively unaffected based on the observed copper capacities which are only slightly lower than for the **CMPh** only silica gel. Analysis of the residual chlorine content after polymer loading allows an estimate of the average number of anchor points per polymer molecule

after correcting for the mass gains. The much smaller number of anchor points for the mixed silane has only a minimal effect on polymer loading as the copper capacities remain fairly high relative to **CMPh** only. We observed a similar constancy in copper capacities in our prior studies using polymers of very different molecular weights and silica gels with different surface areas.[22] Thus polymer loading seems to be related to available surface area on the silica rather than to the number of covalent anchor points or the overall size of the polymer.

Material	Ph	PAA CH_2, CH	Si–Me	CH_2 (silane)	Carboxyl
CMPh	125, 128, 132, 138			41.7	
PhCMPh	125, 128, 132, 137[b]			41.3[b]	
MCMPh	128, 135, 141		−6.0	45.0[b]	
CMPhBP-1[c]	129, 133, 141	34.9		44.1	
PhCMPhBP-1[c]	125, 131	31.7		[d]	
MCMPhBP-1[c]	140, 131, 124	33.6	−6.0	42.6	
CMPhBP-2	129	25.6		46.0	165
PhCMPhBP-2	126, 132	28.3		[b]	168
MCMPhBP-2	125, 136	33.7	−6.0	[b]	171

Table 3.1. ^{13}C Chemical shifts for silanized gels and composites.[a]

[a] All chemical shifts are given relative to external TMS and were run in the CPMAS mode.

[b] Peaks of lower intensity than the other peaks due to reactant ratios.

[c] All the **BP-1** spectra showed a relatively low intensity peak at 162 ppm. We tentatively assign this resonance to a formamide carbonyl formed by the reaction of the primary amines with carbon dioxide.

[d] Resonances hidden by polymer carbon resonances.

Material	%C	%H	%N	%Cl	#Anchors[a]	Cu Cap[b]
CMPh	9.99	0.93		4.94		-
PhCMPh	9.20	0.93		0.36		-
MCMPh	2.67	0.75		0.29		-
CMPhBP-1	19.25	3.1	4.18	0.02	101	128
PhCMPhBP-1	16.55	2.44	3.32	0.04	9	106
MCMPhBP-1	11.58	2.19	3.30	0.03	7	98
CMPhBP-2	20.93	2.88	3.42			17
PhCMPhBP-2	17.83	2.77	2.93			18
MCMPhBP-2	13.07	2.40	2.76			20

Table 3.2. Elemental analyses, anchor points and Cu^{2+} capacities for silanized gels and composites made with aromatic silanes and aromatic/methyl mixed silanes.

[a] Number of anchor points per molecule of polymer calculated from the difference in Cl content before and after polymer grafting, %N and MW of polymer.

[b]Batch capacity at pH = 2 for **BP-2** and 3.5–4 for **BP-1** in mg/g as measured by AA.

In order to understand the impact of modifying the basic amine polymer with an acidic substituent on silica leaching we converted the **BP-1** composites made with the **CMPh** anchor to **BP-2** by reaction with sodium chloroacetate according to the literature procedure used for the chloropropylsilane analog.[19] The ^{13}C NMR data and elemental analyses for these **BP-2** composites are given in Table 3.1 and Table 3.2, respectively. This composite was designed to capture metal ions at lower pH than **BP-1** and the copper capacities are measured

at pH = 2 while those for **BP-1** are measured at intrinsic copper solution pH (3.5–4.0). The copper capacities for **CMPh-BP-2** composites are much lower than for their **BP-1** precursors. This is also the case for the **BP-1** chloropropylsilane analogs where copper capacities decrease to 30–35 mg/g from 90 to 105 mg/g on conversion to **BP-2**.[19] The decrease in copper capacity for the 4-(chloromethyl)phenylsilane analogs is even more drastic decreasing from 98–106 mg/g to 17–20 mg/g on going from **BP-1** to **BP-2**. This could be because the more rigid aromatic anchors prevent some metal chelating active sites from participating in metal binding. The overall decrease in copper capacity on modification with the chloroacetate ligand suggests that the equilibrium binding constant for the acetate modified surface at pH = 2 is significantly lower for the amino acetate ligand than that for the amine ligand at pH = 3–4. We have previously shown that almost all of the amine groups in **BP-1** are modified with 1–2 acetate groups.[19] Polymer leaching is not considered significant for the mixed silane composites with fewer anchor points reported here as this has been previously demonstrated in our prior work with methyl/chloropropyl mixed silanes.[15,16]

3.2.3. Silica leaching from the silanized silica surfaces

The results of the silica leaching studies on silica gels silanized with different silanes: chloropropyl (**CP**), methyl mixed with chloropropyl in a 7.5:1 ratio (**M:CP**), methyl mixed with 4-(chloromethyl)phenyl in a 7.5:1 ratio (**M:CMPh**), phenyl mixed with 4-(chloromethyl)phenyl in 7.5:1 ratio (**Ph:CMPh**) and 4-(chloromethyl)phenyl only (**CMPh**) are illustrated in Figure 3.3. The use of the 4-(chloromethyl)phenyl silane on its own or mixed with the methyl silane gives silica leaching values similar to the chloropropyl and mixed methyl-chloropropyl silane. However, if the 4-(chloromethyl)phenyl is mixed with the

phenyl silane, leaching is significantly lowered. This suggests that the use of a bulky and non-polar silane is necessary to reduce surface leaching of silica. Although the 4-(chloromethyl)phenyl is bulkier and more hydrophobic than the **CP** or **M:CP**, the presence of the polar benzylic chloride which probably undergoes hydrolysis on extended exposure to alkaline solutions, presents a more polar surface to the aqueous phase and gives higher leaching rates.

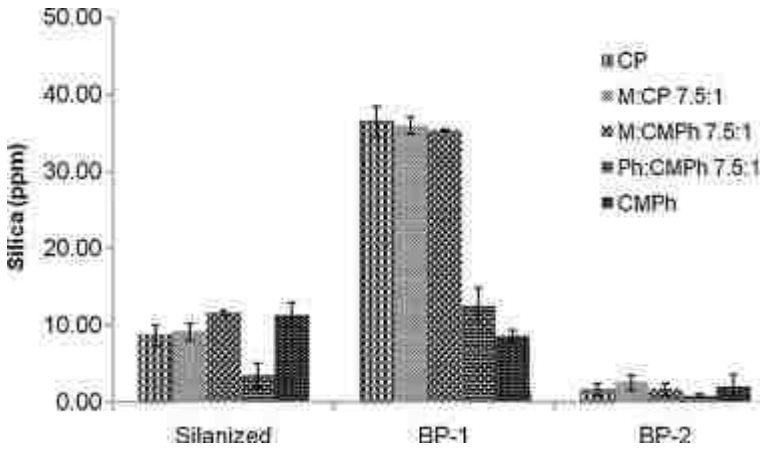

Figure 3.3. Silica leaching from silanized silica gels using different silanes: chloropropyl (**CP**), methyl mixed with chloropropyl in a 7.5:1 ratio (**M:CP**), methyl mixed with 4-(chloromethyl)phenyl in a 7.5:1 ratio (**M:CMPh**), phenyl mixed with chloromethyl phenyl in 7.5:1 ratio (**Ph:CMPh**) and 4-(chloromethyl)phenyl (**CMPh**).

3.2.4. Silica leaching from silica polyamine composites made with different silane anchors

Interestingly, the conversion of these silanized silica gels to the corresponding silica–polyamine composites, **BP-1**, results in a dramatic increase in the silica leaching for the less bulky and less rigid **CP** and **M:CP** as well as the **M:CMPh** but not for the **Ph:CMPh** and

CMPh only. We interpret this phenomenon in terms of an amine assisted hydrolysis of surface siloxane bonds (Figure 3.4a). In the case of **Ph:MCPh** and **CMPh** these more rigid and longer polymer anchors prevent the amine polymer from directly interacting with the surface. In the case of **M:CMPh** dilution of the aromatic anchor with methyl silane leaves enough flexibility in the polymer to interact with the surface. Modification of all of these poly(allylamine) composites with sodium chloroacetate to give the corresponding aminoacetate composites, **BP-2**, almost completely eliminates silica leaching at pH = 10 (Figure 3.3). Our prior work with this modification indicated that almost all of the amine sites are modified with at least one if not two acetate groups.[19] At pH = 10 the aminoacetate groups would be negatively charged inhibiting the diffusion of the negatively charged hydroxide ions to the silica surface. Furthermore, substitution of the amines on the polymer would be expected to impart an additional degree of conformational rigidity thus limiting access of any unmodified basic amine groups to the surface (Figure 3.4b).

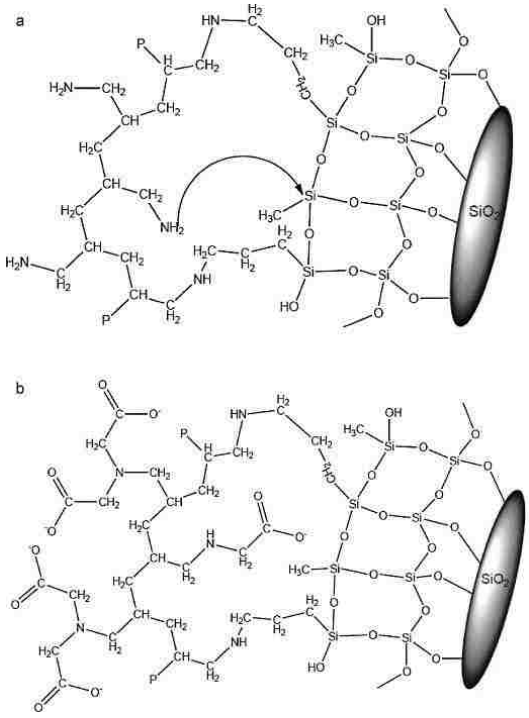

Figure 3.4. (a) schematic diagram of the mechanism of amine promoted silicate leaching in **BP-1**; (b) schematic diagram of the quenching of silicate leaching in **BP-2**.

3.2.5. Synthesis, characterization and silica leaching of SPC made by the sol–gel method

As part of the general development of the **SPC** technology we have been looking into alternatives to the commercially available amorphous silica gels. This goal prompted us to synthesize the **SPC** composite **BP-1** by the sol–gel method. These studies were undertaken not only to evaluate their resistance to silica leaching for comparison with the **SPC** materials previously reported but also to see if these alternatives offered other advantages with regard to the commercial development of the **SPC** technology. In the case of the sol–gel method a more uniform surface, more careful control over pore size distribution and the possibility of development of a one pot **SPC** synthesis were the primary goals. The sol–gel matrix was

synthesized by a two-step hydrolysis-polymerization process using trimethoxy(chloropropyl)silane and trimethoxy(methyl)silane in a 7.5:1 ratio according to previously published procedures.[72] This ratio was chosen as it proved to have the best metal adsorption properties for the **SPC**s made from the commercial silica gel.[15,16] The sol–gel made by this method was ground and sieved to the particle size distribution, 150–250 μm, commonly used for the **SPC**s and then converted to the **BP-1** by a procedure given in the experimental section, which is similar to the previously reported method.[15,16] Mercury porosimetry analysis revealed a surface area of 163 m^2/g and an average pore diameter of 13.2 nm. This material appeared to have good mechanical strength but without the addition of a tetraalkoxysilane to the sol–gel formulation there will not be a bulk silica phase within the sol–gel. The bulk siloxane adds mechanical stability and creates the surface and pore structure of the **SPC**. Therefore the above procedure was repeated using both tetramethoxysilane (**TMOS**) and tetraethoxysilane (**TEOS**). The ratio of the alkoxysilanes used was 7.5:1:4.25 for **CP:M:TMOS** or **TEOS**. This ratio provides two tetraalkoxysilanes for each trialkoxy(organo)silane. These **TMOS** and **TEOS** derivatives were converted to the corresponding **BP-1** composites by reaction with **PAA** and mercury porosimetry analysis revealed a surface area of 50 m^2/g and of 48 m^2/g and an average pore diameter of 6.7 nm and 7.4 nm for the **TMOS** and **TEOS**, respectively. The corresponding values for the **BP-1** made from the commercial silica gels are 165 m^2/g and have an average pore diameter of 9.1 nm. It should be pointed out here that binding of the polymer to the silica matrices lowers both pore size and surface area.[90]

As expected, elemental analyses for the composites reveal that the addition of the tetraalkoxysilanes lowers the carbon content of the resulting sol–gels due to the formation of

bulk silica regions (going from 20.3% in the original sol–gel to 8.30 and 11.02% in the **TMOS** and **TEOS** gels, respectively) while the percentage of chlorine is in a much narrower range for all three materials (3.66–2.59%) and suggests a similar rate of incorporation of the chloropropyl silane. On conversion to **BP-1** only 32 and 22% of the chlorines are utilized in reaction with the polyamine in the case of **TMOS** and **TEOS** respectively. The better utilization of the chlorines in the case of **TMOS** is probably due to less steric interference with the chloropropyl groups by the methyl group compared with the ethyl group in TEOS. This makes **TMOS** a better choice for future work. Chlorine analyses of these sol–gels before and after reaction with **PAA** allows estimates of the number of anchor points per polymer chain by making use of the nitrogen analysis and the average molecular weight of the polymer. The **BP-1** made without **TMOS** or **TEOS** showed very little change in chlorine content and gave a value of ~0.2 anchors per polymer molecule. This means that the polymer molecules have very few or no anchor points but the chlorine data is not precise enough to discern which is the case. This, in turn, indicates that the chloropropyl groups are not accessible to the polymer on the pore surfaces. This situation changes entirely when the poly(allylamine) is reacted with the gels made with **TMOS** or **TEOS**. Here the change in chlorine content is more substantial and we calculate 19 and 27 anchors per polymer molecule for the **BP-1** composites made with **TEOS** and **TMOS** respectively, even though there remain many unreacted chloride sites. These values compare more favorably with the value of 24, obtained for **BP-1** made with the commercially available silica gels, although here there are fewer chlorine sites and so almost all react with the **PAA**. The **TMOS** and **TEOS** containing poly(allylamine) composites have lower copper capacities than the commercially produced **BP-1**. The initial sol–gel **BP-1** gave a copper capacity of 87.1 mg/g,

the **TMOS** sol–gel **BP-1** had a copper capacity of 68.7 mg/g and the **TEOS** sol–gel **BP-1** had a copper capacity of 56.8 mg/g.

The silica leaching data for the composites synthesized from the sol–gels are shown in Figure 3.5. All of these materials show leaching values comparable to values seen for the **BP-1** composites made from the commercial silica gel and higher than the silanized commercial silica gels. In the case of the sol gels we attribute this to the presence of unpolymerized methoxysilyl and silanol groups most likely situated on pore peripheries. Conversion of the sol–gels to the corresponding polyamine composites however, does not lead to increased leaching as observed for the composites made from the silanized commercial silica gels. We suggest here that this result is because there are not any bare silica areas or unpolymerized surfaces within the pores where the polymer resides. This conclusion is borne out by the fact that when the silanized commercial silica gels are reacted with trimethyl chlorosilane we observe ~75% decrease in leaching presumably due to the reaction of unreacted silanol sites after silanization. These interpretations are supported by the solid state NMR data discussed below.

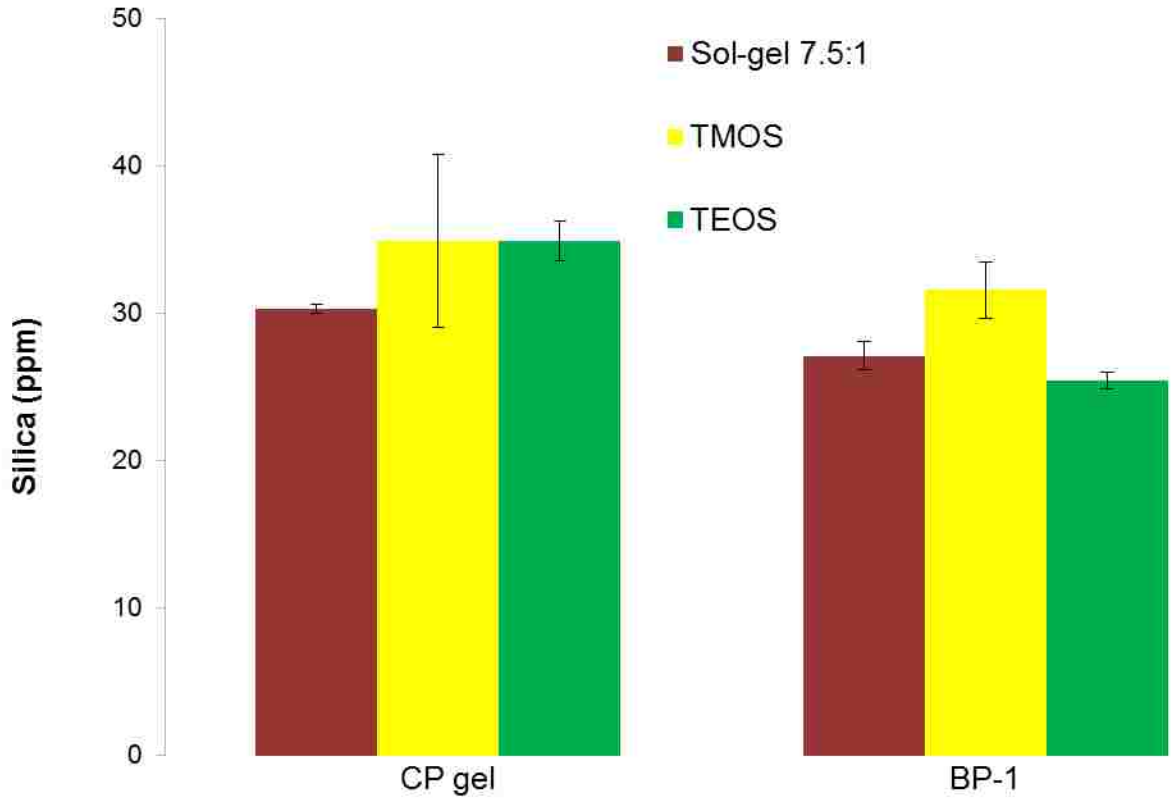

Figure 3.5. Silica leaching from sol–gel materials and the corresponding **PAA** composites at pH = 10.

3.2.6. Solid state CPMAS ^{13}C and ^{29}Si investigations of the polymer surface interface

Solid state CPMAS ^{13}C and ^{29}Si investigations of silica based hybrid organic–inorganic materials have proven to be valuable tools for characterizing the surface compositions of these materials.[91-95] The CPMAS ^{29}Si NMR of the materials synthesized for this report are shown in Figure 3.6 and the assignments are based on the well-established chemical shifts for similar silica gel and sol–gel materials.[91-95] Although we cannot interpret these data

quantitatively, the expected similarities in the extent of cross polarizations for these materials allows some important qualitative conclusions. Figure 3.6a shows the surface siloxane species of the commercial silica gels. Figure 3.6b shows the CPMAS ^{29}Si NMR of the silanized silica gels made from commercial silica as well as the sol–gel made with **TMOS**. There are some notable differences. As expected, the sol–gel where the Q sites can be controlled by the amount of added **TMOS** has a^{29}Si NMR with more T_3 sites than T_2 sites but here the Q_3 and Q_4 sites are of equal intensity whereas in the amorphous silica gels there are more Q_3 sites than Q_4 sites. Figure 3.6c shows the ^{29}Si NMR of the same two materials (as in Figure 3.6b) after reaction with **PAA**. Here the sol–gel and the silica gel made from commercial silica gel both show a significant decrease in the number of T_2 relative to the T_3 sites. This is consistent with the idea that the amine polymer interacts with the surface and perhaps promotes formation of siloxane bonds from residual silanols in addition to increasing leaching.

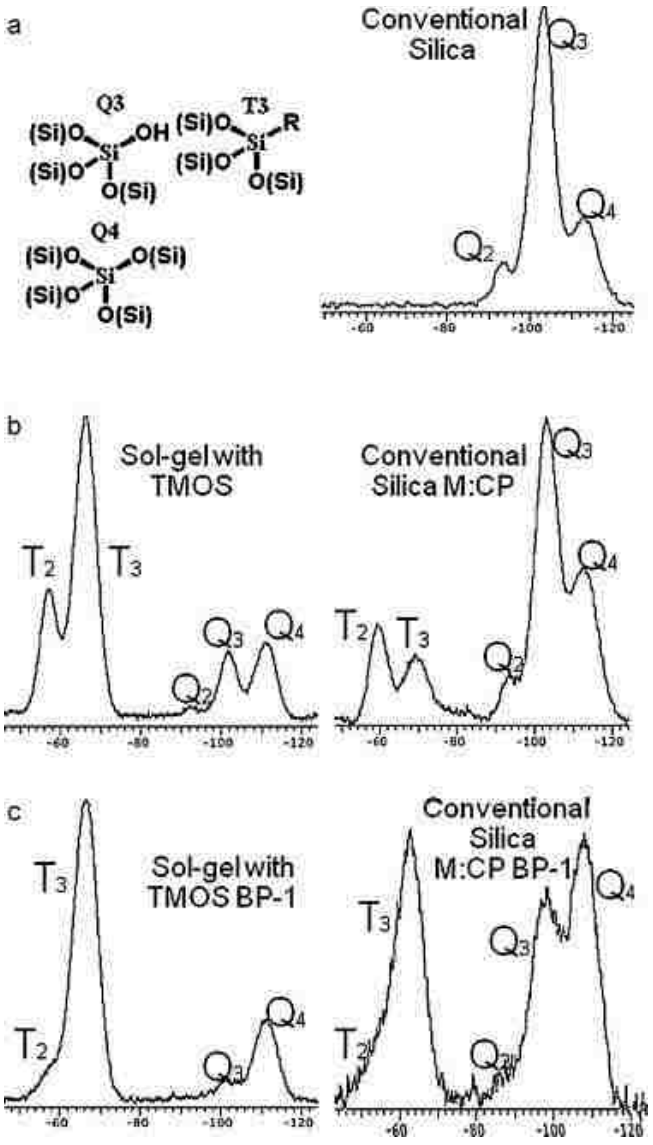

Figure 3.6. Solid state CPMAS ^{29}Si NMR of: (a) commercial silica gel; (b) silanized silica gels made from commercial silica gel and a sol–gel matrix made with the addition of **TMOS**; (c) silica polyamine composites (**BP-1**) made from silanized silica gel and from the sol–gel with added **TMOS**.

Further corroboration of the interpretations presented here comes from an experiment in which a silanized silica gel made with only chloropropyltrichlorosilane (**CPTCS**) was reacted with trimethylchlorosilane (**TMCS**). The **CPTCS** gels have been shown to have less

surface coverage relative to the mixed silane silanized gels.[15,16] This suggests that the poorer surface coverage leaves more unreacted surface hydroxyl groups. The ^{29}Si NMR of a **CPTCS** gel before and after reaction with **TMCS** is shown in Figure 3.7. The overall increase in T sites relative to Q sites is the result of the silanization of unreacted surface hydroxyl groups and the reaction of silanols on surface alkyl silanes with the **TMCS**. The trimethyl silyl group would give a T_3 chemical shift where R = $SiMe_3$ and similarly for the T_2. The small amount of T_1 observed could arise from the reaction of a surface –O–$Si(OH)_3$ site. This experiment verifies our earlier reports where the **SPC** properties implied a poorer surface coverage for gels made with only **CPTCS**.[15] Indeed, leaching of the 7.5:1 **MTCS:CPTCS** gel decreased by 53% after treatment with **TMCS**.

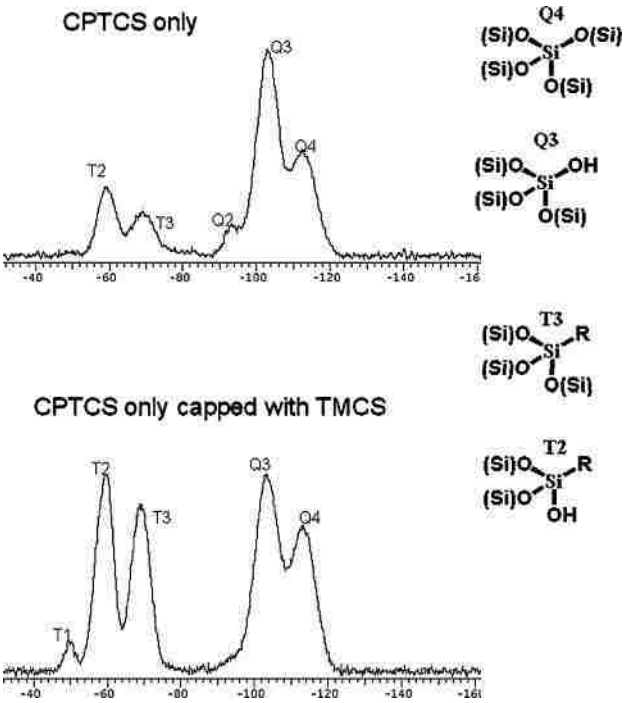

Figure 3.7. Solid state CPMAS ^{29}Si NMR of a silanized silica gel made with only **CPTCS** before (top) and after reaction with **TMCS** (bottom).

The choice to use **TMOS** as the preferred tetraalkoxysilane for synthesis of the polyamine composites is additionally based on the analysis of the CPMAS ^{13}C NMR of the sol–gels made with this compound versus **TEOS** (Figure 3.8). It can be seen that there are resonances that can be assigned to unreacted ethoxy groups in the case of **TEOS** while for **TMOS** no residual methoxide is observed (the methoxide resonance would be expected to appear at ~55 ppm, Figure 3.7(top).[22] In addition, on conversion of the **TEOS** sol–gel to the polyamine composite the resonances associated with the ethoxy groups are significantly diminished (Figure 3.8(bottom)). This observation gives strong support for our hypothesis that the **PAA** interacts directly with the surface and is responsible for the increased leaching observed for the composites relative to the silanized silica gels. Finally, it should be noted

that the C_3 carbon of the propyl group has two different chemical shifts. This is only observed when mixed methyl- and chloropropylsilanes are used in the silanization process and is also observed in the CPMAS ^{13}C NMR for the composites made with commercial silica gels. We tentatively interpret this in terms of the existence of two gross environments on the gel surface. One chemical shift arises from C_3 carbons that are surrounded by methyl groups and one where some of the near neighbors are other propyl groups. This idea is supported by the observation of this splitting in the case of silanized silica gels made with methyl and propylsilanes but not with gels silanized with only propyl or chloropropyl silanes. It seems reasonable that the carbon most remote from the surface would most feel the presence of a neighboring propyl group.

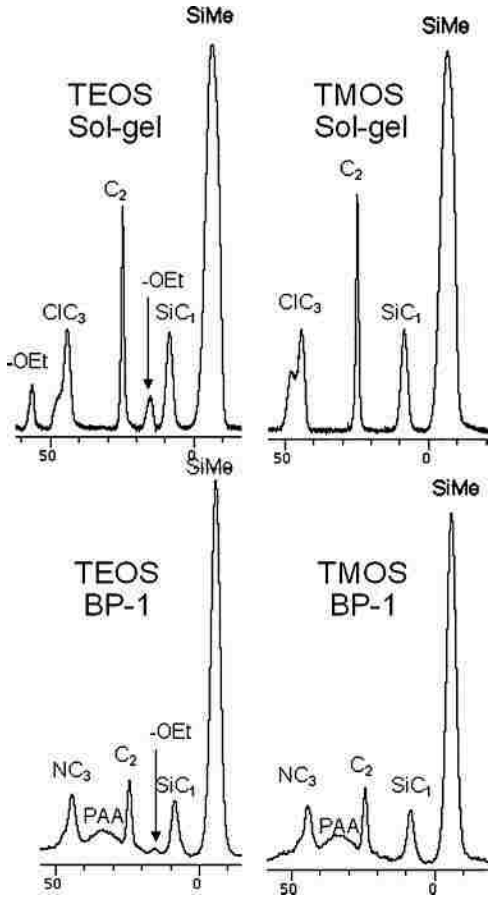

Figure 3.8. Solid state CPMAS ^{13}C NMR of the sol–gels made with **TMOS** and **TEOS** (top) and the resulting composites after reaction with **PAA** (bottom). The resonances labeled SiC_1, C_2, ClC_3, and NC_3 are due to the propyl groups of the silane anchor.

3.2.7. SEM and pore size distributions of BP-1 made by the two different methods

Scanning electron microscopy (SEM) imaging was performed on the **SPC** organic–inorganic hybrid material **BP-1** made on the two different matrices: (a) commercial amorphous silica gel purchased from Qing Dao Mei Gow; (b) a sol–gel xerogel made with **TMOS**, **MTMOS** and **CPTMOS**. In Figure 3.9 the surface morphologies of the three **SPC** materials are illustrated at the same scale and magnification. The sol–gel **BP-1** has a

distinctly smoother appearance than the other two materials and suggests a smaller average pore size (*vide supra*) and/or a tighter pore size distribution. Figure 3.10 shows the pore size distribution curves for the two materials measured on a mercury porosimeter up to 30,000 psi. In the region between 5 and 10 nm (region with highest pore populations) it can be seen that the sol–gel **SPC** has a much sharper pore size distribution than the amorphous silica gel. Although the formulation of the sol–gel **SPC** is still under development, these preliminary results hold out the promise that the sol–gel method for making these **SPC** could provide a more uniform material with better flow properties.

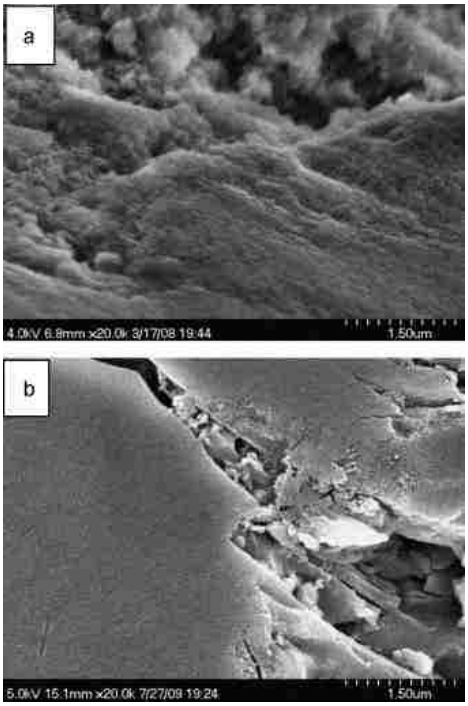

Figure 3.9 Scanning electron micrographs at 20,000 magnification of **BP-1** made from: (a) commercial silica gel; (b) a sol–gel with 4.25:7.5:1 **TMOS:MTMOS:CPTMOS**.

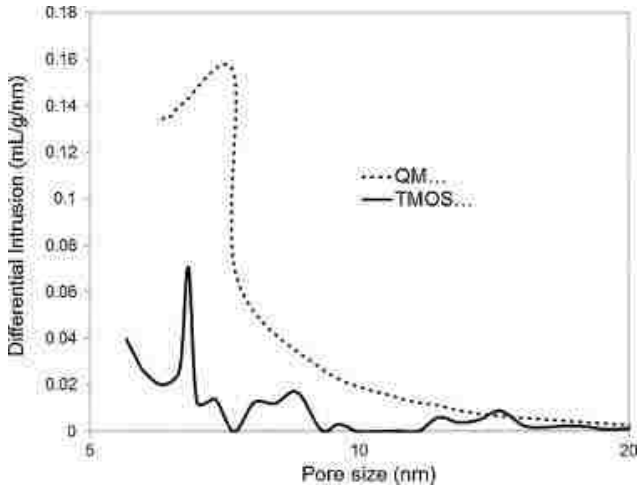

Figure 3.10. Mercury porosimetry data for **BP-1** made from commercial silica gel; and a sol–gel with 4.25:7.5:1 **TMOS:MTMOS:CPTMOS**.

3.3. Conclusions

There are a number of important conclusions that can made from the work reported here:

1. Silicate leaching is a significant process for the silanized surfaces at pH > 10 and the use of bulkier hydrophobic silanes is only marginally effective in mitigating the rate of leaching.

2. On conversion to the **SPC**, silicate leaching increases significantly as a result of base promoted hydrolysis by the polyamine directly interacting with the surface but this effect is almost completely mitigated by modification of the amine functionality with a chloroacetate moiety suggesting that surface pH and zeta potential have profound effects on the leaching process.

3. Sol–gel chemistry offers an alternative to commercial silica gels as a matrix for synthesizing the **SPC**. Although silicate leaching from the sol–gel is greater than that of the silanized silica gels, introduction of the polyamine does not result in an increase in leaching, thus the sol-gel polyamine composites show similar leaching properties to those derived from conventional **SPC**'s. The spectroscopic studies reported here indicate that this is due to the more complete coverage of the sol–gel surface by T_3 sites. In order to use this approach, the incorporation of tetraalkoxysilanes is needed or the halide functionalized alkyl group is not accessible to surface reactions.

4. The number of anchor points to the polyamine has little effect on overall polymer loading as evidence by the comparable capacities of the **CMPh BP-1** versus the mixed silane analogs but we have previously shown that reducing the number of anchor points does impact polymer modification with metal selective ligands.[15]

Further studies to optimize the ratios of the mixed silanes and the tetraalkoxysilanes using the sol–gel approach are underway, as well as the application of surface analytical techniques (AFM, TEM) to deepen our understanding of molecular interactions at the polymer–surface interface.

3.4. Experimental

3.4.1. Materials and methods

All chemicals were purchased from Sigma–Aldrich and used as received. The silanized silica gels, the poly(allylamine) composite (**BP-1**), and the chloroacetic acid modified **BP-1** (**BP-2**) were prepared according to the published literature procedures.[14-16] Raw silica gel

(10 nm average pore diameter, 150–250 μm particle size, 450 m^2/g surface area) was obtained from INEOS, UK or from Qing Dao Mei Gow, Qing Dao, China. Poly(allylamine) **PAA**-15B (15,000 MW) was obtained from Summit Chemicals Inc., NJ, USA as a 15% by weight aqueous solution. Alkoxysilanes for the sol–gel preparations were purchased from Gelest Inc. Alkylchlorosilanes were purchased from Aldrich Chemicals.

Atomic absorption (AA) analyses were done on an S series Thermo Electron corporation AA spectrometer. Metal ion solutions were run in a 2% nitric acid solution and were diluted to give approximately 0.1–0.2 absorbance units. AA analysis was used to determine the metal ion remaining bound on the surface of composites by measurement of the difference between the total in the initial solution and the total metal ion in the filtrate and rinses. Solution silica concentrations were measured on a PerkinElmer Inductively Coupled Plasma Atomic Emission Spectrophotometer (ICPAES) on the acidified leach solutions (5%HCl/5%HNO_3). Standards were run every 10–15 samples, and the initial leach solutions were examined to make sure they contained no silica. Mercury porosimetry measurements were performed on a 9500 Micromeritics Autopore Series Mercury Porosimeter operating at a maximum pressure 36,000 psi corresponding to a minimum intrusion diameter of 5 nm. Elemental analyses were done by Galbraith Analytical Labs, Lexington, KY.

Stock solutions of Cu^{2+} were prepared using $Cu(SO_4)\cdot 10H_2O$. Solution pH was adjusted from the intrinsic pH, where necessary, using hydrochloric acid or sodium hydroxide. Stripping and recovery of copper was achieved with $2M-H_2SO_4$. Metal standards for AA/ICP analyses were obtained from Fisher Scientific Co.

Solid state ^{13}C and ^{29}Si CPMAS NMR were done on a 500 MHz Varian NMR spectrometer using a 4 mm rotor with parameters describes in Figure 2.2. FT-IR spectra were recorded as KBr pellets on a Nicolet Nexus 670 FT-IR.

3.4.2. Synthesis of xerogels by the sol–gel method

Sol–gel syntheses used the two step process modeled after the work of Brennan and Dong.[72] To a 50 mL polyethylene beaker was added 6 mL of MeOH and 3.7 mL of pH = 2 HCl solution. To this mixture was added 20 mL of premixed methyl(trimethoxy)silane (**MTMOS**) and 3-chloropropyl(trimethoxy)silane (**CPTMOS**) in a 7.5:1 molar ratio (17.1 mL **MTMOS** and 2.9 mL **CPTMOS**).

For the synthesis of sol–gels containing tetramethoxysilane (**TMOS**), which was added for the formation of quaternary silica structures, a similar procedure was used.To a 50 mL polyethylene beaker was added 6 mL of MeOH and 3.7 mL of pH = 2 HCl solution. To this mixture was added 20 mL of premixed **MTMOS**, **CPTMOS**, and **TMOS** in a 7.5:1:4.25 molar ratio (11.4 mL **MTMOS**, 1.9 mL **CPTMOS**, and 6.7 mL **TMOS**).

For the synthesis of sol–gels containing tetraethoxysilane (**TEOS**), the same procedure was used. To a 50 mL plastic beaker was added 6 mL of MeOH and 3.7 mL of pH = 2 HCl solution. To this mixture was added 20 mL of premixed **MTMOS**, **CPTMOS**, and **TEOS** in a 7.5:1:4.25 molar ratio (9.8 mL **MTMOS**, 1.7 mL **CPTMOS**, and 8.6 mL **TEOS**).

After 1 h of magnetic stirring, 3.7 mL of 7 M ammonium hydroxide was added to each sol–gel reaction. Upon gelation of the materials, stirring is stopped, and they are allowed to age overnight at room temperature. This is followed by aging at 40 °C for 24 h followed by

aging at 100 °C for 24 h. The materials are then crushed with a mortar and pestle followed by sieving to a particle size of 150–250 μm.

3.4.3. Conversion of the sol–gel xerogels to the polyamine composite BP-1

The reaction of the resulting sol–gels with poly(allylamine) (**PAA**) was done by placing 2.0 g of sol–gel in a 250 mL 3 neck round bottom flask, 16 mL of methanol is added and the mixture degassed for 5 min. 64 mL of 15% by volume **PAA** is then added. The reaction mixture was fitted with a condenser and fitted with an overhead stirrer. The mixture was then heated to 60–70 °C and stirred for 48 h. The solution was decanted from the solid while still warm and then washed 5 times with 80 mL water, 1 time with 80 mL 1 M NaOH, 3 times with 80 mL water, 2 times with 80 mL methanol, and 1 time with 80 mL acetone. All washes are stirred for 15 min. After washing the composite is dried overnight at 70 °C. Copper capacities for the three sol–gel composites were determined as described in the equilibrium batch experiment below.

Elemental analyses for the sol–gel: 20.27% C, 4.69% H, 3.66% Cl. Sol–gel made with **TMOS**: 8.30% C, 3.39% H, 2.73% Cl. Elemental analyses for sol–gel made with **TEOS**: 11.02% C, 3.35% H, 2.59% Cl. Elemental analyses for the sol–gel **BP-1**: 24.3% C, 5.29% H, 3.27% Cl, 2.59% N. Sol–gel **BP-1** with **TMOS**: 18.37% C, 4.19% H, 1.86% Cl, 2.34% N. Sol–gel **BP-1** with **TEOS**: 17.69% C, 4.02% H, 2.01% Cl, 2.04% N.

3.4.4. Silicate leaching protocol

The silica leaching as a function of pH was determined by combining 0.5 mL of methanol with 9.5 mL of water adjusted to the desired pH in a 30 mL Nalgene screw cap

bottle. The pH was then checked and 100 mg of silica or composite was added and allowed to stand for 48 h. The vials were not put on a shaker so the particles would not stick to the sides of the plastic vials. For the subsequent measurements at pH = 10: to 100 mg of composite in a 30 mL Nalgene screw cap bottle was added 0.5 mL of MeOH to wet the materials for testing. To this mixture was then added 9.5 mL of pH = 10 NaOH solution. This mixture was allowed to equilibrate for 48 h, after which it was filtered using a 1.0 μm nylon syringe filter and then analyzed for concentration of silicon via ICPAES after a 1:10 dilution with 5%HCl/5%HNO_3. The raw data were converted to ppm of SiO_2 and all the data are reported as SiO_2. All leaching experiments were done in triplicate and the error bars in Figure 3.3 and Figure 3.4 are based on the standard deviations of the triplicate data.

3.4.5. Equilibrium batch experiments

Batch extraction tests were conducted by adding 100 mg of **SPC** to 10 mL of metal solution at selected pH values. To ensure equilibrium, the metal ion and **SPC** mixtures were placed in a shaker bath. After 24 h the mixtures were allowed to settle. Each supernatant was extracted and diluted using a 2% nitric acid solution for analysis using the AA method. The sol–gel **BP-1** gave copper capacity of 87.1 mg/g, the **TMOS** sol–gel **BP-1** had a copper capacity 68.7 mg/g and the **TEOS** sol–gel **BP-1** had a copper capacity of 56.8 mg/g. The copper capacities for the **BP-1** and **BP-2** composites made with the silane anchors shown in Figure 3.11 are reported in Table 3.2.

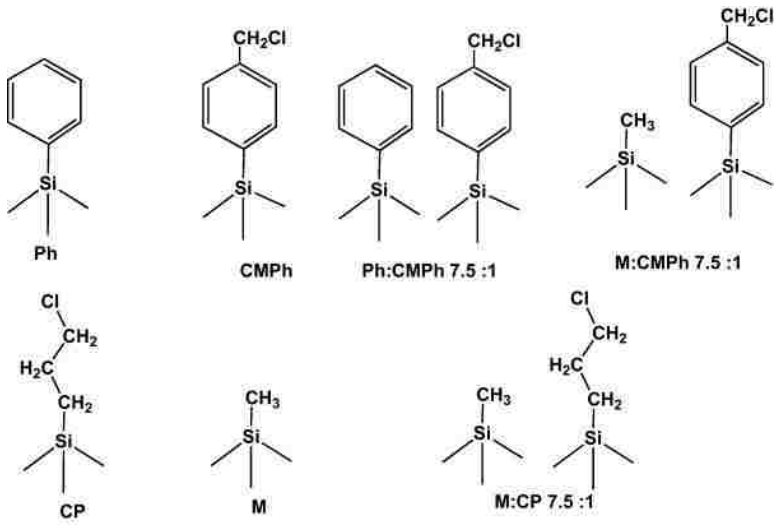

Figure 3.11. Surface silanized anchors and diluents

3.4.6. Method for calculating the number of surface anchor points per polymer molecule

The following stepwise method was used to calculate the number of anchor points per polymer molecule. The following assumptions were made:

1. All nitrogen is from **PAA** of MW = 15,000.

2. Change in mass is only due to polymer addition.

3. Each chloride that reacts does so with the polymer, forming an anchor point.

(1) Amount of chlorine

$$\%\mathrm{Cl}\frac{\mathrm{mol\ Cl}}{35.45\ \mathrm{g}}/100 = \frac{\mathrm{mol\ Cl}}{\mathrm{g\ composite}}$$

(2) Amount of nitrogen

$$\%\mathrm{N}\frac{\mathrm{mol\,N}}{14.01\,\mathrm{g}}/100 = \frac{\mathrm{mol\,N}}{\mathrm{g\,BPcomposite}}$$

(3) PAA loaded

$$\frac{\mathrm{mol\,N}}{\mathrm{g\,BPcomposite}}\frac{57g\ \mathrm{PAA}}{15,000\,\mathrm{g\,PAA}} = \frac{\mathrm{mol\,PAA}}{\mathrm{g\,BPcomposite}}$$

(4) PAA mass%

$$\frac{\mathrm{mol\,N}}{\mathrm{g\,BPcomposite}}\frac{57\,\mathrm{g\,PAA}}{\mathrm{mol\,N}} * 100 = \%\ \mathrm{PAA}$$

(5) Mass correction

$$\frac{\mathrm{mol\,Cl\,on\,CP}}{\mathrm{g\,CPcomposite}}\left(1 - \frac{\%\mathrm{PAA}}{100}\right) = \frac{\mathrm{mol\,Cl\,on\,CP}}{\mathrm{g\,BPcomposite}}$$

(6) Reacted chlorines

$$\frac{\mathrm{mol\,Cl\,on\,CP}}{\mathrm{g\,BPcomposite}} - \frac{\mathrm{mol\,Cl\,on\,BP}}{\mathrm{g\,BPcomposite}} = \frac{\mathrm{mol\,Cl\,reacted}}{\mathrm{g\,BPcomposite}}$$

(7) Number of anchor points

$$\frac{\mathrm{mol\,Cl\,reacted}}{\mathrm{g\,BPcomposite}}\frac{\mathrm{g\,BPcomposite}}{\mathrm{mol\,PAA}} = \frac{\#\ \mathrm{of\,anchor\,points}}{\mathrm{molecule\,PAA}}$$

CHAPTER 4: SOL-GEL SPC ANALOGS

4.1. Introduction

Recent developments in silica based composite materials have demonstrated viability as competitive solid-state ion exchange matrices.[14-28] The potential use of these materials on an industrial scale has advanced investigations of their methods of synthesis. Recent progress has been made in synthesizing silica from a waste material, rice hull ash, which may be a less costly procedure compared to existing silica syntheses methods.[17] Other studies are also underway to improve both material performance and the economics of silica composite synthesis.

The development of sol-gel materials and their potential for improved performance is an area currently under investigation.[32] **SPC** materials have several deficiencies that could be improved. Many of these shortcomings, such as incomplete surface coverage, non-uniform porosity, and susceptibility of the modified composites to alkaline attack could be improved by the synthesis of analogous materials by a sol-gel method. Furthermore, the synthesis of the materials themselves could ideally be economically competitive and could be produced in a more environmentally friendly manner.

This work and prior art[96] have shown that the condensation of two-component silica sols can proceed without favoring the condensation of individual monomeric units, and that the reaction rates of individual components (self-polymerization) are only weakly related to the concentration of cross-condensed species.[96] The prevalence of cross-polymerization

results in the ability to incorporate tethers during the formation of sol-gel composites. The sol-gel method offers the complete coverage of the surface with alkyl silanes, and the lack of exposed surfaces could result in greater alkaline stability of the material.

Many factors affect the formation of pores during the polymerization and precipitation of sol-gels. Pore definition can be strongly affected by substituent groups on the monomeric units, as well as by the conditions under which polymerization, precipitation, and gelation occur.[71] In this work, the term precipitation in relation to the formation of a gel is defined as the phase separation of the material, often (but not exclusively) evidenced by high levels of internal reflection and refraction (cloudiness). Gelation, in this case, is referred to as the formation of a spanning polymer which thickens and then hardens the material. Porous structures have classically been controlled by the use of templating agents, and while this can be effective, the method also requires the removal of the template, which is an undesirable step often requiring calcination.[97-99]

The work of Dong and Brennan has shown that morphological control of silsesquioxane monoliths can be achieved using a two-step processing method which does not require the use of templates, but can allow the tailoring of pore structure to desired sizes and distributions.[72] This method has been reported previously and produces monolithic silica polyamine composites which show very similar characteristics to the currently produced **SPC** materials.[32]

We report here an attempt to systematically improve the characteristics of the sol-gel **SPC** materials by modifying the composition of monomeric units while also changing the conditions under which the polymerization, precipitation, and gelation occur. The methods described here are an attempt to increase understanding of pore formation processes.

Increased understanding of conditions affecting pore formation will then hopefully lead to control of pore formation.

Direct comparison of sol-gels with currently available **SPC** materials is investigated with solid-state multinuclear NMR to define structural characteristics. Mercury porosimetry is used to determine the average pore size distributions of the sol-gels and **SPC** materials. Additionally, metal loadings are discussed for materials further functionalized with metal selective ligands.

4.2. Results and Discussion

4.2.1. Silsesquioxane polymerization tracking via ^{1}H NMR

The sol-gels reported here have been synthesized by the two-step method previously outlined by Dong and Brennan, using an initial acid catalyzed step and a following base catalyzed step.[72] Initial studies of the sol-gel polymerization focused solely upon the use of polysilsesquioxanes (**MTMOS** and **CPTMOS**) to investigate the effects that each stage of the polymerization has upon reaction progression. The initial studies utilized a molar ratio of 7.5:1 for **MTMOS**:**CPTMOS** which was chosen based upon previous work.[14,16]

^{29}Si NMR nomenclature examples are shown in Figure 4.1. Q_4 species represent atoms of Si with four Si-O-Si bonds. Q_3 species represent atoms of Si with three Si-O-Si bonds and one Si-O-R bond where R can be a hydrogen or alkyl group. Q_2 species represent atoms of Si with two Si-O-Si bonds and two Si-O-R bonds. Q_1 species represent atoms of Si with one Si-O-Si bond and three Si-O-R bonds. T_3 species represent atoms of Si with

three Si-O-Si bonds and one Si-R' bond where R' is an alkyl group. T_2 species represent atoms of Si with two Si-O-Si bonds, one Si-R' bond, and one Si-O-R bond. T_1 species represent atoms of Si with one Si-O-Si bond, one Si-R' bond, and two Si-O-R bonds.

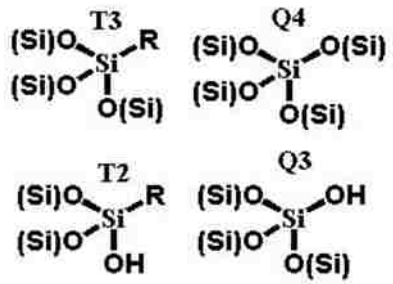

Figure 4.1. Structures of different types of silicon sites in composites

The initial, acid catalyzed step of the reaction involves rapid hydrolysis of the monomers to form low molecular weight oligomers and linear chain oligomers. Cyclization is limited during this step, owing to the reduced rate of condensation with increased connectivity around the silicon center ($T_0>T_1>T_2$).[100] This limited condensation then produces oligomers with low molecular weights and narrow molecular weight distributions. This reaction has been monitored by solution phase ^{29}Si NMR.[96] ^{1}H NMR can also be used to follow reaction progress, as seen in Figure 4.2. The changes in the intensities of the methoxy CH_3 relative to the methanol CH_3 can be used to monitor reaction progress.

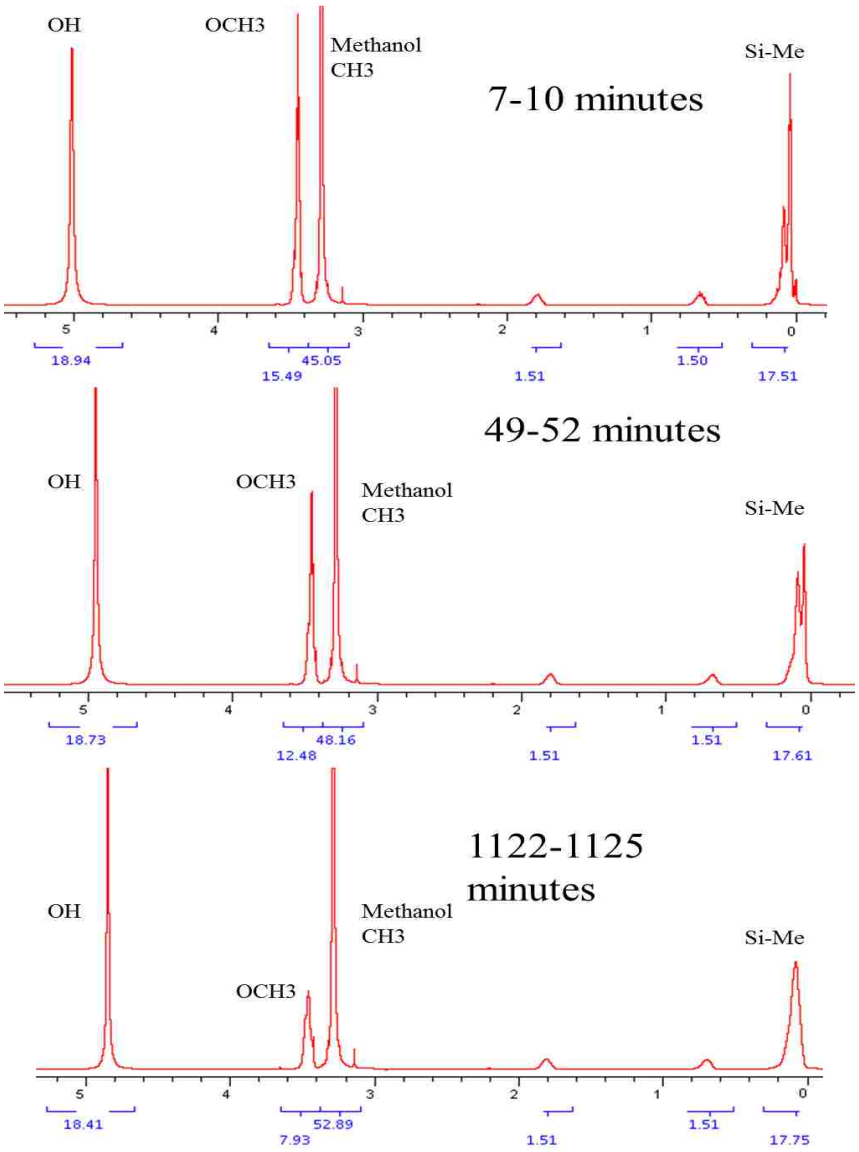

Figure 4.2. Solution state ^{1}H NMR of a 7.5:1 molar ratio **MTMOS**:**CPTMOS** sol during the acid catalyzed stage at 7 minutes, 49 minutes, and 1122 minutes.

It can be seen in Figure 4.2 that as time lapses and the polymerization progresses, ^{1}H NMR gives evidence of reaction progress. The furthest upfield peak(s) (0.0-0.2 ppm) represent H-C-O bound protons. It can be seen that, as time lapses, the peaks here are averaged together as a result of the formation of Si-O-Si bonds creating multiple

environments. The peaks at 0.7 ppm and 1.8 ppm represent the CH_2 and CH_2Cl of the chloropropyl group. The unique chloropropyl peaks are seen to maintain constant shape and chemical shift throughout the reaction, as would be expected from their distance to the reactive centers. At ppm values of 3.3 and 3.45 peaks can be seen representing the CH_3 on MeOH and Si-O-Me groups, respectively. The sum of the integrations of these peaks can be seen to remain constant over time, with the MeOH peak increasing in intensity while the Si-O-Me peak decreases in intensity proportionally. The furthest downfield peak is assigned as a hydroxyl group from the combination of methanol and water. It can be seen that, as the reaction progresses, the OH peak shifts from 5.0 ppm to 4.95 ppm to 4.85 ppm at times of 7 min, 49 min, and 1122 min, respectively. This increased shielding is a result of the increased concentration of methanol released from the hydrolysis of Si-O-Me bonds.

4.2.2. The effect of the acid catalyzed step on polysilsesquioxane pore formation

As the formation of linear chain polysilsesquioxanes progresses in the acid catalyzed step, oligomeric chains grow longer (Figure 4.3). Upon transition to the base catalyzed step, cyclization is inhibited and cluster agglomeration is promoted. This cluster agglomeration is very rapid relative to the acid catalyzed step, with the larger clusters reacting more rapidly, leading to broader size distributions. The larger clusters agglomerate throughout the entire solution, leading to decreased flow and eventually gelation. This effect, in conjunction with solvent hydrogen bonding effects, then leads to pore formation and definition.[72] Using shorter times for the acid catalyzed step results in smaller pores due to the aggregation of smaller clusters, though at very short times in acid, a flocculated, nonporous precipitate forms without gelation. Larger pores form as the time in acid increases. However, at very

long times in acid, a non-porous resin forms due to high levels of chain cyclization, as seen in Figure 4.4.

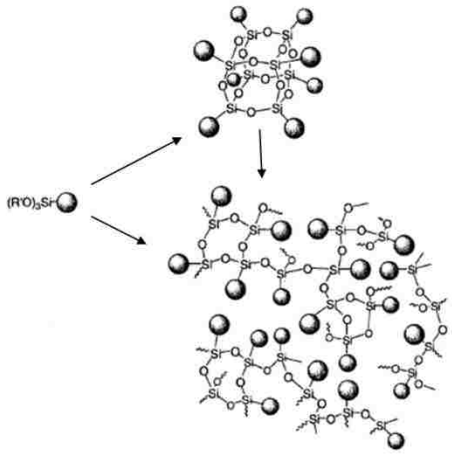

Figure 4.3. Chain elongation and oligomer formation during the acid-catalyzed step

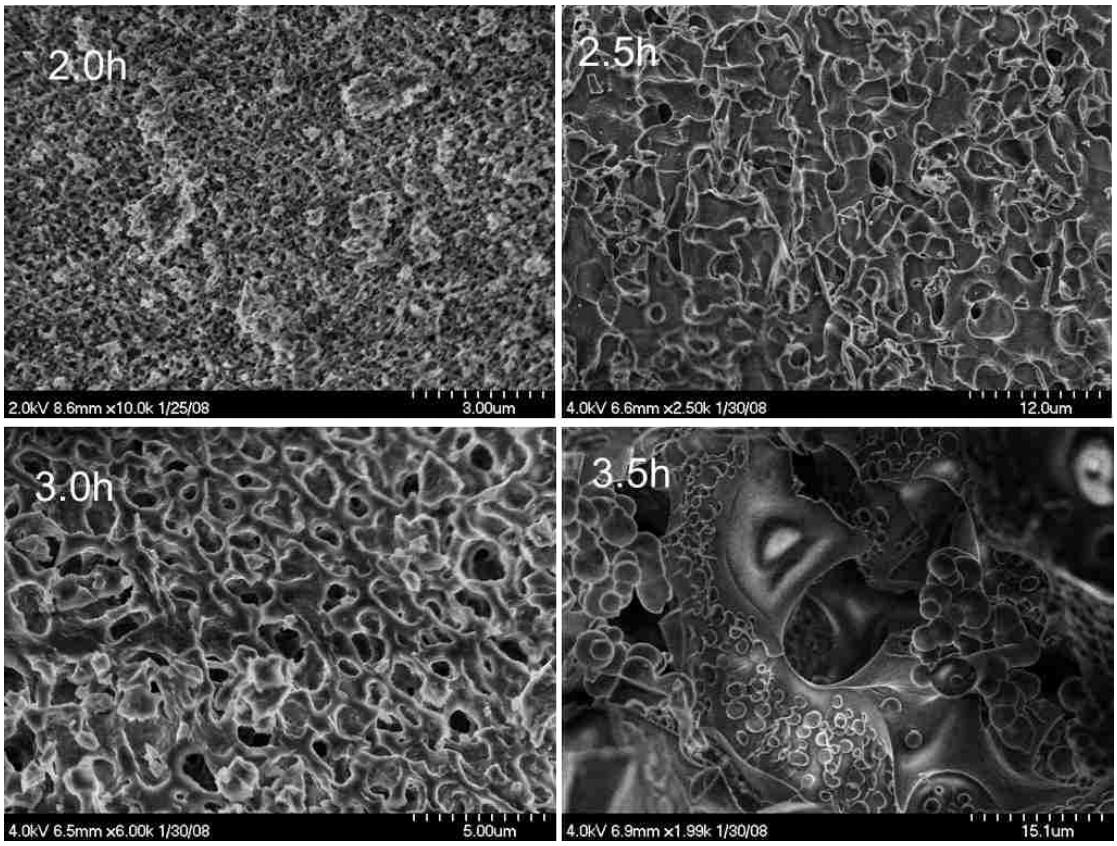

Figure 4.4. SEM images varying times in the acid catalyzed step showing the formation of a collapsed pore structure at very long acid times. Times of gelation were from 12 - 17 minutes.

Figure 4.4 shows the variation in characteristics of gels produced using varying times in the acid catalyzed step. At 3.5 hours in the acid catalyzed step, the material synthesized has undergone collapse of the porous structure, resulting in a flocculated material that precipitated without gelation. At 3.0 hours, the material formed with gelation, however, the pores formed were rather large, on the micron scale, and had variability in diameter.

4.2.3. The effect of the base catalyzed step on polysilsesquioxane pore formation

As previously discussed in Section 4.3.2, the base catalyzed step utilized in the synthesis of sol-gels is a faster process promoting cluster-cluster binding, leading to increased cluster sizes, and eventually a single cluster would span the entire solution, restricting flow to the point where gelation occurs. The properties of the resulting gel show a dependence upon the length of time between base addition and gelation, which can be partially controlled by the concentration of base during this step in the catalysis. At low concentrations of base, gel formation proceeds at a slower rate, resulting in increased pore size, as seen in Figure 4.5.

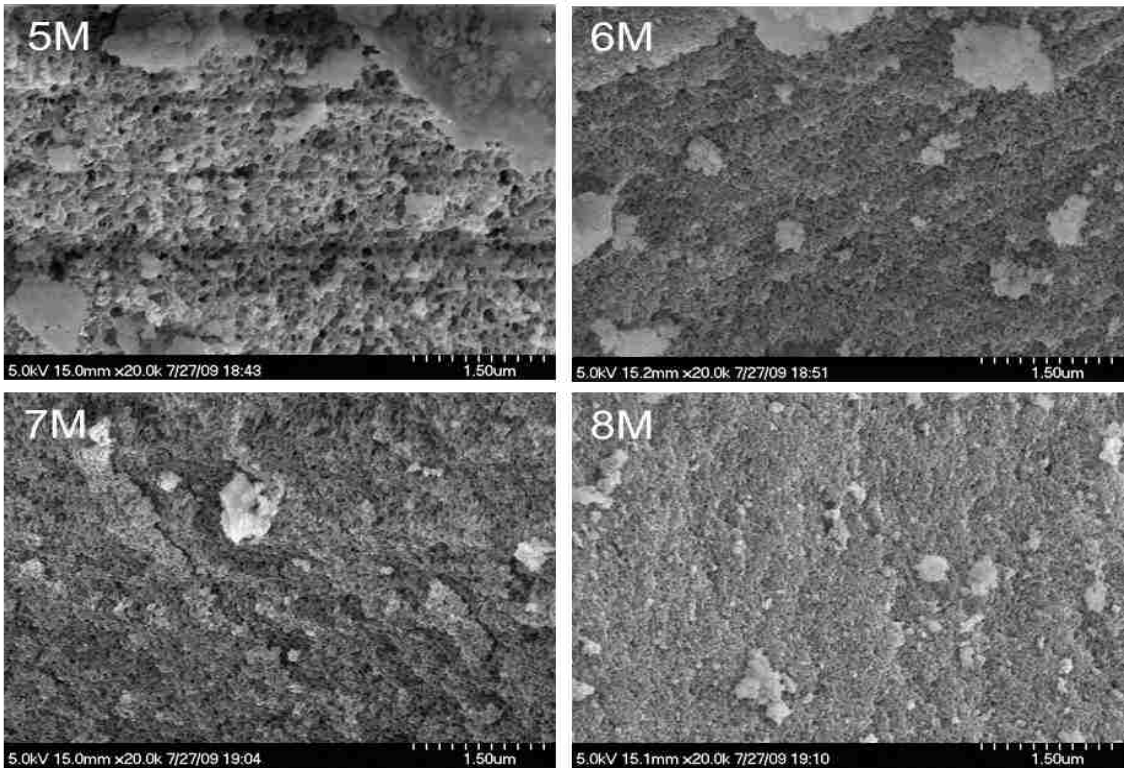

Figure 4.5. SEM images showing the formation of smaller pores with increased base concentration,. Times of gelation were from 30 seconds to 17 minutes.

Figure 4.5 shows the effect of increasing the base concentration in the base catalyzed step upon pore size distribution. At a 5 M base concentration, it is observed that pore size diameters are relatively large, larger than desired for further modifications with polyamines. At 6 M base concentration, pore sizes are decreased, and at 7 M and 8 M base concentrations, pore size diameters appeared approximately equivalent and in the range desired for materials with characteristics designed for ion exchange.

4.2.4. The effect of tetraalkoxysilane addition on material characteristics

Materials designed utilizing only alkyltrialkoxysilyl monomeric units showed that it was possible to exercise some control over the characteristics of pores formed during the polymerization process. Upon **PAA** addition to form **BP-1**, however; the best of these materials showed only 87.1 mg/g copper loading, though repeated syntheses had widely varying properties, resulting in average pore diameters ranging from 9-13.6 nm and copper capacities ranging from 41.5-87.1 mg/g. A proposed reason for the difficulty in reproducing the materials is internalization of the hydrophobic alkyl groups present in the alkyltrialkoxysilanes.[101]

The **SPC** materials tested have so far shown very long usable lifetimes, with <10% capacity loss in more than 3000 copper loading – acid stripping – base regeneration cycles.[11] Much of this stability is attributed to the multiple point covalent anchoring of the polyamine to the surface, as well as to the bulk silica matrix present, which provides increased mechanical stability. It was thought that the addition of a tetraalkoxysilane to the reaction mixture would not only increase mechanical stability through cross linking, but may also

increase the reproducibility of the sol-gel reaction, and expose more of the chloropropyl silanes to reaction with **PAA**.

Initial introduction of tetraalkoxysilanes was attempted using **TMOS** and **TEOS**, however **TEOS** did not fully react under the experimental conditions tried, and it was found that **TMOS** was a more suitable monomer for the intended purpose.[32] Initial reactions used a 4.25:7.5:1 **TMOS**:**MTMOS**:**CPTMOS** ratio in an attempt to form a structure similar to the idealized structure shown in Figure 4.6.

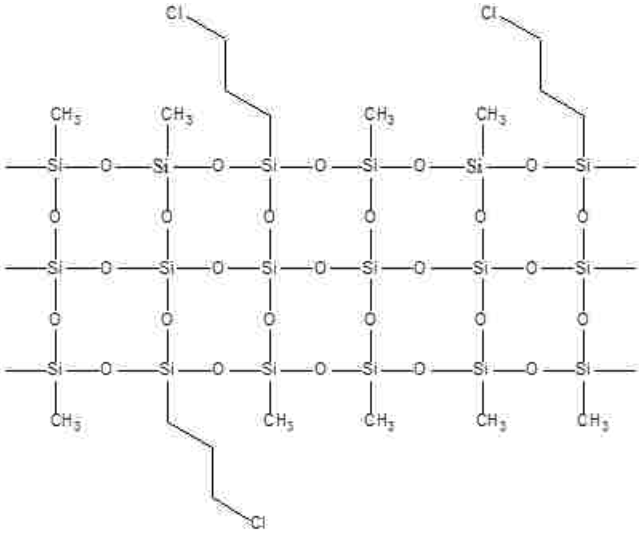

Figure 4.6. Structure of an idealized sol-gel surface with **TMOS:MTMOS:CPTMOS** ratio of 4.25:7.5:1

^{13}C NMR of the resulting composite made from this material suggests the same rates of incorporation of all of the monomeric units, despite their different rates of self-polymerization. This is evidenced by the splitting of the halocarbon peak on C_3 of the chloropropyl group as seen in Figure 4.7. This splitting has been assigned to a neighboring group effect and is present in commercial **SPC** materials with mixed silanes, but not in those

utilizing only 3-chloropropyltrichlorosilane as the monomer for surface silanization. This then suggests that the two main environments experienced by the 3-chloropropyl groups are:

1) Including one or more neighboring 3-chloropropyl group

2) Only including neighboring methyl surface groups.

Predominant agglomeration of 3-chloropropyl groups would result in this peak not being split. [32]

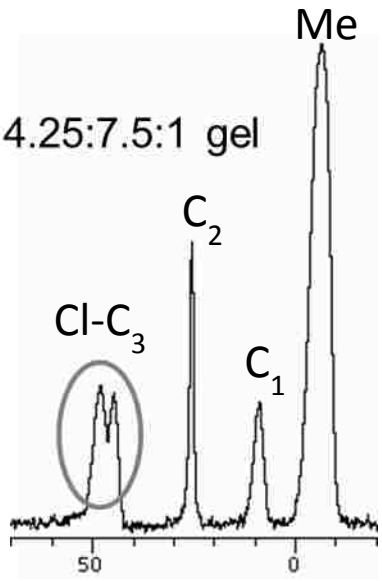

Figure 4.7. ^{13}C CPMAS NMR of sol-gel with a **TMOS:MTMOS:CPTMOS** molar ratio of 4.25:7.5:1, with the halocarbon peak circled to emphasize splitting

Copper capacities of materials using the 4.25:7.5:1 ratio still varied significantly, ranging from 68.7 mg/g up to 100 mg/g. It was found that the reaction of **PAA** was incomplete, with only 35-38% of surface halocarbons being reacted. Though this resulted in multi-point anchoring at ~38 anchors per polymer molecule on average, the low level of chloride utilization further supports the concept that non-polar alkyl groups were being internalized into the support matrix. Further gels were created with increasing amounts of

MTMOS, resulting in increasingly lower chloride utilization, down to 31% on a gel made with 4.25:30:1 **TMOS**:**MTMOS**:**CPTMOS**. Copper batch capacities decreased with increasing ratios of **MTMOS** to **CPTMOS**.

4.2.5. The effect of increasing TMOS to push halocarbons to the surface

The low chloride utilization observed prompted us to investigate further increasing the relative concentration of **TMOS**, increasing the internal framework and 'pushing' the nonpolar alkyl groups to the surface, effectively increasing the number of halocarbons available for nucleophilic attack by **PAA**. This increased crosslinking and internal framework development can be followed by the solid state ^{29}Si NMR spectra in Figure 4.8. The ^{29}Si NMR spectra in Figure 4.8 show that increasing amounts of **TMOS** results in increasing amounts of Q peaks (those assigned to the bulk siloxane). In addition to this effect, there is also some broadening of the T peaks (those assigned to the alkyltrialkoxysilanes) and a decreased T_2 peak intensity, suggesting more complete reaction of alkyltrialkoxysilanes.

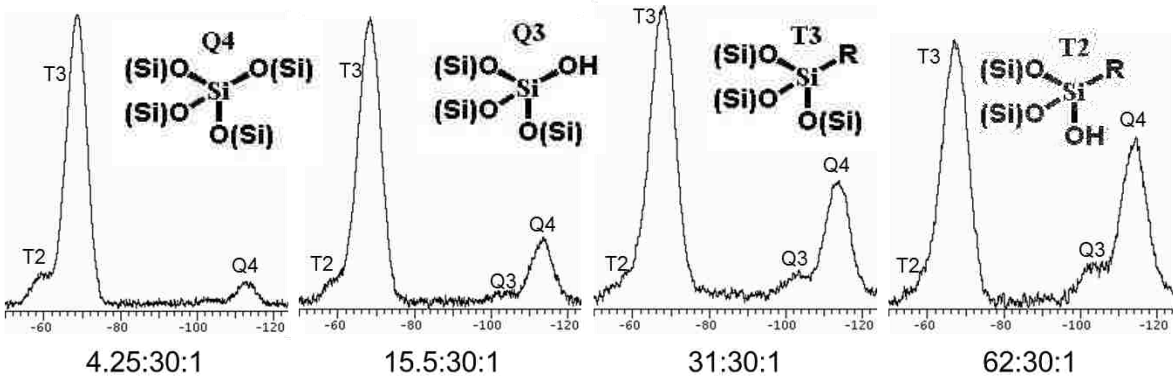

Figure 4.8. ^{29}Si NMR showing increasing internal framework with increasing **TMOS**

Sol-gels were prepared using four mixtures with increasing molar ratios of **TMOS** relative to the other monomers. The four ratios chosen were 4.25:30:1, 15.5:30:1, 31:30:1, and 62:30:1 for **TMOS**:**MTMOS**:**CPTMOS**. **BP-1** composites made from these gels showed several significant trends with improved characteristics as the level of **TMOS** increased. Both chloride utilization and copper binding of the resulting composites showed strong correlations with increasing amounts of **TMOS** (Figure 4.9). Chloride utilization in the commercially available **SPC BP-1** was found to be ~80%. Chloride utilization for the sol-gel **BP-1** materials with varying amounts of **TMOS** was from 31-51%, still utilizing less of the surface anchors than conventional materials. Interestingly, however, this did not have a significant impact on polymer tethering, which was found to range from 12.2-13.3 anchors per polymer molecule (Table 4.1). For the material with the highest molar ratio of **TMOS**, copper capacity was found to be 118 mg/g, which is slightly higher than the copper capacities found in conventional **SPC** materials (95-105 mg/g). This observation is consistent with the

internalization model proposed earlier, where increasing internal cross-linking increased the number of available halocarbons.

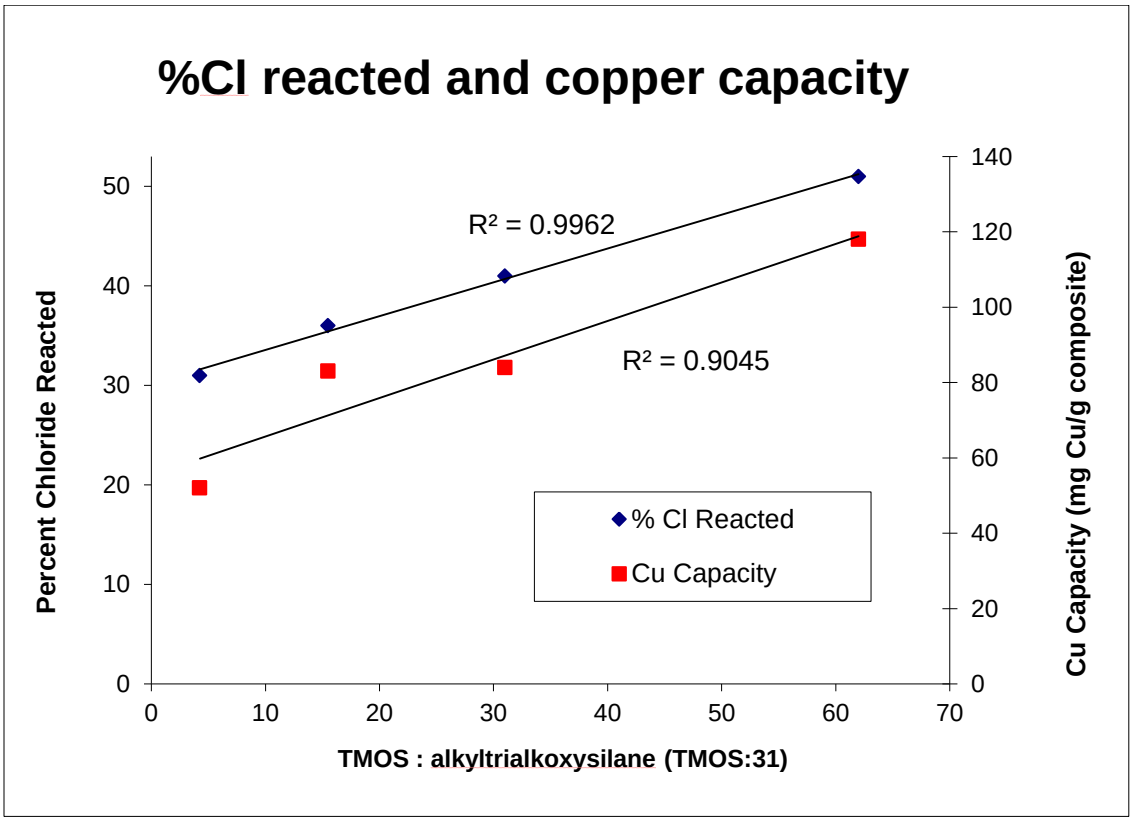

Figure 4.9. Copper capacities and chloride utilizations for sol-gels with varying relative amounts of **TMOS**.

Figure 4.9 details the relationship between chloride utilization, copper capacity, and the relative amount of **TMOS** used in the synthesis of the resulting gels. At 4.25 moles of **TMOS** to 31 moles of alkyltrialkoxysilanes, the copper binding capacity and chloride utilization of the resulting **BP-1** composite are low, at 52 mg/g and 31%, respectively. Increasing the relative amount of **TMOS** showed marked improvements in both chloride utilization and copper capacities, which seem to be correlated for these materials.

Ratio of Silanes (TMOS:MTMOS:CPTMOS)	Anchor Points per Polymer Molecule	Percent Chloride Utilization	Batch Copper Capacity (mg Cu/g composite)
4.25:7.5:1	37.7	38	100
4.25:30:1	13.3	31	52
15.5:30:1	12.8	36	83
31.0:30:1	12.2	41	84
62.0:30:1	12.5	51	118

Table 4.1. Copper capacities, chloride utilizations, and anchor points for sol-gel **BP-1** materials with varying relative amounts of **TMOS**.

Gelation and pore structure are also highly affected by the addition of **TMOS**. Figure 4.10 shows the effects of three different ratios of **TMOS**:**MTMOS**:**CPTMOS** upon the average pore size distribution. At very low amounts of **TMOS**, little porosity is observed and the average pore size distribution is relatively broad. The composite resulting from a 4.25:30:1 ratio of **TMOS:MTMOS:CPTMOS** showed this low level of porosity. As the amount of **TMOS** increases, porosity increases and pore sizes decrease. The composite resulting from a 31:30:1 ratio of **TMOS:MTMOS:CPTMOS** showed greatly increased porosity and much narrower average pore size distribution, with an average pore diameter of 9.1 nm. The composite resulting from a 62:30:1 ratio of **TMOS:MTMOS:CPTMOS** showed even higher porosity and decreased average pore diameter of 8.0 nm. This is expected for materials having increased cross-linking. Additionally, the gelation times were seen to decrease with increasing levels of **TMOS**, which would result in smaller clusters agglomerating and the formation of smaller pores.

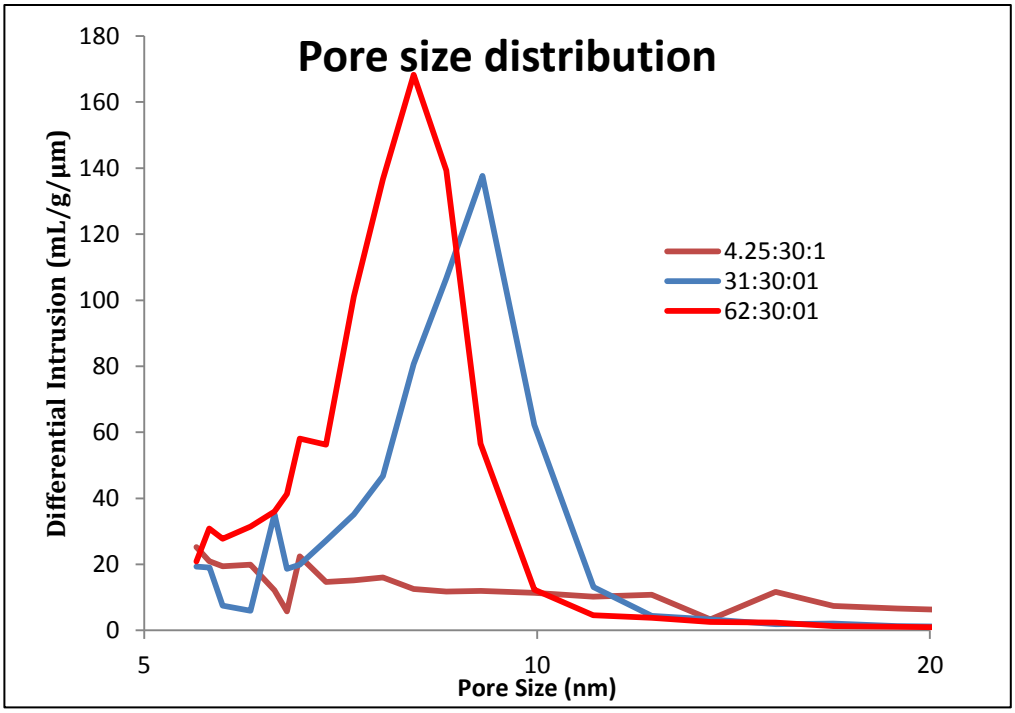

Figure 4.10. Average pore size distributions for sol-gels with varying relative amounts of **TMOS**.

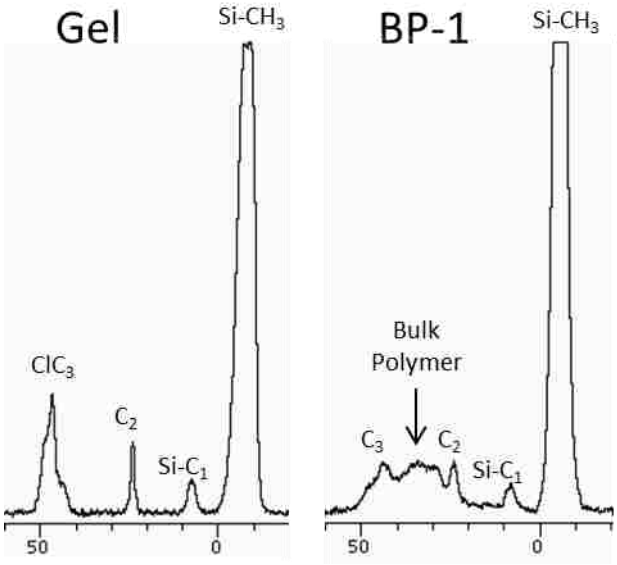

Figure 4.11. Solid state CPMAS ^{13}C NMR of the sol–gel (left) made with 62:30:1 **TMOS:MTMOS:CPTMOS** and the resulting composite after reaction with **PAA** (right). The resonances labeled SiC_1, C_2, ClC_3, and C_3 are due to the propyl groups of the silane anchor.

Evidence of polymer binding to the sol-gel can be seen in Figure 4.11. The ^{13}C CPMAS NMR of both the gel (left) and the **BP-1** (right) show the regular peak for the Si-Me group at -6.0 ppm. The three peaks corresponding to the 3-chloropropyl group can also be seen at 9, 23, and 46 ppm in the gel and 9, 23, and 44 ppm on the **BP-1**. The shift of the #3 carbon is due to the binding of the polyamine to the surface. The bulk polymer can be seen as a broad peak ranging from ~25-45 ppm. Mass gains of these materials on conversion of the gel to **BP-1** were measured. However, the small scale of the reactions necessary for these experiments resulted in negligible mass gains which were unreliable for calculations of polymer binding. Conventional silica composites exhibit mass gains of 10-13% on polymer binding to the silanized surface.

4.2.6. The effect of polymer binding on gel reorganization

Binding of **PAA** on the surface of the sol-gel composites is performed using a very similar procedure to that used for conventional **SPC** composites. The conditions under which the polymer addition proceeds appear to result in further conversion of the T_2 sites to T_3 sites. This is evident by the decrease in Q_3 and T_2 peaks at -102 ppm and -56 ppm, respectively, in Figure 4.12. This is seen in the ^{29}Si NMR before and after polymer addition. It is proposed that this reorganization is not due to one effect, but rather due to the combination of effects (heating under aqueous conditions).

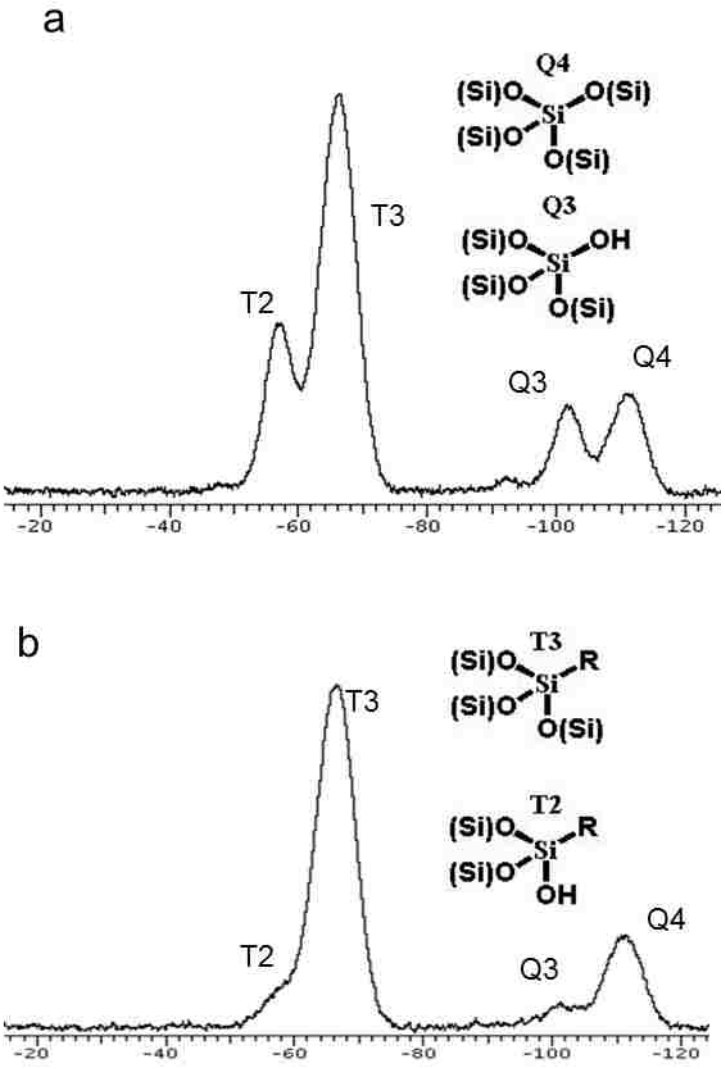

Figure 4.12. ^{29}Si NMR of a) 4.25:7.5:1 **TMOS:MTMOS:CPTMOS** sol-gel and b) 4.25:7.5:1 **TMOS:MTMOS:CPTMOS BP-1**

The Q_3 and T_2 peaks represent unreacted silanol or alkoxysilane sites. These sites are more receptive to alkaline attack, and their decreased level upon polymer addition is also corroborated by silica leaching studies. (Figure 4.13)

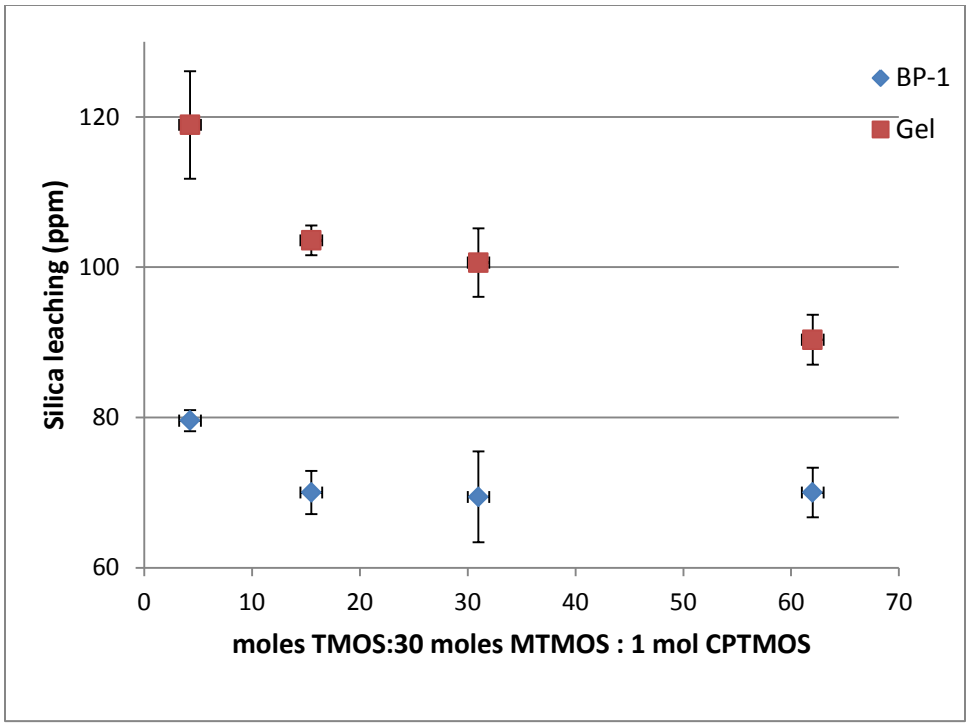

Figure 4.13. Silica leaching for sol-gels with varying relative amounts of **TMOS**. All gels showed significantly decreased leaching upon conversion to **BP-1**.

The decreased leaching shown upon modification distinguishes a fundamental difference between **SPC** and sol-gel materials. The surface of conventional silica composites becomes more susceptible to alkaline attack upon modification with **PAA**. This suggests that the materials made by sol-gel methods, though they show greater leaching than the conventional **SPC** materials, do lack the surface interactions shown to increase leaching in conventional **BP-1** upon covalent binding of **PAA**.

4.2.7. Comparisons with SPC materials

SPC based materials have been shown to be highly effective for metal separations. **CuSelect** has been produced commercially and been shown to be effective for the separation of Cu^{2+} from Fe^{3+}. Sol-gel materials synthesized to date have shown very comparable characteristics to conventional silica composites, and even improvements in some areas. Average pore size distributions of sol-gels are narrower than those of **SPC** materials. Control of the pore size also shows potential for sol-gel materials to be designed for specific purposes, a major advantage over conventional **SPC** materials.

4.2.7.1. SEM and mercury porosimetry of "best" BP-1's

Polymer binding has been shown to lower both pore size and surface area. It is suggested that some of the decrease in surface area is due to the covering of smaller pores,[90] and that the formation of slightly larger pores could result in increased composite performance following polymer addition. The ability to design pores of specific sizes is a great advantage for an ion exchange material. As seen in Figure 4.10, conditions of the sol-gel reaction can be altered to achieve a level of control over pore formation. Figure 4.14 illustrates the differences between the most desirable sol-gel **BP-1** to date (made from 62:30:1 **TMOS:MTMOS:CPTMOS**) and a typical **SPC BP-1**. The sol-gel **BP-1** demonstrates pore sizes with a narrower distribution than the conventional **SPC** materials. Conventional materials have many of their pores present in sizes smaller than the 5 nm minimum that can be measured by the mercury porosimeter used for these measurements. Many of these pores would become inaccessible upon polymer binding. The maximum for

average pore diameter of the conventional **BP-1** was 6.3 nm. This compares with the more desirable, larger average pore diameter of 8.0 nm for the sol-gel **BP-1**.

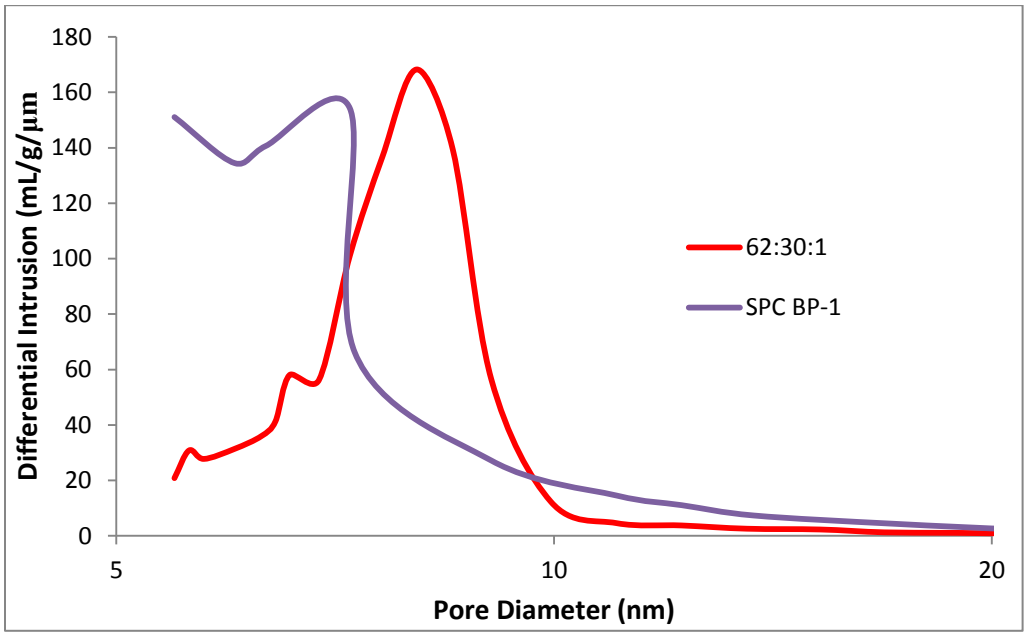

Figure 4.14. Average pore size distributions for **SPC BP-1** and 62:30:1 **TMOS:MTMOS:CPTMOS BP-1**

4.2.7.2. BP-1 silica leaching comparison of SPC with 62:30:1 and previous materials

The susceptibility to silicate leaching under alkaline conditions is considered to be the greatest weakness of **SPC** materials. It was thought that with sol-gel materials, some of this susceptibility could be avoided through both a decreased amount of bulk silica and the avoidance of 'bare' silica surfaces which have not been silanized. Though both of these effects are observed in sol-gel composites, and alkaline stability of **BP-1** materials was improved for initial materials, leaching increased upon dilution of chloropropyl anchors (Figure 4.15). The large increase in leaching from 9.2 ppm to 36.0 ppm for the conventional

SPC materials upon polymer addition is thought to be a direct result of polymer-surface interactions. The initial sol-gel experiments, using only silsesquioxanes or small relative amounts of **MTMOS**, showed similar silica leaching levels to conventional materials. However, materials produced with very low levels of **CPTMOS**, such as the **BP-1** made from a ratio of 62:30:1 **TMOS:MTMOS:CPTMOS**, show strong increases in the level of silica leaching at pH = 10, up to 70.0 ppm for the **BP-1**. Interestingly, the sol-gel material with very low amounts of **CPTMOS** also shows a decrease in leaching upon polymer immobilization. This is thought to be a direct result of the decreased number of Q_3 and T_2 sites upon surface reorganization during the polyamine addition step.

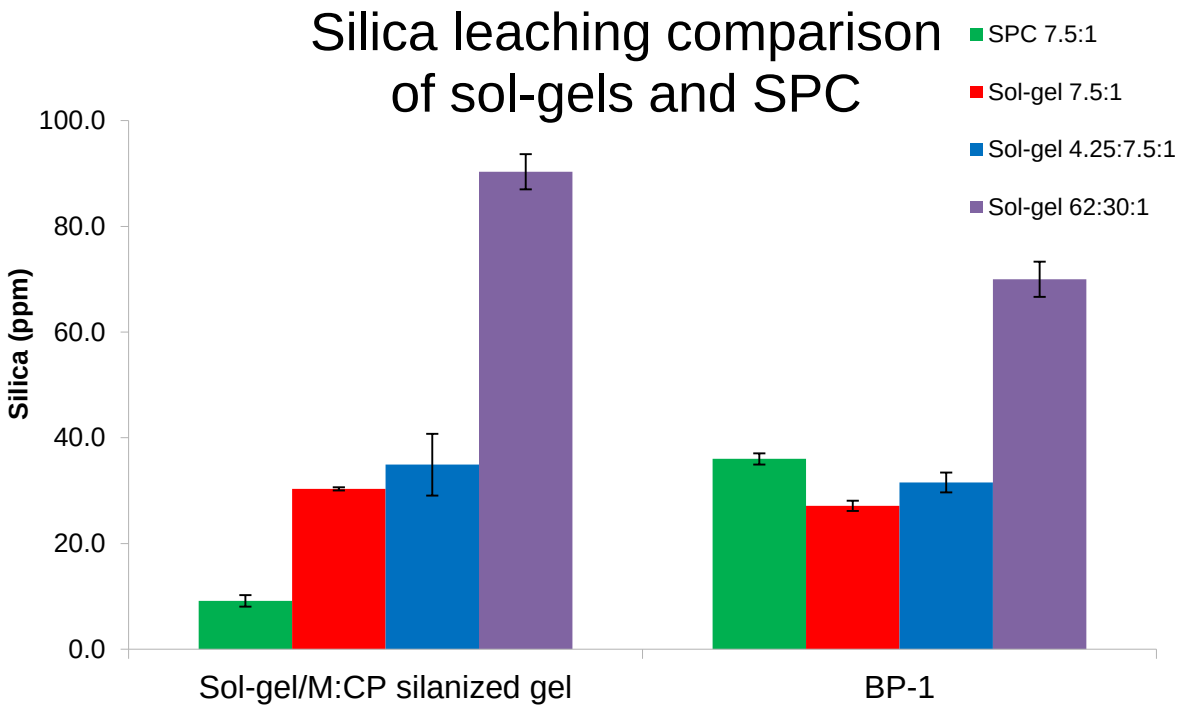

Figure 4.15. Silica leaching for **SPC BP-1**, 7.5:1, 4.25:7.5:1, and 62:30:1 **TMOS:MTMOS:CPTMOS BP-1**

4.2.7.3. BP-1 copper capacities, chloride utilization, anchor points, and elemental analyses

Name of Sample	%C	%H	%Cl	%N	Anchor Points / Polymer Molecule	% Chloride Utilization	Copper Capacity (mg/g)
7.5:1 silanized gel	3.8	0.97	1.05	N/A	N/A	N/A	N/A
7.5:1 SPC BP-1	11.56	2.36	0.17	3.26	24	81	95-105
7.5:1 sol-gel	20.13	4.75	5.46	N/A	N/A	N/A	N/A
7.5:1 sol-gel BP-1	24.92	5.31	4.44	2.47	20	10	92
4.25:7.5:1 sol-gel	10.366	3.442	2.66	N/A	N/A	N/A	N/A
4.25:7.5:1 sol-gel BP-1	20.176	4.458	1.73	3.023	21	26	96
4.25:30:1 sol-gel	14.115	4.321	1.19	N/A	N/A	N/A	N/A
4.25:30:1 sol-gel BP-1	22.732	5.064	0.73	2.612	13	31	80
62:30:1 sol-gel	6.69	2.37	0.51	N/A	N/A	N/A	N/A
62:30:1 sol-gel BP-1	12.02	2.73	0.23	1.99	12.5	51	118

Table 4.2. Elemental analyses, copper capacities, chloride utilizations, and anchor points for conventional silica based materials as well as sol-gels with varying monomeric unit composition.

Table 4.2 shows, as expected, that elemental analyses on the different composites show higher levels of carbon, hydrogen, and chlorine relative to **SPC** materials due to having less bulk silica framework. At very high ratios such as 62:30:1, this effect is diminished. All of the **BP-1** materials showed increased amounts of carbon, and nitrogen is not observed prior to the addition of **PAA** to the composite surface. Copper capacities determined for the sol-gel **BP-1** from 62:30:1 **TMOS:MTMOS:CPTMOS** were slightly higher than in conventional materials. Anchor points on the polymer are less for all of the sol-gel synthesized materials, and this effect increases to some extent with deceasing relative ratio of **CPTMOS**. Chloride utilization is greater with sol-gel materials utilizing large relative amounts of **TMOS**, and, for the 62:30:1 material, chloride utilization rises to 51%. This

begins to approach the 81% chloride utilization of conventional **SPC** materials. It is currently under further investigation whether increasing the relative amount of **TMOS** will further increase the level of chloride utilization, and therefore the copper capacity.

4.2.7.4. BP-2 and CuSelect composite performance

Further modification of polyamine composites provides the ability to design composites with ligands selective for certain metal separations. Solid phase ion exchange materials utilizing aminoacetate functional groups have been shown to be effective for the extraction of divalent transition metal ions from aqueous solutions at low pH.[19] Picolylamine functionalized materials (**CuSelect**) have been shown to be effective copper selective ligands at low pH, such as the selective removal of Cu^{2+} in the presence of high quantities of Fe^{3+}.[27] Aminoacetate functionalized materials (**BP-2**) have been shown to be effective for the separation of Cu^{2+} from Ni^{2+} at low pH.[19] A synthetic scheme for these materials is shown in Figure 4.16. **CuSelect** is synthesized by the use of a sodium triacetoxyborohydride solution in MeOH as a hydride donor in the reaction of 2-pyridinecarboxaldehyde with the primary amines of **BP-1**. The resultant 2-picolylamine modified composite is given the name **CuSelect**. **BP-2** is synthesized by the use of sodium chloroacetate under basic conditions. The amines of **BP-1** undergo nucleophilic attack upon the halocarbons of sodium chloroacetate, resulting in the aminoacetate modified composite, **BP-2**.

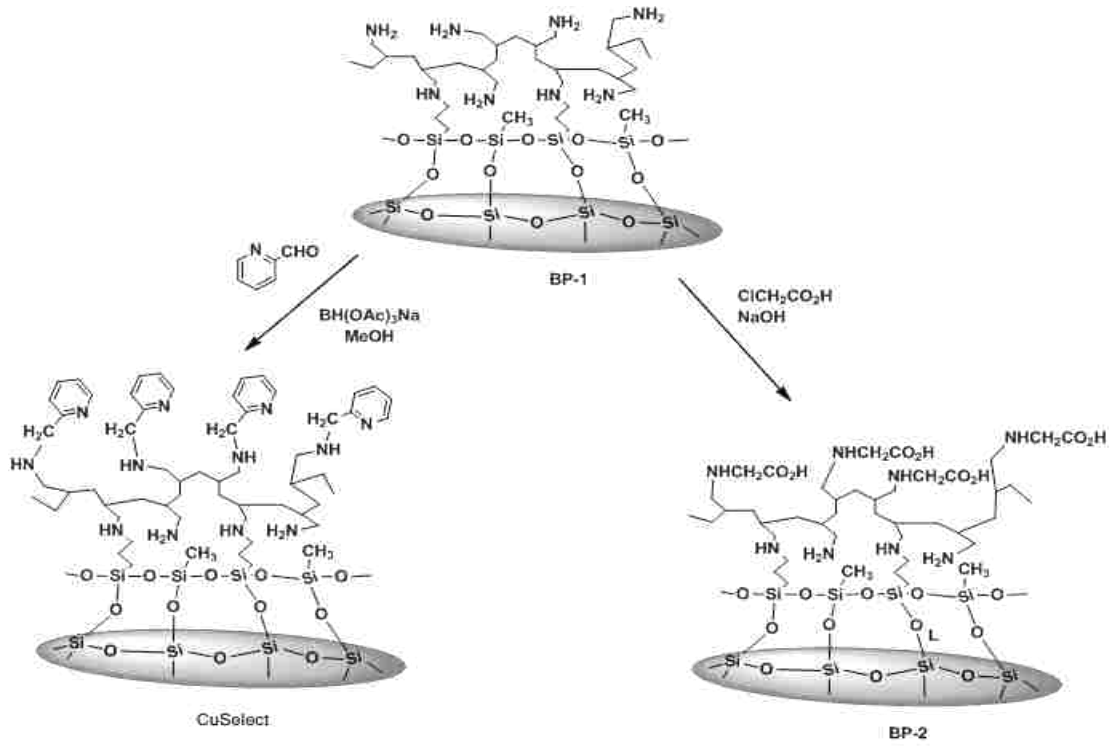

Figure 4.16. Synthesis of ligand modified sol-gel composites

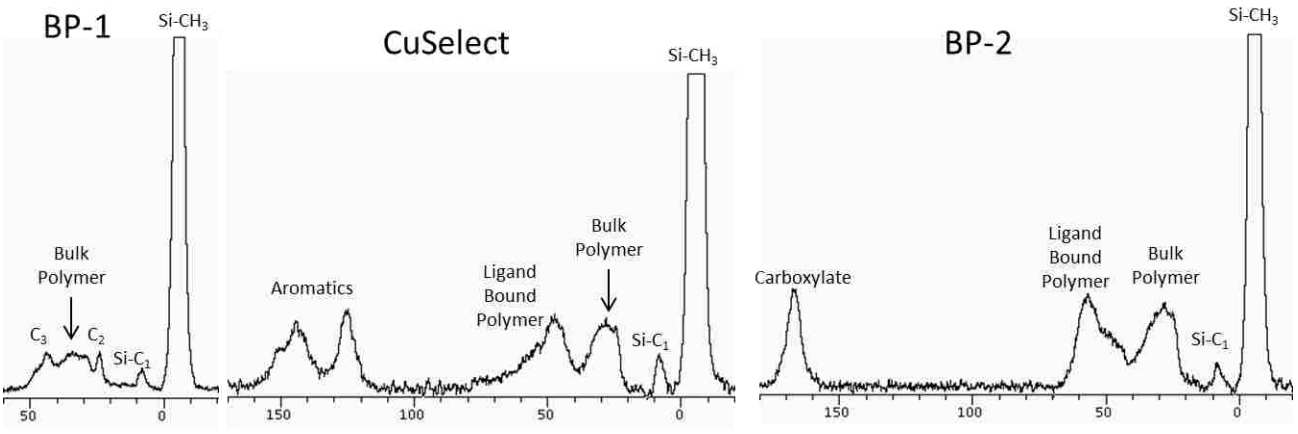

Figure 4.17. Solid state CPMAS ^{13}C NMR of the sol–gel **BP-1** (Left), **CuSelect** (Center), and **BP-2** (Right) made with 62:30:1 **TMOS:MTMOS:CPTMOS**. The resonances labeled SiC_1, C_2, and ClC_3 are due to the propyl groups of the silane anchor.

Evidence of ligand loading on the composites **CuSelect** and **BP-2** can be seen in Figure 4.17. All three materials (**BP-1**, **CuSelect**, and **BP-2**) show the regular peak for the Si-Me group at -6.0 ppm. The three peaks corresponding to the 3-chloropropyl group can also be seen at 9, 23, and 44 ppm on the **BP-1**. The **CuSelect** and **BP-2** show the Si-C_1 peak from the 3-chloropropyl group at 9 ppm, but the other two peaks are overshadowed by the bulk polymer and ligand bound polymer peaks. The bulk polymer can be seen as a broad peak ranging from ~25-45 ppm for the **BP-1** and ~20-40 ppm for the **CuSelect** and **BP-2**. The **CuSelect** shows a ligand bound polymer peak at 48 ppm which is very broad, beginning at ~40 ppm then tailing off to ~80 ppm. The ligand bound polymer peak in **BP-2** is seen ranging from ~40-65 ppm with the apex at 56 ppm and a shoulder at ~48 ppm. The aromatic carbons on **CuSelect** show two peaks: one ranging from ~120-133 ppm and the other ranging from ~133-160 ppm. The carboxylate group on **BP-2** can be seen as a broad peak from ~160-175 ppm.

The **SPC BP-2** made from amorphous silica has many doubly modified amine groups after reaction of **BP-1** with chloroacetic acid. This **BP-2** has ~2.7 mmol ligand/g composite, while **CuSelect** has ~2.0 mmol ligand/g composite.[19] This is significantly higher than the 0.4-1.1 mmol/g and 0.7-1.0 mmol/g found for sol-gel materials made into **BP-2** and **CuSelect**, respectively. Figure 4.18 shows the comparison of ligand loading and copper capacities for the ligand modified **BP-1** composites **CuSelect** and **BP-2**. When compared with Figures 4.9 and 4.10, it can be seen that with increasing relative amounts of **TMOS**, the **BP-1** chloride utilization and copper capacity increase. This trend also carries through to ligand loading on modified composite materials.

CuSelect made from 4.25:7.5:1 **TMOS:MTMOS:CPTMOS** showed a ligand loading of 0.7 mmol ligand/g composite. This increased to 0.83 and 0.96 mmol ligand/g composite for 31:30:1 and 62:30:1 **TMOS:MTMOS:CPTMOS** ratios, respectively. **BP-2** made from 4.25:7.5:1 **TMOS:MTMOS:CPTMOS** showed a ligand loading of 0.42 mmol ligand/g composite. This increased to 0.72 and 1.07 mmol ligand/g composite for 31:30:1 and 62:30:1 **TMOS:MTMOS:CPTMOS** ratios, respectively.

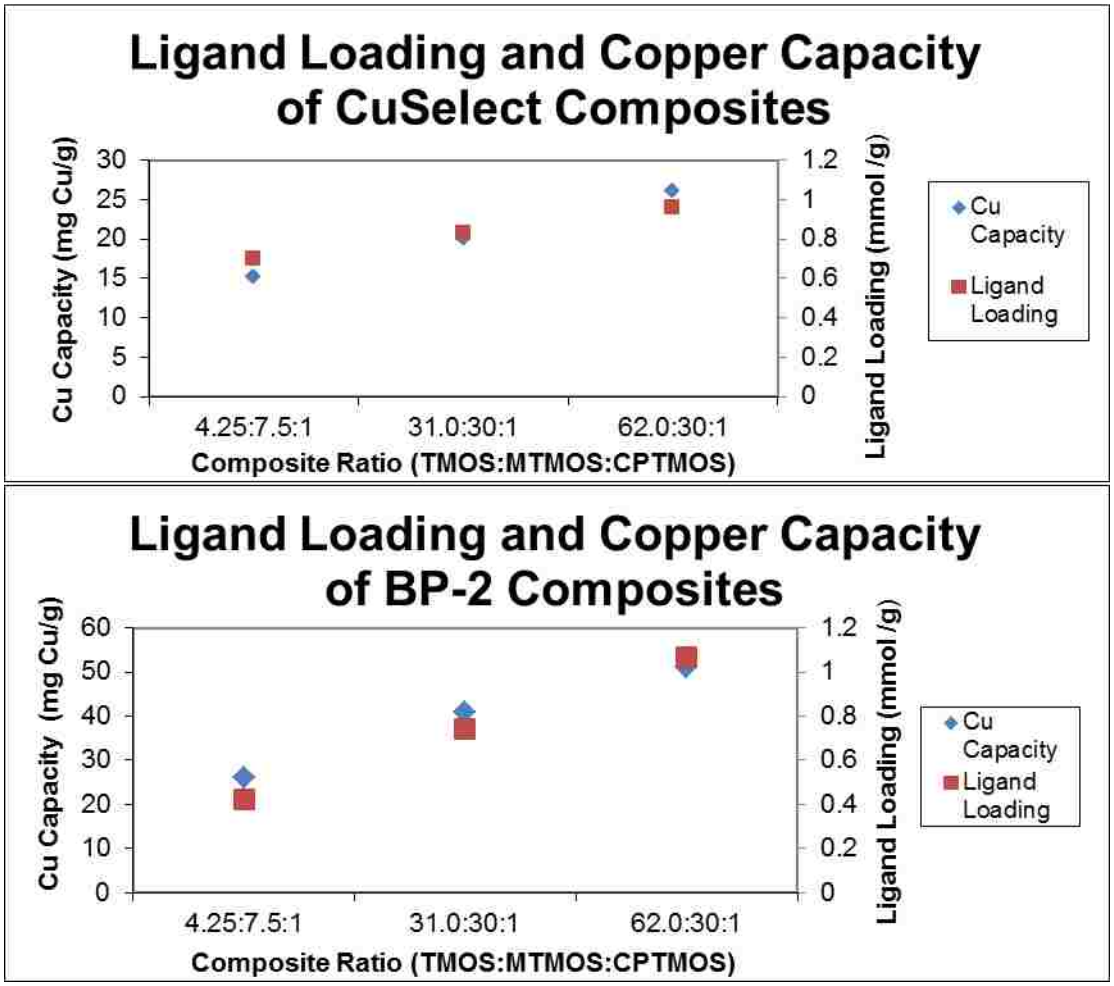

Figure 4.18. Ligand loading and copper capacity for sol-gel **CuSelect** and **BP-2**

However, when a comparison of copper capacities at pH = 2 for **BP-2** is made, the sol-gel materials show improved capacities over conventional materials (51 vs 38 mg/g). This is thought to be an effect of the increased pore sizes resulting in more availability for active sites after ligand modification. For **CuSelect**, however, the capacities at pH = 1.5 are somewhat lower (25 vs 35 mg/g), which is thought to be due to decreased ligand loading combined with the bulky ligand being too large for the available average pore diameters seen in Figure 4.14.

The breakthrough experiments show metal capacities that are significantly decreased for both materials relative to **SPC** materials. **BP-2** synthesized from sol-gels had Cu^{2+} capacities of 36 mg/g under breakthrough conditions in competition with Ni^{2+}. **CuSelect** synthesized from sol-gels had Cu^{2+} capacities of 15 mg/g under breakthrough conditions in competition with Fe^{3+}. **BP-2** synthesized from sol-gels and **SPC** materials gave selectivities for Cu^{2+} over Ni^{2+} of 11:1 and xx:1, respectively. **CuSelect** from sol-gels and **SPC** materials gave selectivities for Cu^{2+} over Fe^{3+} of 40:1 and 67:1, respectively. The decreased selectivity for the ligand-modified sol-gel **SPC** materials is tentatively assigned to the decreased ligand loading, though further investigation is warranted.

4.3. Conclusions

There are a number of important conclusions that can made from the work reported here:

1. Sol-gel materials offer an alternative to conventional silica gels as a matrix with selectable pore size. Pore size distributions are narrower, and the ability to change the pore size provides additional potential for modification with bulkier ligands.

2. Studies into reaction conditions gave a better understanding of the method of pore formation, allowing more effective tailoring of pore size. Both the acid catalyzed step and the base catalyzed step can have significant impacts on pore formation. Modifications to each of these steps (as well as other conditions) can result in control over pore size.

3. Silicate leaching at pH=10 from sol-gel materials is similar to that of conventional silica for the polymer modified composites. The studies presented here suggest that the lack of available T_2 sites prevents polymer-surface interactions. Higher concentrations of methyl groups relative to chloropropyl groups increases leaching, which is thought to be an effect of decreased steric hindrance and/or hydrophobicity due to the small size of the methyl group.

4. The introduction of **TMOS** showed improvements in sol-gel composite performance, particularly in providing narrower pore size distributions. The internal framework developed also is shown to increase the availability of surface halocarbons by prevention of internalization. This effect also seems to be related to increased copper capacities due to increased polymer loading.

5. **BP-1** copper capacities equal to or greater than those of conventional materials have been achieved using sol-gel based materials, showing increased potential as a replacement material in some applications.

6. Equal or greater batch copper loading capacities were expressed for sol-gel derived **BP-2** relative to conventional silica. Lower batch copper loading capacities were expressed

for sol-gel derived **CuSelect**, due to low levels of ligand loading. Similar or slightly less selectivity was found for ligand modified materials in breakthrough experiments. **CuSelect** selectivity was 40:1, which is significantly less than the 67:1 for conventional materials. **BP-2** selectivity was 11:1 (Cu^{2+}:Ni^{2+}).

Further studies regarding the effects of the acid-catalyzed step on pore formation when **TMOS** is present are underway, as are ^{29}Si NMR studies of the acid-catalyzed sol step to develop a complete picture of pore formation. The application of surface analytical techniques (AFM, TEM) will deepen our understanding of molecular interactions at the polymer–surface interface.

4.4. Experimental

4.4.1. Materials and Methods

All chemicals were purchased from Sigma-Aldrich and used as received unless otherwise noted. The silanized silica gels, the poly(allylamine) (**PAA**) composite **BP-1**, and the chloroacetic acid modified **BP-1** (**BP-2**), and the 2-picolylamine modified **BP-1** (**CuSelect**) were prepared according to the published literature procedures.[14-16,18,27,29] The synthesis of sol-gel **BP-1** analogs will be outlined in section 4.4.4. The methods of preparation of the analogous sol-gel ligand modified **BP-1** composites were unchanged from those using **SPC** materials. Raw silica gel (10 nm average pore diameter, 250-600 μm particle size, 450 m^2/g surface area) was obtained from Qing Dao Mei Gow, Qing Dao, China. Poly(allylamine) **PAA**-15B (15,000 MW) was obtained from Summit Chemicals

Inc., NJ, USA as a 15% by weight aqueous solution. Alkoxysilanes for the sol-gel preparations were purchased from Gelest Inc. as well as Sigma-Aldrich. Alkylchlorosilanes were purchased from Aldrich Chemicals.

Atomic Absorption (AA) analyses were done on an S series Thermo Electron corporation AA spectrometer. Metal ion solutions were run in a 2% nitric acid solution and were diluted to give approximately 0.1-0.2 absorbance units. AA analysis was used to determine the metal ion remaining bound on the surface of composites by measurement of the difference between the total metal ion in the initial solution and the total metal ion in the filtrate and rinses. Solution silica concentrations were measured on a PerkinElmer ICPAES on the acidified leach solutions (5%HCl/5%HNO_3). Standards were run every 10-15 samples, and the initial leach solutions were examined to make sure they contained no silica. Mercury porosimetry measurements were performed on a 9500 Micromeritics Autopore Series Mercury Porosimeter operating at a maximum pressure of 36,000 psi, corresponding to a minimum intrusion diameter of 5nm. Elemental analyses were done by Galbraith Analytical Labs, Lexington, KY.

Scanning Electron Microscopy was performed using a Hitachi S-4700 Field Emission Scanning Electron Microscope at 3,000x and 20,000x magnifications. Sample preparation consisted of placing the sample on a conductive carbon tab on an aluminum stub. When necessary, samples were lightly sputter coated with a gold/palladium coating using a Pelco Model 3 Sputter Coater from Ted Pella Inc. Redding, CA.

Solid-state ^{13}C and ^{29}Si CPMAS NMR were done on a 500 MHz Varian NMR spectrometer using a 4mm rotor with parameters described in Figure 2.2. Solution-state ^{1}H

NMR was done on a 500 MHz Varian NMR spectrometer spinning at 20 Hz with a resonance frequency of 500 MHz.

Stock solutions of Cu^{2+} were prepared using $Cu(SO_4)\cdot 10H_2O$. Stock solutions of Cu^{2+} mixed with Fe^{3+} were prepared using $Cu(SO_4)\cdot 10H_2O$ and $Fe_2(SO_4)_3\cdot xH_2O$. Solution pH was adjusted from the intrinsic pH, where necessary, using hydrochloric acid or sodium hydroxide. Stripping and recovery of copper was achieved with 2 M-H_2SO_4. Metal standards for AA/ICP analyses were obtained from Fisher Scientific Co.

4.4.2. Synthesis of xerogels by the sol-gel method

Sol-gel syntheses used the two step process modeled after the work of Dong and Brennan.[72] To a 50 mL polyethylene beaker was added 6 mL of MeOH and 3.7 mL of pH = 2 HCl solution. To this mixture was added 20mL of a premixed solution in the desired ratios of: methyltrimethoxysilane (**MTMOS**), 3-chloropropyltrimethoxysilane (**CPTMOS**), and tetramethoxysilane (**TMOS**) or tetraethoxysilane (**TEOS**). These monomeric units were included in varying molar ratios for different studies.

After one hour of magnetic stirring, 3.7 mL of 7 M ammonium hydroxide was added to each sol-gel reaction. Upon gelation of the materials, stirring is stopped, and the mixture is allowed to age over night at room temperature. This step is followed by aging at 40°C for 24 hours followed by aging at 100°C for 24 hours. The materials are then crushed with a mortar and pestle and sieved to the desired particle size range, 250-600 μm for comparisons with commercial materials, and 150-250 μm for other studies.

4.4.3. Acid catalyzed sol step tracking via ^{1}H NMR

To a 20 mL polyethylene vial was added 600 μL MeOH and 370 μL pH = 2 HCl solution. To this was added 2 mL of premixed **MTMOS** and **CPTMOS** in a molar ratio of 4.5:1. The solution was mixed by pipetting up and down, then inserted into an NMR tube. ^{1}H NMR spectra averaged over three minutes were taken every three minutes to track the progression of the acid catalyzed polymerization step.

4.4.4. Conversion of the sol-gel xerogels to the polyamine composite BP-1

For gels with particle sizes 150-250 μm, the reaction of the resulting sol-gels with **PAA** was done by placing 2.0 g of sol-gel in a 250 mL 3 neck round bottom flask; 16 mL of methanol is added and the mixture degassed for 5 min. 64 mL of 15% by volume **PAA** is then added. The reaction mixture was then heated to 60-70°C and stirred for 48 h. The solution was decanted from the solid while still warm and then washed 5 times with 80 mL water, 1 time with 80 mL 1 M NaOH, 3 times with 80 mL water, 2 times with 80 mL MeOH, and 1 time with 80 mL acetone. All washes were stirred for 15min. After washing, the composite is dried over night at 70°C.

For gels with particle sizes 250-600 μm, the reaction of the resulting sol-gels with **PAA** was done by placing 5.0 g of sol-gel in a 250 mL 3 neck round bottom flask; 8 mL of methanol is added and the mixture degassed for 5 min. 32 mL of 15% by volume **PAA** is then added. The reaction mixture was then heated to 60-70°C and stirred for 48 h. The solution was decanted from the solid while still warm and then washed 5 times with 40 mL

water, 1 time with 40 mL 1 M NaOH, 3 times with 40 mL water, 2 times with 40 mL MeOH, and 1 time with 40 mL acetone. All washes were stirred for 15min. After washing, the composite was dried over night at 70°C.

Copper capacities for the sol-gel composites were determined as described in the equilibrium batch experiment below. Elemental analyses for the sol-gels are included in Table 4.2.

4.4.5. Method for calculating the number of surface anchor points per polymer molecule

The calculation of the number of surface anchor points per polymer molecule was performed using chlorine and nitrogen elemental analyses of the **CP** gels and corresponding **BP-1**'s. The method for this calculation is detailed in Section 3.4.6. of this document.

4.4.6. Silicate leaching protocol

The silica leaching was determined by placing 100 mg of composite in a 30 mL Nalgene screw cap bottle was added 0.5 mL of MeOH to wet the materials for testing. To this was then added 9.5 mL of pH = 10 NaOH solution. This mixture was allowed to equilibrate for 48 h, after which it was filtered using a 0.22 µm PES syringe filter and then analyzed for concentration of silicon via ICPAES after a 1:200 dilution with 2%HCl/2%HNO_3. Raw data were converted to ppm of SiO_2 and all the data are reported as SiO_2. All leaching experiments were done in triplicate and the error bars are based on the standard deviations of the triplicate data.

4.4.7. Equilibrium batch experiments

Batch extraction tests were conducted by adding 100 mg of **SPC** to 10 mL of metal solution at selected pH values. All batch extractions were done in triplicate. To ensure equilibrium, the metal ion and **SPC** mixtures were placed in a shaker bath. After 24 h the mixtures were allowed to settle. Each supernatant was extracted and diluted using a 2% nitric acid solution for analysis using the AA method.

4.4.8. Breakthrough column experiments

Breakthrough column experiments on **CuSelect** were conducted by packing a 5 mL plastic column fitted with frits on both ends and packed with 3.3 g of composite. The columns received flow from a variable flow FMI Lab Pump, Model QG150 from Fluid Metering Inc., NJ. The flow rate was 0.15 column volumes/minute. The column was conditioned for metal ion extraction by passing the following solutions in order:

1) 25 mL pH = 1.5 di H_2O
2) 300 mL pH = 1.5 aqueous solution of 1.7 g/L Fe^{3+} and 0.5 g/L Cu^{2+}
3) 20 mL di H_2O
4) 70 mL 2M H_2SO_4
5) 20 mL di H_2O

The breakthrough column experiment on **BP-2** was conducted by packing a 10 mL adjustable Omnifit glass column with 3.3 g of composite. The columns received flow from a variable flow FMI Lab Pump, Model QG150 from Fluid Metering Inc., NJ. The flow rate

was 0.15 column volumes/minute. The column was conditioned for metal ion extraction by passing the following solutions in order:

1) 25 mL pH = 2 di H_2O
2) 170 mL pH = 2 aqueous solution of 1.5 g/L Ni^{2+} and 1.5 g/L Cu^{2+}
3) 25 mL di H_2O
4) 50 mL H_2SO_4
5) 25 mL di H_2O

Fractions were taken every 10 mL and measured for metal ion content by AA analysis.

CHAPTER 5: HYDROGENATION OF OLEFINS‡

5.1 Introduction

Hydrogenation plays a central role in petroleum hydrotreating and upgrading processes, as well as in saturated oil hydrogenation processes in the food industry and in petrochemistry.[50] In addition to these bulk chemical processes, a large number of pharmaceutical and fine chemical syntheses target the selective hydrogenation of specific olefin bonds.[53] In industry, catalytic hydrogenations have been accomplished using heterogeneous systems because of their many advantages over homogeneous systems, such as catalyst stability, ease of separation of product from catalyst and a wide range of applicable reaction conditions. Homogeneous catalysts are preferred for selective organic transformations for fine chemical synthesis. In heterogeneous systems catalyst performance is strongly influenced by the nature of the support which controls molecular access to the active sites and can change electronic properties of supported catalytically active particles or complexes.[51,52] The most common type of heterogeneous catalysts are metal crystallites on metal oxide surfaces.[102] Often these metal crystallites are made by reduction of metal salts which have been adsorbed onto the metal oxide surface or by thermal decomposition of metal cluster complexes.[102,103] More recently, the immobilization of well-defined homogeneous catalysts on polymers and on surface-silanized silica gels has received considerable attention.[55,56] The utmost advantage associated with the last strategy resides in the ready recovery and reuse of the usually expensive catalysts through a simple filtration

‡This chapter was published as reference #30.

manipulation. The immobilization improves catalyst stability and increases regioselectivity, but often also decreases catalytic activity.[104]

We have been working with silica polyamine composites (**SPC**), organic–inorganic hybrid materials that offer the high ligand loading of polymeric supports and the greater porosity and matrix rigidity of amorphous silica. These patented and commercialized materials were developed as metal sequestering materials for the mining and remediation industries.[18-21,25-28,31] The fast capture kinetics that these materials exhibit also make them a promising platform for catalytic applications. Our initial investigation into using the **SPC** matrix for catalysis involved the immobilization of an EDTA ligand on the poly(allylamine) (**PAA**) **SPC**, **BP-1** ([poly(allylamine) on amorphous silica; Fig. 5.1] to form the composite called **BPED** (Fig. 5.1.).[105] Ferric ion was coordinated to this ligand-modified **SPC** and the system was examined for the selective oxidation of phenol to catechol. Using hydrogen peroxide as the oxidant, excellent selectivity and conversion were realized compared with homogeneous ferric ion and polymer supported catalysts.[105] The poly(ethyleneimine) (**PEI**) **SPC**, **WP-1** [poly(ethyleneimine) on amorphous silica] (Fig. 5.1) loaded with copper ion was also evaluated for this reaction and proved to be less efficient than the ferric system, although good conversions were observed. Given these initial results, we decided to investigate the catalytic activity of the **SPC** materials **WP-1**, **WP-2** (**WP-1** modified with chloroacetic acid), **BP-1** and **BP-2** (**BP-1** modified with chloroacetic acid; Fig. 5.1) loaded with simple salts of the transition metals Pd, Rh and Ru, towards the hydrogenation of olefins. The goal of these preliminary studies was to understand how the nature of the polymer (branched **PEI** vs linear **PAA**) and the nature of the coordinating ligand (amine vs amino acetate) influence the selectivity and catalytic activity of these metals immobilized on the **SPC** hybrid materials.

The results are compared with more conventional heterogeneous catalysts for hydrogenation, and an attempt has been made to characterize the nature of the active catalysts using X-ray photoelectron spectroscopy (XPS), transmission electron microscopy (TEM) and solid-state ^{13}C CPMAS NMR.

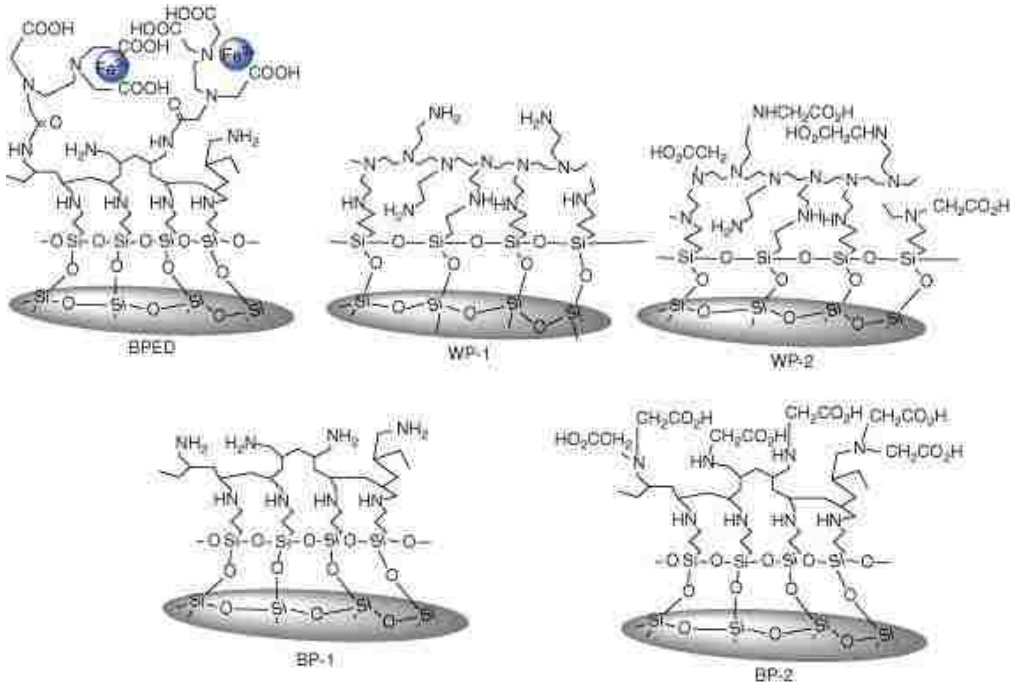

Figure 5.1. Schematic representations of the silica polyamine composites used in the catalytic studies

5.2. Results and Discussion

5.2.1. Metal Loadings

The metal loadings shown in Table 5.6 in the experimental section are in the range of 0.10–1.2 mmol g^{-1}. In general, the mmol g^{-1} of metal compound adsorbed reflects the expected ligand binding preferences of the three metals investigated. The Pd(II) loadings of

~0.65 mmol g^{-1} for the two amine based composites, **WP-1** and **BP-1**, are somewhat lower than reported in our previous studies on the adsorption of $PdCl_2$ on **WP-1** which had a loading of 0.95 mmol g^{-1} and where elemental analysis was in accord with the formation of a diammine, dichloro Pd(II) complex on the composite.[23] The high metal loading realized with **BP-2** can be rationalized in terms of our prior work which showed that this composite has a large number of 3-coordinate amino-acetate binding sites.[19] The $RuCl_3$ on the other hand shows its highest loadings on the carboxylate modified composites **WP-2** and **BP-2**, not surprising for this more oxophilic metal while $RhCl_3$ shows metal loadings that are intermediate between the high loading of Pd(II) on the amine ligands and the high loadings of Ru(III) on the carboxylate modified ligand, consistent with the intermediate hardness of Rh(III) relative to Pd(II) and Ru(III). There are two anomalous outliers to these trends, the exceptionally low loading of Rh(III) on **BP-2** (0.10 mmol g^{-1}) and the high standard deviation reported for $RhCl_3$ on **WP-1** the analysis was only done in duplicate because of sample shortage.

5.2.2. Hydrogenation Catalysis

The results of the hydrogenation experiments are summarized in Tables 5.1-5.4 for each of the four substrates investigated, 1-octene, 1-decene, 1-hexene and 1,3-cyclohexadiene. The turnover frequencies given in Tables 5.1-5.4 must be taken as minimum values because all of the experiments were done in 1 h and we cannot exclude the possibility that reaction reached equilibrium in less than 1 h. The turnover frequencies were calculated based on conversion to alkane and to cyclohexene in the case of the hydrogenation of 1,3-cyclohexadiene.

Composite	TOF (min^{-1})	TON	Percentage octane	Percentage 1-octene	Percentage isomerization
WP-1-Ru	0.51	30	2.4	7.8	89.8
WP-2-Ru	3.70	222	29.2	4.9	65.9
BP-1-Ru	1.34	80	10.5	68.0	21.5
BP-2-Ru	5.45	327	42.0	6.8	51.2
WP-1-Rh	4.19	252	46.5	9.1	44.4
WP-2-Rh	0.58	35	2.1	7.5	90.4
BP-1-Rh	14.9	896	69.5	1.1	29.4
BP-2-Rh	27.7	1664	25.6	0.1	74.3
WP-1-Pd	13.6	816	81.3	0.5	18.3
WP-2-Pd	26.0	1558	97.8	0.1	2.1
BP-1-Pd	15.2	911	95.9	0.2	3.9
BP-2-Pd	17.2	1032	99.8	0.1	0.1

TOF, turnover frequency.

Table 5.1. Hydrogenation of 1-octene at 90°C

Composite	TOF (min^{-1})	TON	Percentage decane	Percentage 1-decene	Percentage isomerization
WP-1-Ru	2.68	161	15.1	41.2	43.7
WP-2-Ru	0.98	59	9.3	63.2	27.6
BP-1-Ru	0.21	12	1.9	90.3	7.7
BP-2-Ru	2.26	136	20.9	64.4	14.6
WP-1-Rh	3.43	206	45.6	26.2	28.2
WP-2-Rh	10.6	636	46.5	0.7	52.8
BP-1-Rh	12.5	752	70.0	0.4	29.7
BP-2-Rh	34.5	2069	38.2	37.0	24.8
WP-1-Pd	10.0	602	71.9	0.2	28.0
WP-2-Pd	17.5	1048	78.9	0.0	21.1
BP-1-Pd	12.0	719	90.8	0.0	9.2
BP-2-Pd	14.3	861	99.9	0.0	0.1

TOF, turnover frequency.

Table 5.2. Hydrogenation of 1-decene at 90°C

Composite	TOF (min^{-1})	TON	Percentage hexane	Percentage 1-hexene	Percentage isomerization
WP-1-Ru	0.94	57	3.5	93.2	3.2
WP-2-Ru	0.36	21	2.3	94.5	3.2
BP-1-Ru	1.63	98	10.2	75.2	14.6
BP-2-Ru	0.54	32	3.3	92.6	4.1
WP-1-Rh	4.99	299	44.0	37.7	18.2
WP-2-Rh	17.3	1041	50.5	27.4	22.0
BP-1-Rh	9.81	589	36.4	53.6	10.0
BP-2-Rh	43.2	2594	31.8	8.7	59.5
WP-1-Pd	5.47	328	26.0	39.6	34.3
WP-2-Pd	12.6	756	37.8	5.3	56.9
BP-1-Pd	8.66	520	43.6	4.1	52.4
BP-2-Pd	7.79	467	36.0	2.6	61.4

TOF, turnover frequency.

Table 5.3. Hydrogenation of 1-hexene at 70°C

As expected, the results obtained for 1-octene and 1-decene at 90 °C are fairly similar. Hydrogenation efficiency decreases in the order Pd ≫ Rh > Ru and isomerization to internal olefins is highly competitive with reduction (Tables 5.1 and 5.2). The isomerization to hydrogenation ratio was higher for Ru and Rh catalysts, although previous work with heterogeneous Pd catalysts showed unusually high activity of palladium for olefin isomerization.[106] The higher reaction rates of the palladium based catalysts reported here apparently lead to low yields of isomers in the reaction mixture after 1 h.

Visual examination of the catalysts after hydrogenation revealed that in the case of Pd(II) on **WP-2 BP-1** and **BP-2** the catalysts had turned black indicating the formation of metal crystallites or nano-particles (see below). This was not the case for **WP-1**, which maintained the pale yellow color of the starting catalysts but still showed efficient hydrogenation relative to isomerization compared to any of the Ru or Rh loaded composites.

Pd(II) on **WP-1** thus represents a relatively unusual example of a heterogeneous Pd(II) olefin reduction catalyst.[51,106-108] The stability of Pd(II) on **WP-1** can be rationalized in terms of the branched nature of the polymer **PEI** and the expected lability of the acetate ligand which results in the formation of stable tetraammine complexes on the surface. The turnover numbers (TON) realized for Pd hydrogenations are comparable to other heterogeneous catalysts under similar conditions and catalyst loadings.[51,106] The one experiment where reduction of 1-octene differed drastically from the results for 1-decene was Rh on **WP-2**. Almost no reduction and almost complete isomerization was observed with 1-octene while for 1-decene almost equal amounts of reduction and isomerization were observed. This experiment was repeated but nonetheless seems anomalous in light of the similarity of these two olefins.

The complete conversion to octane observed for the Pd on **WP-2**, **BP-1** and **BP-2** prompted us to take a look at this reduction at shorter reaction times. Reactions done under the same conditions as in Table 5.1 but for 15 min revealed that complete conversion to octane was still observed for Pd on **BP-2**, making the turn-over frequencies shown in the table at least four times higher (Fig. 5.2). On the other hand, **WP-2** and **BP-1** showed conversion to 60% octane and 40% isomerized olefin, suggesting that the isomerized olefin can also be reduced by the Pd catalysts but at a lower rate than 1-octene.

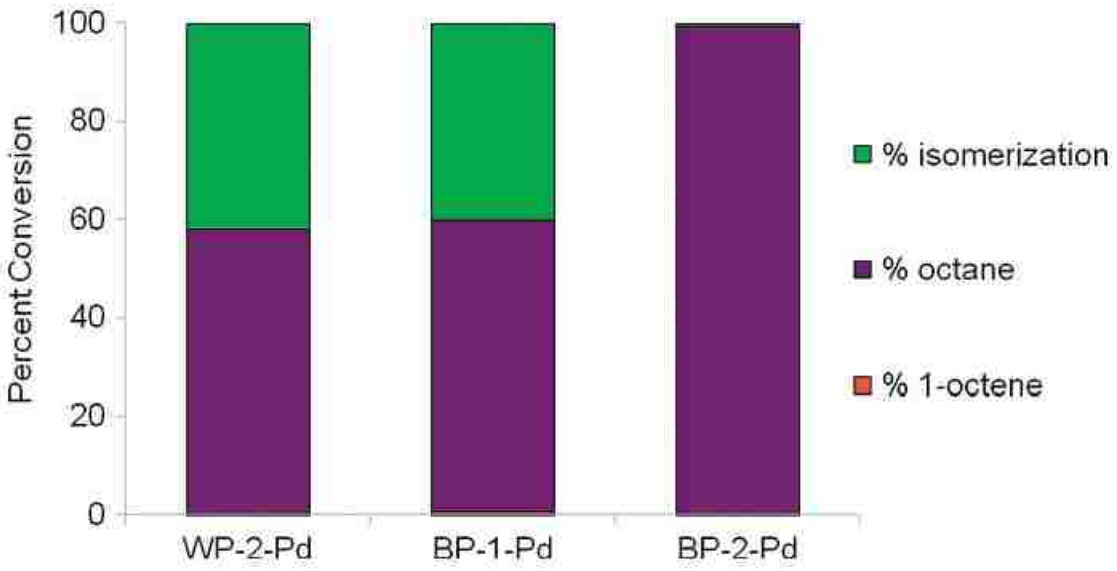

Figure 5.2. Hydrogenation of 1-octene at 90 °C and 5 atm hydrogen for 15 min using 10 mg of Pd on**WP-2**, **BP-1** and **BP-2**

The reduction of 1-hexene was studied at 70 °C with the composite catalysts and the results are summarized in Table 5.3. At 70 °C the Ru catalysts showed low activity for both reduction and isomerization. At 70 °C the Rh catalysts were more comparable to the Pd systems in terms of hydrogenation vs isomerization and, in one case, Rh on **WP-2**, a greater percentage of hydrogenation was realized than for any of the Pd systems. This suggests that reduction with Pd is dependent on the formation of the metallic Pd particles while isomerization is not.

The conversion of dienes to monoenes is one of the most useful applications of hydrogenation in petrochemistry. It is used for the removal of traces of 1,3-butadiene from the C4 fraction and for synthesis of cyclooctene from 1,5-cyclooctadiene and cyclododecene from 1,5,9-cyclododecatriene. The model hydrogenation of 1,3-cyclohexadiene at 50 °C was done with the desired goal of selective reduction to cyclohexene. Conjugated dienes are

usually more reactive than simple olefins. However, selectivity for the formation of monoenes with most heterogeneous catalysts is not high and the reaction does not usually stop at the monoene stage. The most active hydrogenation catalyst¸ Pd on **BP-2**, gave the lowest selectivity for this product while several of the Ru and Rh catalysts showed both excellent conversion and good selectivity for cyclohexene. Overall, the best combinations of selectivity and conversion for cyclohexene were realized for Ru on either **BP-1** or **WP-2** and Rh on **WP-2**. For the Pd catalyst, in which large crystallites of Pd were formed during the reaction, the activity observed was considerably higher with lower selectivity. Thus, formation of metal particles gives a catalyst that is too active for selective hydrogenation of conjugated dienes to monoenes.

Composite	TOF (min-1)	TON	Percentage Selectivity	Percentage cyclohexene	Percentage 1,3-cyclohexadiene	Percentage benzene	Percentage cyclohexane
WP-1-Ru	37.9	2275	96	68.9	25.5	2.7	2.9
WP-2-Ru	19.9	1194	97	92.4	0.0	4.8	2.8
BP-1-Ru	24.8	1491	96	93.7	0.0	2.8	3.4
BP-2-Ru	7.19	431	95	33.6	64.0	0.7	1.7
WP-1-Rh	22.7	1364	92	86.7	5.8	0.0	7.4
WP-2-Rh	46.3	2775	97	91.5	0.8	5.1	2.5
BP-1-Rh	18.6	1114	97	54.3	43.5	0.5	1.7
BP-2-Rh	174.7	10481	91	88.4	0.4	2.1	9.1
WP-1-Pd	14.9	891	95	61.0	28.6	7.2	3.1
WP-2-Pd	37.7	2265	89	81.0	0.0	8.8	10.2
BP-1-Pd	14.9	897	75	64.8	0.0	13.7	21.5
BP-2-Pd	9.27	556	46	42.2	0.0	7.8	50.0

Table 5.4. Hydrogenation of 1,3-cyclohexadiene at 50°C

Interestingly, small to moderate amounts of benzene were formed in all cases, suggesting that hydrogen transfer catalysis is an accessible side reaction in these systems. The disproportionation of cyclohexene to cyclohexane and benzene is irreversible.[109] The Pd

catalysts showed the largest amounts benzene and this contributes to the lower selectivity for cyclohexene.

5.2.3. Characterization of the Surface Bound Catalysts

To gain a better understanding of the changes that the catalysts undergo after use, we recorded the TEM images and XPS of the starting metal loaded composites before and after hydrogenation of 1-hexene at 70 °C for 1 h. Binding energies for the observed spectral lines of the metals are summarized in Table 5.5 and the assignments are based on comparison with related compounds in the NIST XPS database.[110] It is not possible to match the actual values of the binding energies to a specific compound(s) because of the amorphous nature of the surface that provides many related but slightly different environments for the metal sites. The purpose of these measurements was to provide some insight into the stability of the surfaces.

	Rh 3d 5/2	Rh 3d 3/2	Ru 3p	Pd 3d 5/2	Pd 3d 3/2
WP-1	313.8	309.8	463.2	343.4	338.2
WP-2	313.2	309.2	461.5	344.9	338.9
BP-1	313.4	309.4	463.9	344.0	338.8
BP-2	311.6	Not resolved	462.8	342.4	338.0
WP-1 used	314.6	309.8	463.4	343.6	338.4
WP-2 used	314.4	309.2	463	343.8	339.4
BP-1 used	314.2	309.8	457.8	344.5	342.1
BP-2 used	312	308	463	Not observed	

Table 5.5. XPS binding energies for metal loaded composites before and after catalysis (eV)

The TEM images of $Pd(OAc)_2$ on **WP-1** before and after use are shown in Fig. 5.3 with the Pd region of the XPS spectrum in the inset. The binding energies correspond to Pd(II) with amine ligands.[110] Deconvolution of the data revealed that Pd(0) (binding energy 336.1–336.3 eV[111]) can be present in small amounts but the surface contains predominantly Pd(II) complexes (Fig. 5.4).

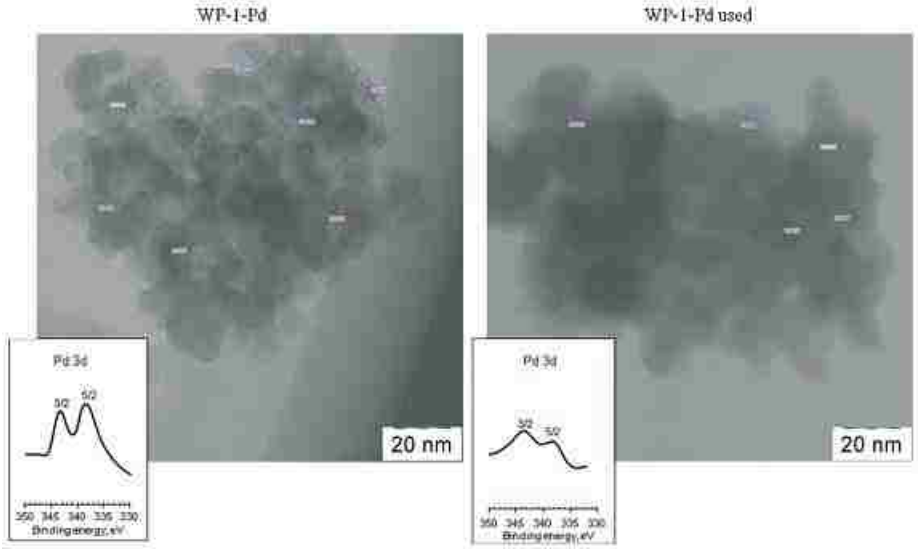

Figure 5.3. TEM images of $Pd(OAc)_2$ on **WP-1** before and after hydrogenation catalysis with Pd portion of the XPS spectrum in the inset

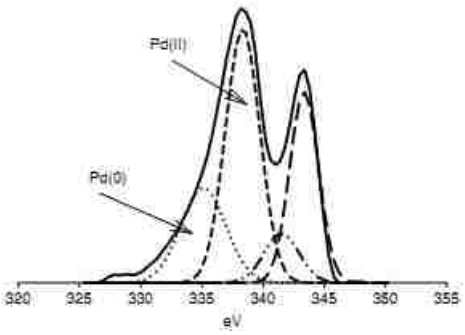

Figure 5.4. Deconvolution of XPS spectral lines for Pd on **WP-1**

It can be seen that, although the XPS is somewhat degraded after use, the same two binding energies are observed and the TEM shows no evidence of the formation of metal nanoparticles of more than 1 nm. This suggests that hydrogenation with this composite is accomplished with Pd(II) with a small quantity of Pd nanoclusters. The degradation of the signal is probably due to interference by organic residues because the samples were allowed to evaporate at ambient temperature and heated gently on a hot plate to dryness before running the XPS. On the other hand, the TEM image of $Pd(OAc)_2$ on **BP-2** clearly shows the formation of metal nanoparticles with diameters in the 5–20 nm range (Fig. 5.5). The XPS spectral lines completely disappear, indicating that the starting Pd(II) species are gone. No XPS signal is observed for the presumably Pd(0) nanoparticles, probably because they reside below the 10 nm depth range of the incident X-Rays. $Pd(OAc)_2$ on **BP-1** and **WP-2** each show similar behavior with the formation of nanoparticles and significant degradation of the XPS lines (see Supporting Information). These results point to the increased stability of Pd(II) on the branched amine polymer **PEI** and suggest that the catalysis by Pd on the other composites is due to the nanoparticles. The ratio amine/metal by XPS is considerably higher for the **WP-1** sample (6.0) compared with the **BP-1** one (2.4). This fact indicates a particular envelopment of the metal ion by the branched polymer chains. After the reaction, the ratio of C/N increases sharply from 3–8 to 12–70. It is likely that the hydrocarbon substrate is absorbed by the metal loaded composite and does not desorb entirely during drying.

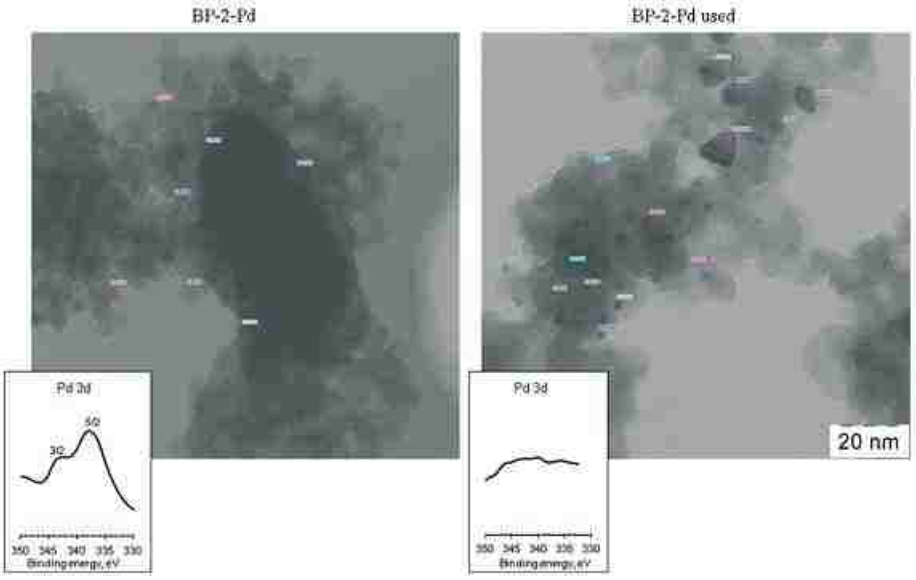

Figure 5.5. TEM images of $Pd(OAc)_2$ on **BP-2** before and after hydrogenation catalysis with Pd portion of the XPS spectrum in the inset

The $RuCl_3$ and $RhCl_3$ on all four composites do not show the formation of nanoparticles based on their TEM images (Figs 5.6 and 5.7). XPS of the 3p spectral line of Ru and the 3d5/2 and 3d3/2 spectral lines of Rh show some degradation as for the Pd loaded composites and, in the case of $RhCl_3$ on **BP-2**, a single broad signal is observed which we suggest is an overlap of the two spectral lines. Unfortunately, XPS of the 3p spectral line for Ru(II) and Ru(III) and the 3d5/2 and 3d3/2 spectral lines of Rh(I) and Rh(III) give very similar binding energies that are very sensitive to ligand environment. Therefore, it is not possible to assign oxidation states to the metals on the composites based on this XPS data. Given the observed activity, it seems likely that the metal species on the surface are Ru(II) and Rh(I) or a mixture of these and their corresponding higher oxidation states. It is well known that amines and alcohols can reduce the Ru(III) and Rh(III) to their lower oxidation states in the presence of chelating or strongly electron donating ligands.[85,112]

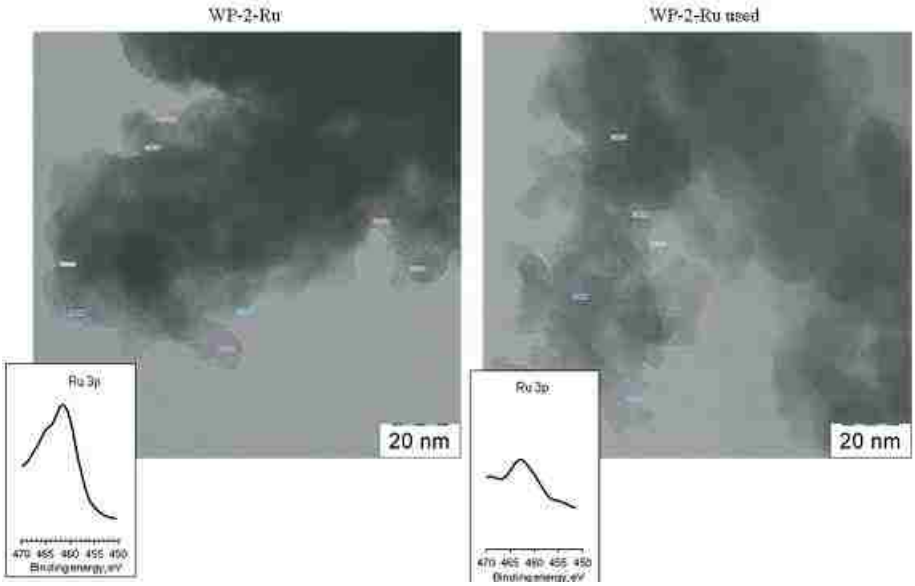

Figure 5.6. TEM images of $RuCl_3$ on **WP-1** before and after hydrogenation catalysis with Ru portion of the XPS spectrum in the inset

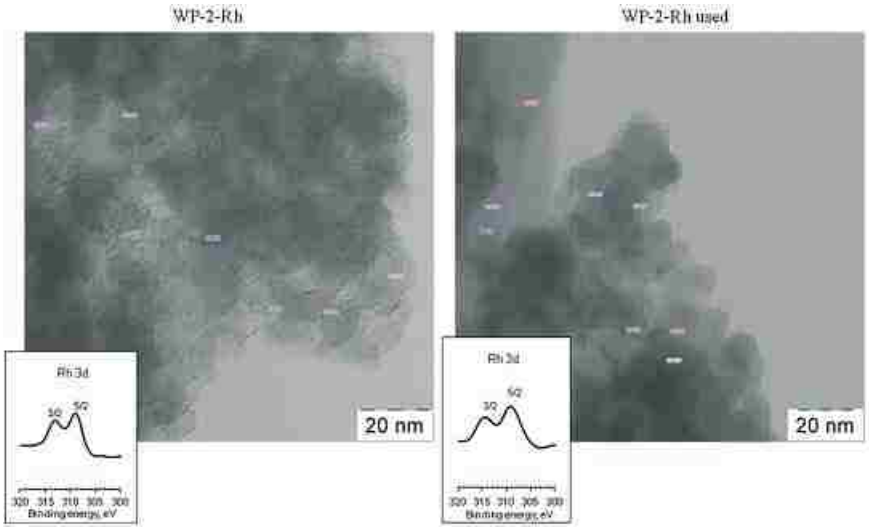

Figure 5.7. TEM images of $RhCl_3$ on **WP-2** before and after hydrogenation catalysis with Rh portion of the XPS spectrum in the inset

Convincing evidence that the $RhCl_3$ on the carboxylate modified composites is covalently bound to the aminoacetate ligand comes from a comparison of the solid-state ^{13}C CPMAS NMR of **WP-2** before and after metal loading (Fig. 5.8). The carboxyl resonance is considerably broadened while the other resonances remain unchanged. The resonance shows 'wings' in addition to broadening and we interpret this in terms a family of overlapping $^{2}J^{13}C–^{103}Rh$ doublets. We tentatively extrapolate this result to the other composites and suggest that the metals are all covalently bound to the polymer except in the cases where they convert to nanoparticles during their use as catalysts.

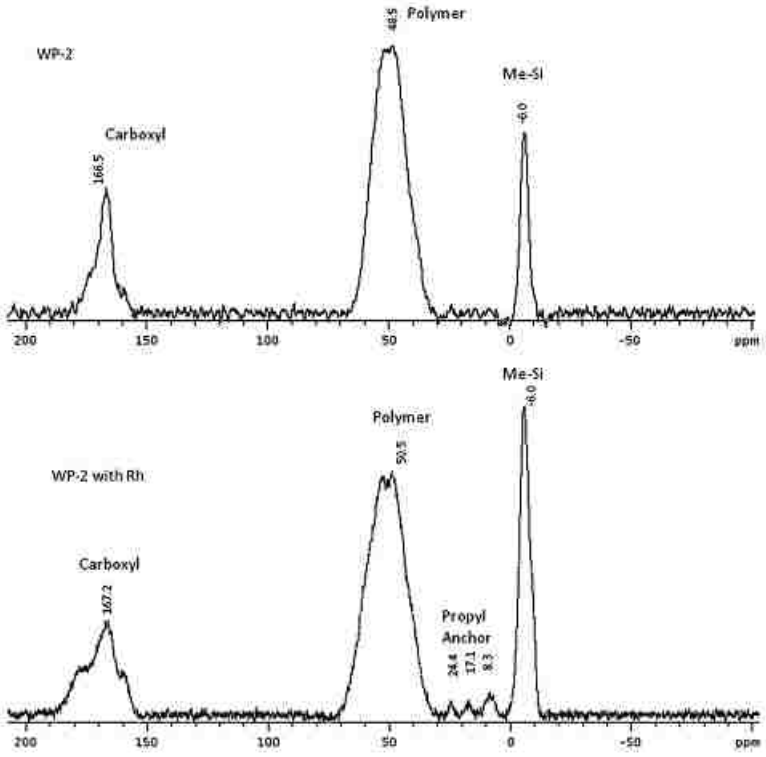

Figure 5.8. Solid state ^{13}C CPMAS NMR of $RhCl_3$ on **WP-2** showing the $^{2}J^{13}C$-^{103}Rh satellites on the carboxyl resonance of the aminoacetate ligand

In light of the very different behavior of **BP-1** vs **WP-1** when loaded with $Pd(OAc)_2$, where **BP-1** goes to mainly Pd nanoparticles and **WP-1** remains mainly as a complex after catalysis (see above), we decided to investigate the ^{13}C NMR of these systems. The solid-state CPMAS ^{13}C NMR of $Pd(OAc)_2$ shows two relatively sharp resonances at 187.5 and 185.8 ppm for the carboxyl carbon (Fig. 5.9b). The solid-state structure of $Pd(OAc)_2$ consists of triangle of Pd atoms with two bridging acetates on each edge of the triangle.[113] All the acetate carbons should be equivalent according to the crystal structure but neighboring molecules in the crystal could make some of them magnetically non-equivalent. The ^{13}C NMR of **BP-1** loaded with $Pd(OAc)_2$ shows a single broader peak at 178.2 ppm and two lower intensity peaks at the same chemical shift as $Pd(OAc)_2$

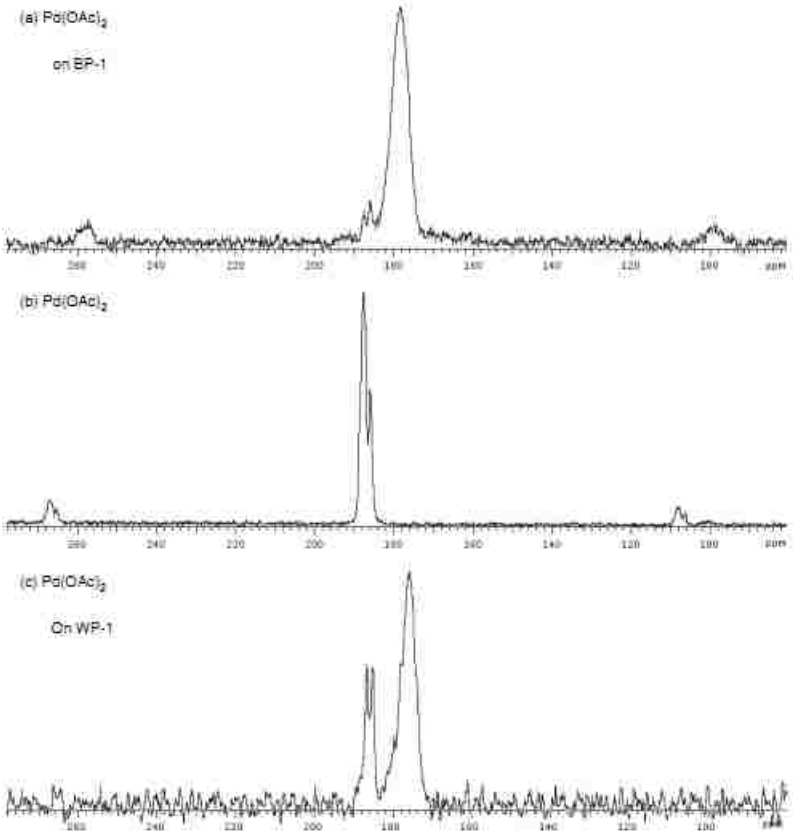

Figure 5.9. Solid-state CPMAS ^{13}C NMR of : (a) Pd $(OAc)_2$ on **BP-1** before catalysis; (b) $Pd(OAc)_2$; c) Pd $(OAc)_2$ on **WP-1**

Given that the reported chemical shift for acetate anion is 182 ppm and that for bridging acetates in Pd complexes containing nitrogen ligands is also 182.2 ppm, we tentatively assign the peak at 178.2 ppm to an acetate group terminally coordinated to Pd.[114,115] This assignment is supported by the fact that coordination of acetate to a Lewis acid leads to upfield shifts of the carboxyl carbon.[116] The ^{13}C NMR of $Pd(OAc)_2$ on **WP-1** shows the $Pd(OAc)_2$ resonances at much higher intensity relative to the resonance at 175.7 ppm assigned to acetate terminally coordinated to Pd. The possibilty of the coordination up to three or four amines with the branched polymer, **PEI**, on **WP-1** would be expected to produce fewer terminally coordinated acetates and leave more starting $Pd(OAc)_2$, and in our prior work we showed that average coordination numbers for **BP-1** and **WP-1** are 2 and 4, respectively.[19,31] These results present evidence to suggest that stability of the $Pd(OAc)_2$ on **WP-1** is indeed due to the formation of mainly di- and triamine complexes

5.3. Conclusions

These studies have demonstrated that adsorption of simple transition metal salts on **SPC** can give a family of catalysts that can reduce alkenes and dienes with some selectivity. The Pd catalysts are the fastest for reducing terminal olefins and, although isomerization is faster than reduction, the resulting internal olefins are still reduced. The Rh and Ru catalysts are much slower for reduction of monoenes but show good selectivity for the reduction of 1, 3-cyclohexadiene to cyclohexene, and this is potentially the most useful outcome of this

work. The conversion of $Pd(OAc)_2$ into nanoparticles for **WP-2**, **BP-1** and **BP-2** but not for **WP-1** is interesting from two points of view. First, the **SPC** environment can be made selective for the generation of nanoparticles. Second, the use of the unmodified branched polymer **PEI** generates an unusual example of a Pd(II) hydrogenation catalyst. Although there were significant differences in the catalytic properties of a given metal on the four different composites, no apparent trends emerged. The main problem with these systems at the time of this writing is the difficulty in fully characterizing the catalytic sites. It is anticipated that further NMR studies, magnetic measurements and EXAFS measurements will address this issue.

5.4. Experimental

5.4.1. Materials and Methods

$Pd(OAc)_2$, $RhCl_3 \cdot 4H_2O$ and $RuCl_3 \cdot nH_2O$ (n = 1–3) were obtained from Strem Chemicals and used as received. 1-Hexene, 1-octene, 1-decene and 1,3 cyclohexadiene were obtained from Aldrich and used as received. The composites **WP-1**, **WP-2**, **BP-1** and **BP-2** were synthesized according to published literature procedures using commercially available silica gel (INEOS or Qing Dao Mei Gao, 10 nm average pore diameter, 150–250 μm particle size, 450 $m^2\ g^{-1}$ surface area).[19]

The metal loaded composite samples were investigated by X-ray photoelectron spectroscopy (XPS) with an LAS-3000 instrument equipped with a WER-150 photoelectron retarding-potential analyzer. For photoelectron excitation, aluminum anode radiation (Al K = 1486.6 eV) was used at a tube voltage of 12 kV and an emission current of 20 mA. Photoelectron peaks were calibrated with reference to the carbon C 1s line corresponding to a

binding energy of 285 eV. Transmission electron microscopy (TEM) was performed with an LEO912 AB Omega transmission electron microscope. Catalyst loadings on the composites were measured on digested samples[117] using a Perkin Elmer inductively coupled plasma–atomic emission spectrometer (ICP-AES) on the acidified leach solutions with standards run every 10–15 samples. Solid-state ^{13}C CPMAS NMR spectra were recorded on a Varian NMR Systems 500 MHz spectrometer using parameters outlined in Figure 2.2.

5.4.2. Preparation of the Metal Loaded Composite Samples

$RhCl_3 \cdot 4H_2O$ (41 mg) or $RuCl_3 \cdot nH_2O$ (n = 1–3; 31 mg) was combined with 100 mg of **WP-1**, **WP-2**, **BP-1** or **BP-2**. To the mixture of these solids was added 30 mL of deionized water and the mixture was stirred with a magnetic stir bar for 1 h. After this time all the solid metal salt appeared to dissolve and a color change of the composite to light orange for Rh and to black for Ru indicated metal loading. $Pd(OAc)_2$(24 mg) was loaded on the composites by mixing it with 150 mg of **WP-1**, **WP-2**, **BP-1** or **BP-2**. To this 7 mL of chloroform was added and the mixture was stirred magnetically for 6 h at reflux (65 °C). The samples were light to medium tan after loading. Subsequent samples were also made using larger amounts of composite and metal salt and proportionately larger volumes of solvent. All samples were filtered and rinsed twice with the same volume of solvent used in the loading procedure and for the rhodium and ruthenium samples a 10 mL rinse of acetone was used to facilitate drying. After loading the samples were placed in glass vials and gently heated on a hot plate. Metal loading was evaluated by digesting 1–3.5 mg of loaded composite in 0.25 ml concentrated H_2SO_4 and 0.25 mL concentrated H_3PO_4. The resulting mixture was heated at

~80 °C in a steam bath for 1 h and 2.0 mL freshly prepared aqua regia was added after cooling. The mixture was then heated again at 80 °C for 1 h, during which time significant bubbling of the solution was noted.[117] These samples were diluted to 10 mL in a volumetric flask and metal concentrations were determined by ICP-AES. Metal loadings are listed in Table 5.6.

Catalytic System	Average loading (mmol g^{-1})	SD (mmol g^{-1})
WP-1-Ru	0.50	0.16
WP-2-Ru	0.84	0.03
BP-1-Ru	0.83	0.16
BP-2-Ru	0.82	0.04
WP-1-Rh	1.18	0.72
WP-2-Rh	0.39	0.05
BP-1-Rh	0.49	0.02
BP-2-Rh	0.10	0.01
WP-1-Pd	0.63	0.07
WP-2-Pd	0.40	0.03
BP-1-Pd	0.67	0.08
BP-2-Pd	0.62	0.16

Table 5.6. Loading of metal ions on composites

5.4.3. Hydrogenation Catalysis Experiments

All catalytic runs were done in a 30 mL water jacketed pressure reactors that were fitted with magnetic stir bars, and hot water was circulated through the jacket by a MLW temperature controlled hot water circulator. The reactor was charged with 10 mg of catalyst and 1.0 mL of substrate. In the case of 1-octene with Pd loaded **WP-2**, **BP-1** or **BP-2**, one additional experiment was run for only 15 min. The reactor was pressurized to 5 atm with

hydrogen and the reactions were run for 1 h at 50, 70 or 90 °C. After reaction the reactor was cooled by flushing the jacket with cold water until cool to the touch and then carefully depressurized. The cooled reaction mixture was diluted with 5.0 mL of diethyl ether, the composite was allowed to settle and then a 0.5–2.0 μL sample of the diluted supernatant was analyzed by gas chromatography using a 0.25 mm i.d. 30 m SE-30 non-bonded silicone gum column on a Chrompack chromatograph using a flame ionization detector and hydrogen as the carrier gas. Peak areas were evaluated with a digital integrator using the Maestro chromatography data system version 1.4. Retention times for the reactants and products were obtained by comparison with authentic samples.

CHAPTER 6: CONCLUSIONS AND FUTURE WORK

6.1. Surface Coordination Environments

The oxidation of Co^{2+} to Co^{3+} was shown to be the cause of irreversible binding of cobalt on the surface of **WP-1**. The same effect was not observed on the surface of **BP-1**. The chelation effect seen with the branching polymer **PEI** on **WP-1** is evident as the source of the ligand field stabilization that allows for this effect. The linear polyamine **PAA** does not have the ability to reach high enough coordination numbers to achieve sufficient ligand field stabilization to allow the Co^{2+} to Co^{3+} oxidation to occur.

Studies into the irreversible binding of cobalt on **WP-1** showed a dependence upon the presence of oxygen. This is direct evidence that the irreversible binding is due to the oxidation of cobalt from its divalent to its trivalent state. Evidence of the full conversion of Co^{2+} to Co^{3+} is found in the ^{13}C NMR of **WP-1** before and after coordination with cobalt. The cobalt coordinated **WP-1** was found to have a nearly identical ^{13}C NMR, where the presence of any Co^{2+} would be expected to cause significant paramagnetic broadening of the spectrum. This is corroborated by the UV-Vis spectra of cobalt bound to **PEI** in solution. When compared with known Co^{3+} amine complexes, the absorption spectra were very similar.

The UV-Vis spectrum of cobalt coordinated to **PEI** in solution was also closest to that of the Co-tren complex, supporting the view that **PEI** is generally a tetracoordinate chelating polyamine. IR spectra of the Ru complex $[Ru(CO)_3(TFA)_3]^-K^+$ (**1**) on **WP-1** and **BP-1**

distinctly show the differences between the coordination environments present on each of these materials. Ligand replacement motifs for **1** indicate that the general coordination number for **WP-1** is 4, and that the general coordination number for **BP-1** is 2. The low coordination number for the cobalt-**PAA** complex does not supply sufficient ligand field stabilization, explaining the lack of oxidation of Co^{2+} on the surface of **BP-1**.

Additionally, this shows that **1** will be a useful probe for studying coordination geometries of surface bound ligands to transition metals. ^{13}C NMR studies on ^{13}CO enriched **1** also show that a certain small number of the branched sites are in close enough proximity to result in the formation of $M_2\mu CO$ species.

6.2. Surface Stability

Silica surfaces are subject to degradation by aqueous solutions at alkaline pH. Batch measurements of silica based materials at pH = 10 have shown that the use of bulky, hydrophobic silanes is only marginally effective in mitigating the rate of leaching.

Silica-based materials show significant increases in silicate leaching on binding of the polymer to the silanized surface. This serves as evidence that the polyamine undergoes direct interaction with the surface, promoting surface hydrolysis and therefore silicate leaching. Functionalization of the amine with an acetate ligand nullifies this effect, further supporting the concept that it is direct interaction of the amine with the silicate surface which is causing the increased leaching effect. The previously described effects suggest that surface pH and zeta potential have profound effects upon the process of surface silicate leaching.

Sol-gel synthesized materials offer an alternative to conventionally produced silica gels. It was expected in the design of the materials that improvements could be made in the surface stability to alkaline conditions. Alkaline stability, however, was similar to that of conventional silica gels, though introduction of the polyamine does not result in the increased silicate leaching that is found for conventional silica. The ^{29}Si NMR studies reported in chapter 3 show more complete coverage of the sol-gel surface by T_3 sites relative to T_2 sites.

Elemental analyses have shown that polyamine loading on the surface of silica composites is only marginally affected by the number of surface anchor points covalently bound to the polymer. This is also evidenced by the comparable copper capacities of **CMPh BP-1** and 7.5:1 **M:CP BP-1**.

6.3. Sol-gel SPC Analogs

Conventional silica gels have shown many favorable characteristics when compared with commonly used commercial ion-exchange materials. The sol-gel based materials reported here have many of the characteristics of the commercially produced **SPC** materials.

Sol-gel analogs of **SPC** materials demonstrated a degree of control over pore size and average pore size distributions. Both polymer immobilization and amine modification with bulky ligands have been shown to render the smaller pores on the surface of these composite materials unusable. Control of average pore size diameters would allow for selection of a more desirable average pore diameter relative to those found in conventional **SPC** materials.

Silicate leaching at pH = 10 for sol-gel materials with low relative amounts of **MTMOS** is similar to that of conventional **SPC** materials. Materials with higher relative amounts of **MTMOS** were found to have increased levels of silicate leaching at pH = 10.

This is attributed to decreased steric hindrance and hydrophobicity due to the smaller size of the methyl group relative to the 3-chloropropyl group. The binding of **PAA** to the sol-gel composite surface showed significant decreases in surface silica leaching, which is attributed to the surface undergoing a reorganization which allows the T_2 and Q_3 sites to finish polymerization. This also shows that the polymer-surface interactions seen with conventional **SPC** materials do not occur with the sol-gel materials.

The introduction of **TMOS** showed improvements in composite performance. Pore size distributions were narrower for sol-gel **BP-1** samples with high levels of **TMOS** relative to those with little **TMOS** and those made from conventional silica. The internal framework resulting from the introduction of bulk siloxane also caused increased availability of surface halocarbons and reduced alkyl group internalization.

BP-1 copper capacities in the 62:30:1 **TMOS:MTMOS:CPTMOS** sample were greater than those of conventional materials, showing the potential to be used as a replacement matrix for ion exchange purposes.

Equal or greater batch copper capacities were expressed for sol-gel derived **BP-2** relative to conventional silica **BP-2**. **BP-2** ligand loading was lower in the sol-gel materials than in the conventional silica **BP-2**, however; this did not seem to affect copper capacity.

Lower batch copper capacities were expressed for sol-gel derived **CuSelect**. This observation is evidence that the pores are still too small to prevent blockage from the bulky picolylamine groups, and that the dominant factor in this case appears to be ligand loading, which was lower for the sol-gel material relative to the conventional **CuSelect**. Selectivity

for the sol-gel **CuSelect** in breakthrough experiments competing with iron was 40:1 (Cu^{2+}:Fe^{3+}), which is significantly less than the 67:1 selectivity for conventional **CuSelect**.

6.4. Hydrogenation of Olefins

The adsorption of simple transition metal salts on the **SPC** materials **WP-1**, **WP-2**, **BP-1**, and **BP-2** gave a family of catalysts that hydrogenate alkenes and dienes with some selectivity. Both TEM and XPS were invaluable in the characterization of these **SPC** supported transition metal catalysts.

The conversion of $Pd(OAc)_2$ into nanoparticles for **WP-2**, **BP-1**, and **BP-2** but not for **WP-1** shows an unusual example of a Pd(II) hydrogenation catalyst. The formation of Pd nanoparticles was seen to occur at elevated temperature, and hydrogenation was dependent upon nanoparticle formation while isomerization was not.

The Pd catalysts expressed the highest hydrogenation efficiency in most cases, and were also the most active. Isomerization was found to be faster than hydrogenation in the case of the Pd catalysts, though the resulting internal olefins were still reduced. The Rh and Ru catalysts had much lower TOF, but showed good selectivity for the reduction of 1,3-cyclohexadiene.

In the case of 1,3-cyclohexadiene, several Ru and Rh catalysts showed both excellent conversion and good selectivity for conversion to cyclohexene. The best combinations of selectivity and conversion were realized for Ru on **BP-1**, Ru on **WP-2**, and Rh on **WP-2**. Pd catalysts were found to be too active for selectivity in this case, and as such were found to be non-selective. Small to moderate amounts of benzene were formed in all cases, suggesting

that hydrogen transfer catalysis is an accessible side reaction for these systems. The Pd catalysts showed the largest amounts of benzene formation.

6.5. Future Work

6.5.1. Luminescence

Silicon nanoparticles have been found to exhibit strong visible emission. The wavelength of this emission is also tunable based upon the nanoparticle size.[102-105,117] The emission characteristics of silicon nanoparticles have also been found to be conserved upon modification of the silicon surface and functionalization with low molecular weight polymers.[106-108,117] When the excitation of the silicon nanoparticles with λ_{ex}=340 nm and λ_{em}=400-450 nm is combined with the **MLCT** of surface Ru(II)diimine complex, the fluorescent resonance energy transfer (**FRET**) can then be made to result in the conversion of ultraviolet (**UV**) to visible light (Figure 6.1). This then has the potential to be used for various applications, including increasing the efficiency of solar cells. Luminescence observed in this manner can also be used as a detector of trace metals which luminesce at different λ_{em} on the surface complex.[33,109] These studies are already underway and are a significant effort in the current research group.

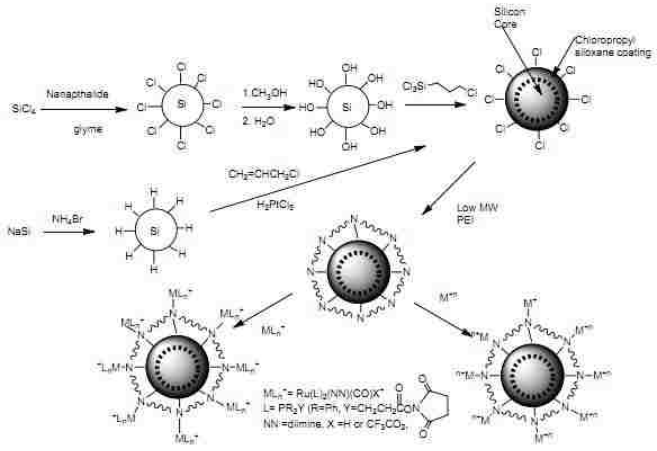

Figure 6.1. Schematic of synthesis of a silicon nanoparticle utilizing FRET for the conversion of visible light to UV.

6.5.2. T1ρ NMR calculations

T1ρ is defined in NMR as the relaxation in the rotating frame. T1ρ is strongly related to T1, the spin-lattice relaxation time, but with the slight difference that the relaxation time is measured while maintaining not only a constant magnetic field B_0, but also a time-dependent magnetic field with a much lower magnitude, B_1. B_1 rotates in the plane transverse to the vector of the field B_0, and does so at the Larmor frequency of the nucleus being measured. T1ρ is the decay constant for recovery of magnetization along B_1. This is a slower process and provides information on slower movements of nuclei.[127]

This could provide valuable information on the surface characteristics of **SPC** and sol-gel materials. **SPC** materials synthesized using bulky aromatic anchors would theoretically show significantly altered T1ρ measurements based upon their environments, and this

technique could further characterize these systems. Sol-gel materials cross-linked with **TMOS** will show significantly altered T1ρ times, and these will be indicative not only of surface environments, but also of matrix effects.[127,128]

6.5.3. Sol-gel ^{29}Si NMR rate constant calculation

Prior art[96] has shown that the use of solution-state ^{29}Si NMR can be employed on two-component sol systems to measure rate constants for cross-condensed species. A series of experiments utilizing the reaction conditions outlined in Section 4.4 can be used to determine rate constants for the sol step of the polymerization. Using various molar ratios of **TMOS:MTMOS:CPTMOS**, the self-polymerization rate constants can be calculated for each monomeric unit, then compared with the cross-condensation products for two-component mixtures for each of the three possible combinations (**TMOS:MTMOS, TMOS:CPTMOS,** and **MTMOS:CPTMOS**), and also to the cross-condensation products for the three component mixture. The changes in rate constants relative to concentrations in the three component mixture could provide a wealth of information in the tailoring of sol-gel materials for specific purposes.

6.5.4. Sol-gel characterizations

Longevity testing of sol-gel materials has yet to be performed. The ability of the material to withstand extended wash-load-strip-regeneration cycles is crucial to its use as an ion exchange resin. Along the same vein, testing of the mechanical strength of the material will be necessary. Mechanical strength will be measured through particle attrition under

agitation, by measuring the amount of crushing observed when the material is water-immersed and rolled in a bottle for a set period of time.

Additionally, adjustments in the acid-catalyzed step such as duration and concentration of acid must be modified with sol-gels using high levels of **TMOS**. The **TMOS** increases cross-linking, leading to smaller pores. Some ligand modifications, such as **CuSelect** would benefit from the production of a gel with slightly larger average pore size diameters. Further investigations with other ligand modifications such as **BPAP** and **BPED** on the sol-gel materials is warranted as well.

6.5.5. Further Catalysis Testing

The selective catalytic conversion of conjugated dienes to monoenes has very high industrial potential. Further investigations using Ru and Rh catalysts immobilized on **SPC** matrices warrants immediate notice. In particular, selective hydrogenation of 1,3-butadiene would be of great value in the petroleum industry.

Further studies of the already investigated catalytic systems for quantitative TON and TOF measurements would provide valuable insight as to the relative activity of these catalysts. Relative specificities for isomerization and hydrogenation could also be measured in catalytic reactions using lesser quantities of catalyst.

6.5.6. Catalytic Site Characterization

Beyond further measurements of catalytic activity, the characterization of the catalytic sites and the differences in the matrices causing the different activities is important for the further development of these systems. NMR studies of the catalysts bound to the **SPC** matrix

such as those in Section 5.2.3 have the potential to elucidate structural information that can help to explain the matrix effects on the catalysts. Extended X-Ray Absorption Fine Structure (EXAFS) can also be used for characterization of these materials. EXAFS has the potential to show whether metal binding occurs with agglomeration or whether it is uniformly spread across the surface.

BIBLIOGRAPHY

1. Feynman, Richard; "The Character of Physical Law", Random House, Inc., New York, 1994.
2. Giddings, J Calvin. "Unified Separation Science", Wiley Interscience, New York, 1991.
3. McCash, Elaine M. "Surface Chemistry", Oxford University Press, Oxford, 2001.
4. Iler, R. K. The Chemistry of Silica, Wiley Interscience, New York, 1978.
5. Alkan, M; Dogan, M. "Silica gels surface chemistry," in Encyclopedia of Surface and Colloid Chemistry, Somasunderan, M, Ed, Taylor and Francis, New York, Volume 7, p5608.
6. Scott, R. P. W. Silica Gel and Bonded Phases, John Wiley and Sons, New York, 1993.
7. Papirer, E. Ed. "Adsorption on Silica Surfaces, Marcel-Dekkar, New York, 2000.
8. Warshawsky, A. "Modern Research in Ion Exchange" in Science and Technology, Rodrigues, A. (Ed.) Martinus Nijhoff Publishers, Dordrecht, 1986
9. Dias-Filho, N. L.; Gushikem, Y *Sep. Sci. and Tech.* **1997**, *32* 2335.
10. M. E. Mahmoud, M. E.; Soliman, E. M *Journal of Liquid Chromatography* & *Related Technologies* **2003**, *26*, 3045.
11. Soliman, E. M. *Analytical Letters* **1997**, *30*, 1739.
12. Dey, R. K.; Jha, U.; Patnaik, T.; Singh, A. C.; Singh, V. K. *Sep. Sci. and Tech.* **2009,** *44*, 1829
13. Wang, J.; Zhang, D.; Lawson, T. R.; Bartsch, R. A. *Talanta* **2009** ,*78*, 477.
14. Hughes, M.; Miranda, P.; Nielsen, D.; Rosenberg, E.; Gobetto, R.; Viale, A.; Burton, S. I n *Recent Advances and Novel Approaches in Macromolecule-Metal Complexes*, Eds. Barbucci,R.; Ciardelli, F.; Ruggeri, G. Wiley-VCH (Macromolecular Symposia 235), Weinheim, 2006, p 161.
15. Hughes, M.; Nielsen, D.; Rosenberg, E.; Gobetto, R.; Viale, A.; Burton, S. D *Ind. Eng. and Chem. Res.* **2006**, *45*, 6538
16. Hughes, M.; Rosenberg, E. *Sep. Sci. and Tech.***2007** *42*, 261.

17. Berlin, Matt; Allen, Jesse; Rosenberg, David; Rosenberg, Edward. Nanoporous Silica Polyamine Composites for Metal ion Capture from Rice Hull Ash. *Submitted for publication*
18. Wong, Y. O.; Miranda,' P.; Rosenberg, E *J. Appl. Polymer Sci*. **2010**, 115, 2855.
19. Hughes, M. A.; Wood, J.; Rosenberg, E *Ind. and Eng. Chem. Res.* **2008**, *47*, 6765.
20. Kailasam, V.; Rosenberg, E.; Nielsen, D. *Industrial & Engineering Chemical Research* **2009**, *48*, 3991.
21. Nielsen, D.; Mckenzie, J.; Clancy, J., Rosenberg, E *Chimica Oggi* **2009**, *26***,** 42.
22. Rosenberg, E. "Silica Polyamine Composites: Advanced Materials for Metal Ion Recovery and Remediation," in *Macromolecules Containing Metal and Metal Like Elements, Volume 4*, C. E. Carraher, C. U. Pittman, A. S. Abd-El-Aziz, M. Zeldin, J. E. Sheats eds. J. Wiley & Sons, New York, 2005, p 51.
23. Anderson, C.; Rosenberg, E; Hart, C. K.; Ratz, Cao, Y. *Proceedings of the 5th International Symposium on Hydrometallurgy, 2003*, Volume 1 Leaching and Purification, Ed. Courtney Young, TMS, Warendale, PA, p393.
24. Rosenberg, E.; Fischer, R. C.; Hart C. K."Removal of Low Level Mercury from Aqueous Streams Using Silica Polyamine Composites," in *2003 EPD Proceedings - Mercury Management* Ed. Schlesinger, M. E. 2003, p 285.
25. E. Rosenberg, D. Pang, U. S. Patent 5,695,882, 1997.
26. E. Rosenberg, David Pang, U. S. Patent No. 5,997,748, 1999
27. E. Rosenberg, R. C. Fischer, U. S. Patent. No. 6,576,590, 2003
28. E. Rosenberg, R. C. Fischer, U. S. Patent. No.7,008,601, 2006.
29. Bandosz, T. J.; Seredych, M.; Allen, J.; Wood, J.; Rosenberg, *Chem. of Materials* 2007 *19*, 2500.
30. Allen, Jesse; Rosenberg, Edward; Maximov, Anton; Karakhanov, Eduard; Zolotukhina, Anna. Catalytic Properties of Transition Metal Salts Immobilized on Nanoporous Silica Polyamine Composites II: Hydrogenation. *Applied Organometallic Chemistry* (2011) *Accepted for publication* doi: 10.1002/aoc.1749
31. Allen, J. J.; Rosenberg, E.; Chierotti, M. R.; Gobetto, R. *Inorg. Chim. Acta* 2010, *363*, 617.

32. Allen, Jesse; Berlin, Matthew; Hughes, Mark; Johnston, Erik; Kailasam, Varadharajan; Rosenberg, Edward; Sardot, Tova; Wood, Jessica. Structural Design at the Polymer Surface Interface in Nanoporous Silica Polyamine Composites. *Materials Chemistry and Physics* (2011) *Accepted for publication* , doi:10.1016/j.matchemphys.2010.11.053
33. Sharmin, A.; Darlington, R.C.; Hardcastle, K.I.; Ravera, M.; Rosenberg E.; Ross, J.B.A. "Tuning Photophysical Properties with Ancillary Ligands in Ru(II) Mono-Diimine Complexes," J Organometal Chem 2009,694: 988.
34. Garino, C.; Gobetto R.; Nervi, C.; Salassa, L.; Rosenberg, E.; Ross. J.B.A.; Chu X.; Hardcastle KI, Sabatini C: Spectroscopic and Computational Studies of a Ru(II)Terpyridine Complex: The Importance of Weak Intermolecular Forces to Photophysical Properties. Inorg Chem 2007, 46:8752.
35. Johnson, D. Barrie and Hallberg, Kevin B. Acid mine drainage remediation options: a review. Science of the Total Environment 338(1-2), 3-14. 2005.
36. Vukovic, Z. Environmental impact of radioactive silver released from nuclear power plant. Journal of Radioanalytical and Nuclear Chemistry 254(3), 637-639. 2002.
37. Meharg, Andrew A. and Rahman, Md. Mazibur. Arsenic Contamination of Bangladesh Paddy Field Soils: Implications for Rice Contribution to Arsenic Consumption. Environmental Science and Technology 37(2), 229-234. 2003.
38. Deorkar, N. V. and Tavlarides, L. L. An adsorption process for metal recovery from acid mine waste: The Berkeley Pit problem. Environmental Progress 17(2), 120-125. 98.
39. Yang, K., Misra, M., and Mehta, R. Removal of heavy metal ions from Noranda tailings water and Berkeley pit water by ferrite coprecipitation process. Waste Processing and Recycling in Mineral and Metallurgical Industries II, Proceedings of the International Symposium on Waste Processing and Recycling in Mineral and Metallurgical Industries, 2nd, Vancouver, B. C., Aug. 20-24, 1995. 425-38. 95.
40. Huang, Hsin Hsiung and Liu, Qi. Bench-scale chemical treatability study of the Berkeley Pit water. ACS Symposium Series 607(Emerging Technologies in Hazardous Waste Management 5), 196-209. 95.

41. Wiener, J. G., Knights, B. C., Sandheinrich, M. B., Jeremiason, J. D., Brigham, M. E., Engstrom, D. R., Woodruff, L. G., Cannon, W. F., and Balogh, S. J. Mercury in Soils, Lakes, and Fish in Voyageurs National Park (Minnesota): Importance of Atmospheric Deposition and Ecosystem Factors. Environmental 197 Science & Technology 40(20), 6261-6268. 2006.
42. Boddu, Veera M., Abburi, Krishnaiah, Talbott, Jonathan L., and Smith, Edgar D. Removal of Hexavalent Chromium from Wastewater Using a New Composite Chitosan Biosorbent. Environmental Science and Technology 37(19), 4449-4456. 2003.
43. Bell, F. G. Environmental Geology and Health. Environmental Geology: Principles and Practice, London: Blackwell Science, **1998**, 487-500.
44. Mendes, F. D. and Martins, A. H. Recovery of nickel and cobalt from acid leach pulp by ion exchange using chelating resin. Minerals Engineering 18(9), 945-954. 2005.
45. Cheng, C. Y. Purification of synthetic laterite leach solution by solvent extraction using D2EHPA. Hydrometallurgy 56(3), 369-386. 2000.
46. Kordosky, Gary A. Copper solvent extraction: the state of the art. JOM 44(5), 40-5. 92.
47. Szymanowski, J. Kinetics and interfacial phenomena in solvent extraction of metals. Mineral Processing and Extractive Metallurgy Review 18(1), 1-66. 98.
48. McGarvey, F. X. and Tamaki, D. Selective ion exchange resins for toxic metal removal. Official Proceedings - International Water Conference 52nd, 228-33. 91.
49. Kekesi, Tamas. Gallium extraction from synthetic Bayer liquors using Kelex 100-kerosene, the effect of loading and stripping conditions on selectivity. Hydrometallurgy 88(1-4), 170-179. 2007.
50. J. S. Speight, B. Ozum. *Petroleum Refining Processes*, Marcel Dekker: New York, **2002**.
51. S. Nishimura Handbook of heterogeneous catalytic hydrogenation for organic synthesis, JohnWiley & Sons: New York, **2001**.
52. J. M. Thomas, J.Mol. Catal. A: Chem. **1999**, 146, 77.
53. R. A. Sheldon, H. Van. Bekkum *Fine Chemicals through the Heterogeneous Catalysis*. John Wiley & Sons: New York, **2002**.
54. Sun, H.P. Wristers, J.P. (1992). Butadiene. In J.I. Kroschwitz (Ed.), *Encyclopedia of Chemical Technology, 4th ed.*, vol. 4, pp. 663–690. New York: John Wiley & Sons

55. V. Udayakumar, S. Alexander, V. Gayathri, V. Shivakumaraiah, K. R. Patil, B. Viswanathan, *J.Mol. Catal. A: Chem.* **2010**, *317*, 111.
56. B. H. G. Swennenhuis, R. Chen, P. W. N. M. van Leeuwen, J. G. de Vries, P. C. J. Kamer, *Eur. J. Org. Chem.* **2009**, *33*, 5796.
57. van Leeuwen, Piet W.N.M. **2004** *Homogeneous Catalysis: Understanding the art*. Dordrecht, The Netherlands: Kluwer Academic Publishers
58. Jessen, S; Larsen, F; Koch, C. B; Arvin, E. Sorption and Desorption of Arsenic to Ferrihydrite in a Sand Filter. Environmental Science & Technology, 2005, 39(20), 8045-8051.
59. Geckeler, Kurt E. and Volchek, Konstantin. Removal of Hazardous Substances from Water Using Ultrafiltration in Conjunction with Soluble Polymers. Environmental Science and Technology 30(3), 725-34. 96.
60. Soper, B., Haward, R. N., and White, E. F. T. Intramolecular cyclization of styrene-p-divinylbenzene copolymers. Journal of Polymer Science, Polymer Chemistry Edition 10(9), 2545-64. 72.
61. Beatty, S.T.; Fischer, R.J.; Hagers, D.L.; Rosenberg, E. *Ind. Eng. Chem. Res.* **1999**, *38*, 4402-08
62. B.R. James, *Homogeneous Hydrogenation*. John Wiley & Sons, New York, 1973.
63. Z. Dobrovolná, P. Kacer, L. Cerveny, *J. Mol. Catal. A: Chem.* 130 (1998) 279.
64. Molnár, A.; Sárkányb, A.; Vargaa, A. *Journal of Molecular Catalysis A: Chemical* 173 (2001) 185–221
65. Nakamura, Y.; Hirai, H. *Chemistry Letters*. **1975** pp. 823-828
66. Naota, T.; Takaya, H.; Murahashi, S. *Chem Rev.* **1998**, 98, 2599-2660
67. T. J. Barton, L. M. Bull, W. G. Klemperer, D. A. Loy, B. McEnaney, M. Misono, P. A. Monson, G. Pez, G. W. Scherer, J. Vartuli, O. M. Yaghi "Tailored Porous Materials," Chem. Mater. 11 (1999) 2633.
68. C. J. Brinker, G. Scherer "Sol-Gel Science: The Physics and Chemistry of Sol-Gel Processing," Academic, New York (1990)
69. S. A. Rodriguez, Luis A. Colón "Study of the Solution in the Synthesis of a Sol-Gel Composite Used as a Chromatographic Phase " *Chem. Mater.* **11** (1999) 754.

70. D. Wang, S. L. Chong and A. Malik "Sol-Gel Column Technology for Single Step Deactivation, Coating and Stationary Phase Immobilization in High-Resolution Capillary Gas Chromatography," Anal. Chem. 69 (1997) 4566.
71. D. A. Loy, B. M. Baugher, C. R. Baugher, D. A. Schneider, and K. Rahimian "Substituent Effects on the Sol-Gel Chemistry of Organotrialkoxysilanes," Chem. Mater. 12 (2000) 3624.
72. H. Dong and J. D. Brennan "Controlling the Morphology of Methylsilssequioxane Monoliths Using a Two-Step Processing Method," Chem. Mater. 18 (2006) 541.
73. M. Streat, NATO ASI Ser., Ser. E: Appl. Sci. 107 (1986) 449.
74. D.L. Jones, US Patent 1999, 18pp., Cont.-in-part of US 5,650,057.
75. P. Devasia and K.A. Natarajan, *Resonance* **9** (2004), p. 27.
76. E. Rosenberg, R.J. Fischer, J. Deming, C. Hart, P. Miranda, B. Allen, in: T. White, D. Sun (Eds.), Symposium Proceedings of the International Conference on Materials and Advanced Technologies, vol. I, Mat. Res. Soc., Singapore, 2001, p. 173.
77. E. Rosenberg, R.J. Fischer, J. Deming, C. Anderson C, in: ALTA 2000 Technical Proceedings, SX/IX-1, ALTA Metallurgical Services, 2000.
78. S.T. Beatty, R.J. Fischer, D.L. Hagars and E. Rosenberg, *Ind. Eng. Chem. Res.* **38** (1999), p. 4402.
79. S.T. Beatty, R.J. Fischer, D. Pang and E. Rosenberg, *Separ. Sci. Technol.* **34** (1999), p. 3125.
80. R. Grinstead, *J. Metal* **31** (1979), p. 13.
81. N. Curtis, G. Lawrance and A. Sargeson, *Austral. J. Chem.* **36** (7) (1983), p. 1327.
82. B. Hammes, M. Kieber-Emmons, R. Sommer and A. Rheingold, *Inorg. Chem.* **41** (2002), p. 1351.
83. P. Crayton, Inorg. Syn. 7 (1963) 207.
84. E. Kimura, S. Young and J. Collman, *Inorg. Chem.* **9** (1970), p. 1183.
85. F. Cotton, G. Wilkinson and P. Gaus, Basic Inorganic Chemistry p. 570 (3rd ed.), John Wiley & Sons Inc. (1995).
86. C. Garino, S. Ghiani, R. Gobetto, C. Nervi, L. Salassa, E. Rosenberg, J. Ross, X. Chu, K. Hardcastle and C. Sabatini, *Inorg. Chem.* **46** (2007), p. 8752.
87. M.R. Chierotti and R. Gobetto, *Chem. Commun.* (2008), p. 1621.

88. M.R. Chierotti, L. Garlaschelli, R. Gobetto, C. Nervi, G. Peli, A. Sironi and R. Della Pergola,*Eur. J. Inorg. Chem.* (2007), p. 3477.
89. L.L. Hench, Sol–Gel Silica: Properties, Processing and Technology Transfer, Prentice-Hall PTR, New York (2005).
90. E. Rosenberg, Z. Fan and D. Li, *Yingyong Huaxue* **20** (2003), p. 867.
91. M.J. Wirth and H.O. Fatumbi, *Anal. Chem.* **65** (1993), p. 822.
92. P.W.J.G. Wijnen, T.P.M. Beelen and R.A. van Santen, *Surf. Sci. Series* **131** (2006), p. 597.
93. M.D. Bruch and H.O. Fatunmbi, *J. Chromatogr. A* **1021** (2003), p. 61.
94. F. del Monte and D. Levy, *Opt. Mater.* **13** (1999), p. 17.
95. T. Kobayashi, J.A. DiVerdi and G.E. Maciel, *J. Phys. Chem. C* **112** (2008), p. 4315.
96. Prabakar, S. and Assink, R.A. *Journal of Non-Crystalline Solids* **211** (1997) 39-48
97. Kresge, C. T.; Leonowicz, M. E.; Roth, W. J.; Vartuli, J. C.; Beck, J. S. Nature 1992, 359, 710.
98. Velev, D. O.; Lenhoff, A. M. *Curr. Opin. Colloid Interface Sci.* 2000, 5, 56.
99. Imhof, A.; Pine, D. *J. Ad. Mater.* 1998, 10, 697.
100. Sanchez, J.; Rankin, S. E.; McCormick, A. V. *Ind. Dng. Chem. Res.* **1996**, *35*, 117.
101. Shimojima, A.; Kuroda, K.; *Langmuir* **2002**, *18*, 1144-1149
102. J. M. Thomas and W.J. Thomas, *Principles and Practice of Heterogeneous Catalysis*. VCH: Weiheim, 1997.
103. J. M. Thomas, R. D. Adams, E. M. Boswell, B. Captain, H. Grönbeck, R. Raja *Faraday Discuss.* 2008, **138**, 301.
104. E. Karakhanov, A. Maximov, in *Metal Complexes and Metals in Macromolecules* (Eds.: D.Wohrle, A.Pomogajlo), John Wiley & Sons:New York, 2003, p. 457.
105. E. Karakhanov, A. L. Maksimov, O. V. Zatolochnaya, E. Rosenberg, V. Kailasam, M. Hughes, *Petroleum Chemistry* 2009, **49**, 107.
106. I. V. Gostunskaya, V. S. Petrova, A. I. Leonova, V. A. Mironova, M. Abubaker, *Kazanskii Neftekhimiya* 1967, **7**, 3.
107. D. K. Mukherjee, N. Ghosh, *Bull. Catal. Soc. India* 2006, **5**, 155.

108. P. C. L'Argentière, E. A. Cagnola, M. E. Quiroga, D. A. Liprandi, *Appl. Catal. A: Gen.* 2002, 253.
109. N. D. Zelinski, P. Pawlow, *Ber. Dtsch. Chem. Ges.* 1924, **57**, 1066, 2055.
110. C. D. Wagner, A. V. Naumkin, A. Kraut-Vass, J. W. Allison, C. J. Powell, J. R. Rumble, Jr. NIST X-Ray Photelectron Database NIST Standard Reference Database 20, Version 3.5 Last updated: August 27, 2007, (Created: June 06, 2000) http://srdata.nist.gov/xps/.
111. E. E. Karakahnov, A. L. Maximov, V. A. Skorkin, A.V. Zolotukhina, A. S. Smerdov, A. Y. Tereshchenko, *Pure Appl. Chem.* 2009, **81**,2013.
112. D. W. Franco *Coord. Chem. Rev.* 1992, **119**, 199.
113. A. C. Skapski, M. L. Smart, *I. Chem. Soc. D* 1970, 568.
114. L. Tasic, R. Ritter *J. Mol. Struct.* 2009, **933**, 15.
115. E. M. Viviente, P. S. Pregosin, M. Tschoerner, *Mag. Res. Ind. Chem.* 2000, **38**, 23.
116. P. M. Tolstoy, P. Schah-Mohammedi, S. N. Smirnov, N. S. Golubev, H. H. Limbach, *J. Am. Chem. Soc.* 2004, **126**, 5621.
117. O. V. Borisov, D. M. Coleman, K. A. Oudsema, R. O. Carter III, *J. Anal. Atomic Spectrom.* 1997, **12**, 239.
118. Zou, J.; Sanelle,P; Pettigrew, K. A.; Kauzlarich, S. M. "Size and Spectroscopy of Silicon Nanoparticles Prepared via Reduction of SiCl4'" J. of Cluster Sci. 2006,17,565.
119. Zhang, X.; Neiner, D.; Wang, S.; Louie, A. Y.; Kauzlarich, S. M. "A new solution route hydrogen-terminated silicon nanoparticles: synthesis, functionalization and water stability Nanotechnology 2007, 18, 1.
120. Canham, L. T. "Silicon quantum wire array fabrication by electrochemical and chemical dissolution of wafers Appl. Phys. Lett.," 1990, 57, 1046
121. Cullis, A. G.; Canham, L.T. Nature "Visible light emission due to quantum size effects in highly porous crystalline silicon,"1991, 353, 335.
122. Wilcoxon, J.P.; Samara, G. A.; Provencio, P. N. "Optical and electronic properties of Si nanoclusters synthesized in inverse micelles,"Phys. Rev. B 1999, 60, 2704.
123. Ouyang, J.-M.; Zhang, Z.-M.; Zhang, X.-L.; Chao, Q.-J.; Ye, C.-J.; Di, H.-W. "Electroluminescent devices with LB films of amphiphilic-8-hydroxyquinoline quinoline as emitter," Thin Solid Films 2000,363 130.

124. Warner J H, Hoshino A, Yamamoto K and Tilley R D 2005 *Angew. Chem. Int. Edn* **44** 4550
125. Zou, J.; Kauzlarich, S. M. "Functionalization of silicon nanoparticles via silanization: Alkyl, Halide and Ester," J. cluster Sci. 2008, 19, 341.
126. Ambili, R.; Biju, S.; Reddy, M. L. P. "Highly luminescent Eu3+ complexes of organosilyl 4,4,555 pentfluoro-1-(napthalen-2-yl) pentane-1,3-dioate ligands grafted on silica nanoparticles," J. Mat.Chem. 2009, 19, 7976.
127. Slichter, C.P. "Principles of Magnetic Resonance", Springer-Verlag, 1990, 242-246
128. Bovey, F.A. and Mirau, P.A. "NMR of Polymers", Academic Press, 1996, 81-83